



**US Army Corps
of Engineers®**
Engineer Research and
Development Center

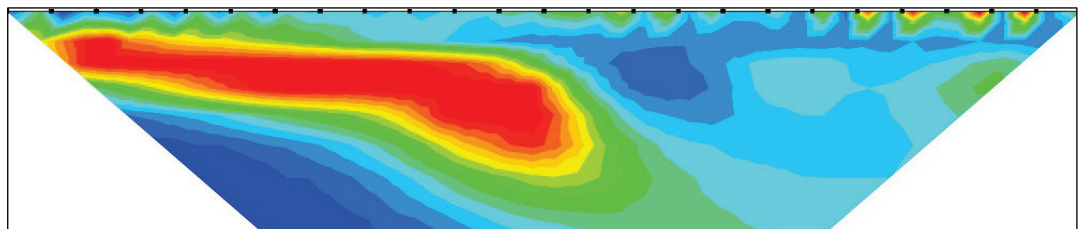


Waterborne Geophysical Investigation to Assess Condition of Grouted Foundation

Old River Control Complex – Low Sill Structure, Concordia Parish, Louisiana

Benjamin R. Breland, Janet E. Simms, William E. Doll,
Jason Greenwood, and Ronald Kaufman

April 2022



The U.S. Army Engineer Research and Development Center (ERDC) solves the nation's toughest engineering and environmental challenges. ERDC develops innovative solutions in civil and military engineering, geospatial sciences, water resources, and environmental sciences for the Army, the Department of Defense, civilian agencies, and our nation's public good. Find out more at www.erdclibrary.on.worldcat.org/discovery.

To search for other technical reports published by ERDC, visit the ERDC online library at www.erdclibrary.on.worldcat.org/discovery.

Waterborne Geophysical Investigation to Assess Condition of Grouted Foundation

Old River Control Complex – Low Sill Structure Concordia Parish, Louisiana

Benjamin R. Breland and Janet E. Simms

*Geotechnical and Structures Laboratory
U.S. Army Engineer Research and Development Center
3909 Halls Ferry Road
Vicksburg, MS 39180-6199*

William E. Doll

*Oak Ridge Institute for Science and Education
P.O. Box 117
Oak Ridge, TN 37831-0117*

Jason Greenwood

*Advanced Geosciences Inc.
2121 Geoscience Drive
Austin, TX 78726*

Ronald Kaufman

*Spotlight Geophysical Services, LLC
4618 NW 96th Avenue
Doral, FL 33178*

Final report

Approved for public release; distribution is unlimited.

Prepared for U.S. Army Corps of Engineers (USACE), New Orleans District (MVN)
New Orleans, LA 70118

Under Project 110712, “Old River Low Sill Evaluation”

Abstract

The Old River Low Sill Structure (ORLSS) at the Old River Control Complex (ORCC) in Concordia Parish, LA, is a steel pile-founded, gated reinforced-concrete structure that regulates the flow of water into the Atchafalaya River to prevent an avulsion between the Mississippi River and the Atchafalaya River. A scour hole that formed on the southeast wall of ORLSS during the Mississippi River flood of 1973 was remediated with riprap placement and varied mixtures of self-leveling, highly pumpable grout. Non-invasive waterborne geophysical surveys were used to evaluate the distribution and condition of the grout within the remediated scour area. Highly conductive areas were identified from the surveys that were interpreted to consist mostly of grout. Resistive responses, likely representing mostly riprap and/or sediment, were encountered near the remediated scour area periphery. A complex mixture of materials in the remediated scour area is interpreted by the more gradual transitions in the geophysical response. Survey measurements immediately beneath ORLSS were impeded by the abundance of steel along with the structure itself. The survey results and interpretation provide a better understanding of the subsurface properties of ORLSS.

DISCLAIMER: The contents of this report are not to be used for advertising, publication, or promotional purposes. Citation of trade names does not constitute an official endorsement or approval of the use of such commercial products. All product names and trademarks cited are the property of their respective owners. The findings of this report are not to be construed as an official Department of the Army position unless so designated by other authorized documents.

DESTROY THIS REPORT WHEN NO LONGER NEEDED. DO NOT RETURN IT TO THE ORIGINATOR.

Contents

Abstract	ii
Figures and Tables	v
Preface	viii
Executive Summary	ix
1 Introduction	1
1.1 Purpose.....	1
1.2 Scope.....	1
1.3 Background.....	1
1.3.1 <i>Geologic setting</i>	2
1.3.2 <i>Old River Low Sill Structure (ORLSS)</i>	4
1.3.3 <i>Physical site properties</i>	8
1.3.4 <i>Previous geophysical surveys</i>	9
2 Geophysical Methods	12
2.1 Electrical resistivity tomography (ERT).....	12
2.2 Seismic refraction and reflection.....	14
3 Field Operations	16
3.1 Weather conditions.....	16
3.2 River elevation and bathymetry.....	17
4 Data Acquisition and Processing	20
4.1 Electrical resistivity data acquisition and processing.....	20
4.2 Seismic data acquisition and processing.....	21
5 Results and Observations	27
5.1 Resistivity.....	27
5.2 Inflow parallel lines.....	29
5.3 Inflow fan lines.....	31
5.4 Outflow dataset.....	34
5.5 Seismic.....	35
5.5.1 <i>Seismic refraction</i>	35
5.5.2 <i>Seismic reflection</i>	37
6 Discussion	42
6.1 Interpretation of ERT survey.....	43
6.1.1 <i>General statements</i>	43
6.1.2 <i>Sub-bottom sediments</i>	45
6.1.3 <i>Left abutment riprap wingwall</i>	46
6.1.4 <i>Resistivity trends associated with rock pile</i>	47

6.1.5	<i>Resistivity trends associated with the estimated scour area</i>	47
6.1.6	<i>Outflow channel and stilling basin</i>	50
6.2	Interpretation of seismic survey	51
7	Conclusions	52
	References	57
	Appendix A: Inverted Resistivity Sections	59
	Appendix B: Seismic Data Processing	66
	Unit Conversion Factors	81
	Report Documentation Page	

Figures and Tables

Figures

Figure 1. Site location map of the Old River Control Complex (ORCC) (modified from Heath et al. 2015).	2
Figure 2. General geologic settings (Saucier 1969).	4
Figure 3. Schematic drawings of ORLSS (courtesy of MVN). Elevations are in feet.	7
Figure 4. Interpreted ERT sections from land surveys: (a) geologic cross section of ORLSS with outline of ERT profiles, (b) ERT line LSNPL parallel to levee embankment on the upstream side near the right abutment, and (c) LSSPL parallel to levee embankment on upstream side near the left abutment.	11
Figure 5. Idealized diagram of a dipole-dipole electrical resistivity configuration. (a) By using different values for a and n , 2-D coverage of the subsurface is obtained (b). In (b), the rectangles along the surface represent electrodes (in this example there are 56), and the dots in the subsurface represent the pseudo-location of a measurement. For a given number of electrodes, and as the electrode spacing increases, the number of measurements at depth decreases.....	13
Figure 6. Idealized diagram of travel times of first-arriving seismic waves indicated by “x” in the top portion of the figure that can be compiled for all shot points.	15
Figure 7. SeaArk boat used for data acquisition at ORLSS.	16
Figure 8. Plot of river elevation, in meters and feet, during the waterborne geophysical survey acquisition.....	18
Figure 9. Bathymetry of the site, in meters with respect to MSL, from December 2019 (provided by MVN) and location of geophysical survey lines. Seismic lines are shown in red, and resistivity lines are in black.	19
Figure 10. SuperSting R8/IP system, GPS, and cable used in ERT data acquisition.	21
Figure 11. Equipment used for seismic survey acquisition: (a) seismic data acquisition configuration, (b) Geometrics SmartSeis used for data recording, (c) hydrophones and cable attached to flotation buoys, (d) airgun used as the seismic source with a control fin and hydrophone, (e) tracking system used to maintain acquisition geometry of prescribed survey layout, and (f) hydrophone cable being towed behind the boat (white floats) after making a turn near the structure. Orange floats on the cable that have not yet turned and are still moving toward the structure can be seen closer to the structure.	23
Figure 12. Marine seismic refraction survey navigation plan and acquired survey lines (magenta).....	24
Figure 13. Example seismic shot records and travel-time picks for both inflow and outflow channels.	25
Figure 14. Resistivity lines with bathymetric map (m, MSL). Green and red points indicate the start and end electrodes, respectively, for each line.	28
Figure 15. ERT profiles acquired in the inflow channel parallel to the weir axis. Dashed line represents the channel bottom.	31

Figure 16. ERT profiles from inflow fan layout. Dashed line represents the channel bottom.....	33
Figure 17. 3-D fence diagrams of ERT profiles acquired in the inflow channel. The left plot is a view looking north-northeast, while the right plot is a view looking north. Color scale (top right) applies to both diagrams.	33
Figure 18. ERT profiles from the outflow channel. Dashed line represents the channel bottom.....	35
Figure 19. Apparent P-wave velocity of shallow sediment.	36
Figure 20. Stacked sections for three lines on the inflow side of ORLSS: (a) line 150 (green dashed line of approximate disturbed area), (b) line 400, and (c) line 675. The blue dashed line represents the channel bottom.	39
Figure 21. Stacked depth sections for three lines from the outflow channel of ORLSS: (a) line 150, (b) line 300, and (c) line 400. Blue dashed line represents the channel bottom.	41
Figure 22. Plan view of interpreted ERT results overlain with feature boundaries. Resistivity values are an average of the resistivity values between the channel-bottom surface and 6 m below.	45
Figure 23. Interpreted areas derived from the geophysical survey.	54
Figure 24. Contours of resistivity in a horizontal plane at 9m below sea level, 21.7m below water surface, shown in color. Gray-scale contours show estimated depth for the deeper part of the scour in meters relative to water surface. The boundary of the estimated scour is shown, and the four resistivity features R1, R2, C1, and C2 are labeled.	55
Figure B1. Idealized diagram of raypaths for types of waves produced at ORLSS. The refracted wave is blue, the primary reflected wave is green, and a multiple reflected wave is solid red. The travel time for the multiple is the same as that for a primary reflection from greater depth with the brown representing a deeper geologic contact. A reflection from a hypothetical deeper contact is shown as a dashed red line, with the interface at twice the depth for simplicity; this assumes the same velocity in the water and the first geologic layers.....	66
Figure B2. Synthetic seismic model parameters.	67
Figure B3. Time-distance plot showing arrival times of seismic waves for five hypothetical bottom sediment velocities, based on the model in Figure B2.	67
Figure B4. Reduced time-distance plot for the synthetic seismic refraction data.	69
Figure B5. Reflected seismic waves observed in three “shot gathers” during fieldwork on line 400N on the inflow side of ORLSS. One of the many reflections is highlighted in green on the left shot gather.	71
Figure B6. The shot gathers from Figure B5 after applying the NMO correction.....	73
Figure B7. Stacked reflection section for Line 400 from the inflow channel of ORLSS, (top) in travel time and (bottom) in depth feet.....	74
Figure B8. Stacked reflection sections for ten lines on the inflow side of ORLSS. Edge of the scour is indicated by the green triangle at the top of each profile.....	77
Figure B9. (a) Unmigrated and (b) migrated depth sections for outflow Line 300.	79
Figure B9. (c) Unmigrated and (d) migrated depth sections for outflow Line 400.	80

Tables

Table 1. Nominal electrical resistivity values for common materials (Telford et al. 1990; Johnson et al. 2017)..... 9

Table 2. Weather conditions during data collection period (NOAA 2019). 17

Preface

This study was conducted for the U.S. Army Corps of Engineers, New Orleans District (USACE-MVN), under Project 110712, “Old River Low Sill Evaluation.” The technical monitor was Dr. Maureen K. Corcoran.

The work was performed by the Geotechnical Engineering and Geosciences Branch (GEGB) of the Geotechnical and Structures Division (GSD), U.S. Army Engineer Research and Development Center, Geotechnical and Structures Laboratory (ERDC-GSL). At the time of publication, Mr. Christopher G. Price was Branch Chief, GSG; Mr. James L. Davis was Division Chief, GS; and Dr. Maureen K. Corcoran was the Associate Technical Director for Water Resources Infrastructure. The Deputy Director of ERDC-GSL was Mr. Charles W. Ertle II, and the Director was Mr. Bartley P. Durst.

ERDC personnel acknowledge appreciation for the support provided by USACE-MVN personnel and ORLSS project office personnel in the planning and coordination of the field acquisition. Also acknowledged are the efforts of the boat operators Patrick Tassin, Christopher “Moon” Lamoine, and Christopher St. Romain for their assistance throughout the investigation. Their professionalism, expertise, and knowledge provided a pivotal role in the success of the data acquisition and is greatly appreciated.

The Commander of ERDC was COL Teresa A. Schlosser, and the Director was Dr. David W. Pittman.

Executive Summary

The U.S. Army Engineer Research and Development Center (ERDC) was tasked by the U.S. Army Corps of Engineers (USACE), New Orleans District (MVN), with assessing the condition of a grouted scour hole located at the southeast wall of the Old River Low Sill Structure (ORLSS) at the Old River Control Complex (ORCC), Concordia Parish, LA. As part of the ORCC, the ORLSS was constructed to prevent an avulsion between the Mississippi River and the Atchafalaya River. The purpose of this investigation was to evaluate the condition of the grout, including any voids and/or water- or sediment-filled zones, used to remediate a scour hole that formed near the left abutment during the Mississippi River flood of 1973. The scour hole was remediated using riprap, which was placed in the inflow channel, and varied mixtures of self-leveling, highly pumpable grout that likely would have exhibited a laterally spreading behavior.

The approach of this investigation was to use waterborne electrical resistivity tomography (ERT) and seismic methods to assess the presence or absence of voids and/or water- or sediment-filled zones in the grout and to better define scour hole boundaries. The interpretation of the results from the waterborne survey was supplemented by the results from a land-based geophysical survey performed in 2018 that characterized the onshore subsurface adjacent to ORLSS.

The waterborne geophysical surveys were performed on both upstream and downstream sides of ORLSS. Both ERT and seismic surveys revealed greater complexity of the subsurface conditions of ORLSS than previous studies had suggested, and more gradual contrasts were encountered in the geophysical response than anticipated. The geophysical response is dependent on the material(s) present and the volume that material occupies. The interpretation process required an understanding of the features at ORLSS from a three-dimensional perspective, in addition to temporal changes of those features. It was not possible to image directly below the structure because of the high concentration of steel piles within that volume. Steel, which exhibits high seismic velocity and high electrical conductivity, will interfere with any seismic or electrical geophysical method.

Two high-resistivity (low-conductivity) regions (i.e., ungrouted regions) were identified: one in the center of the channel adjacent to the estimated scour hole boundary and the other along the left abutment riprap wingwall. The high values in the center of the channel were interpreted to be rock (riprap) with minimal sediment fill. Portions within the scour volume that were not electrically conductive could indicate where grout did not penetrate, and these were presumed to consist of ungrouted riprap blocks. Between the two resistive areas was an electrically conductive area, interpreted as mostly grout and grouted riprap (i.e., grouted region), which partially comprised the scour area on the left abutment side. This low-resistivity area within the scour volume was interpreted as electrically conductive grout that infiltrated riprap blocks now serving as a matrix to the rock. The resistivity surveys show gradual, rather than abrupt, transitions of low and high resistivities between grouted and ungrouted regions.

It is interpreted that the remediated scour hole is not uniform but consists of portions where the riprap has been grouted and portions where the voids (i.e., pore spaces between riprap blocks) are filled with some combination of river sediment and water. Based on the ERT inversion results and their interpretation, there is no evidence to support the presence of air-filled voids greater than 3 m in diameter. It is likely that any former void zones within the grout would be filled with either water, material not associated with the grout (e.g., unconsolidated sediment), or a combination of material and water. Considering that a water-filled cavity would have a low contrasting resistivity compared to a bulk volume of grout, the ERT data do not suggest the presence of water-filled cavities greater than 3 m in diameter. It is possible that water/sediment-filled zones less than 3 m within the grouted area could be present but not detectable using the survey parameters employed.

The seismic survey had limited success because of similarities between the water velocity and the channel-bottom sediment velocities. The shallow sediments along the channel bottom exhibited lower seismic velocities than anticipated. The low seismic velocity of the shallow sediments, combined with the desired depth of investigation, required a longer offset of the seismic source from the hydrophone array to acquire seismic data below the water column. Consequently, this longer offset meant that it was not possible to measure velocities close to ORLSS. The minimal contrast between the water and channel sediment velocities limited the ability to construct two-dimensional (2-D) cross sections from the seismic refraction

data. Although there is limited contrast between the water and channel sediment velocities, the seismic survey was used to identify both higher and lower velocity areas along the channel bottom in the inflow and outflow channels. Typically, a higher seismic velocity suggests the presence of a stiffer material, in contrast to a softer material which would have a lower velocity. The interpretation derived from these results provides a greater understanding of the subsurface properties of ORLSS.

Recommendations for future efforts that could expand on the waterborne geophysical data include: (1) forward modeling and sensitivity analysis of varying resistivity values and geometries to simulate hypothetical water- or material-filled zones, (2) investigating applicability of formation factor to empirically derive an approximate porosity from the ERT data, (3) making laboratory-based measurements on replicated and simulated grout mixtures to correlate the resistivity to compressive strength, and (4) conducting borehole-based geophysical analysis in the event that a borehole is drilled within the scour hole.

1 Introduction

1.1 Purpose

The U.S. Army Engineer Research and Development Center (ERDC) was tasked by the U.S. Army Corps of Engineers (USACE), New Orleans District (MVN), with assessing the condition of a grouted scour hole located at the southeast wall of the Old River Low Sill Structure (ORLSS) at the Old River Control Complex (ORCC), Concordia Parish, LA. This effort involved both land-based and waterborne geophysical surveys led by the ERDC Geotechnical Engineering and Geosciences Branch (GEGB). Geophysical techniques are noninvasive, cover greater spatial area than invasive methods, and can generally be performed in less time and at lower cost than invasive methods. Geophysical investigations were designed to assess the condition of the grout to include delineation of the boundaries of the grout body and riprap-filled volume and identification of anomalies within the grout/riprap body that might be associated with voids, water- or material-filled zones.

1.2 Scope

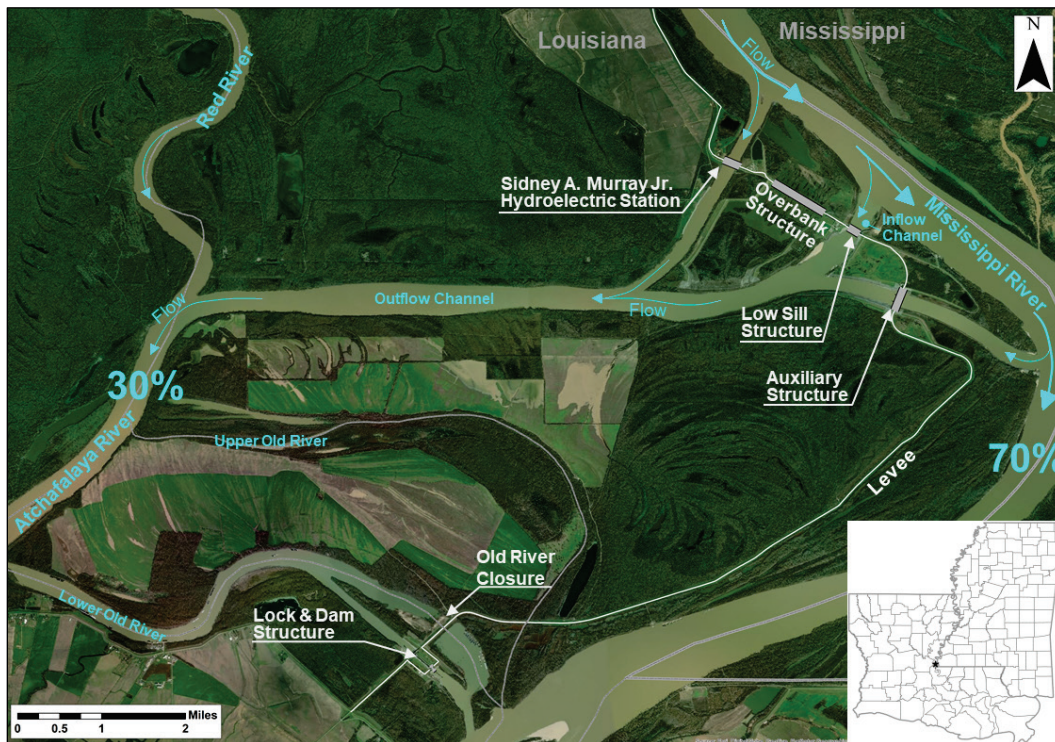
The first phase of the geophysical investigation involved both land-based seismic and electrical resistivity tomography (ERT) surveys conducted in 2018 (Simms et al. 2021). The second phase consisted of a waterborne geophysical investigation conducted at ORLSS between 2 and 6 Dec and between 9 and 11 Dec 2019 and is the focus of this technical report. Two geophysical methods were employed: marine ERT and seismic refraction. The waterborne geophysical investigation is a continuation of the land-based geophysical surveys.

1.3 Background

The ORCC is located along the west bank of the Mississippi River between river miles 317 and 311 in Concordia Parish, approximately 56 km (35 mi) south of Natchez, MS, and 77 km (48 mi) northwest of Baton Rouge, LA (Figure 1). The general location of the survey area is on both the inflow and outflow channels of ORLSS, which is at latitude 31.077328° and longitude -91.598976° and UTM coordinates easting 633648.46 m E and northing 3439015.45 m N. Survey limits extend approximately 300 m (984 ft) upstream and 300 m (984 ft) downstream from the structure.

The ORCC consists of four primary structures: ORLSS, Overbank Control Structure (Overbank), Auxiliary Structure (Auxiliary), and the Sidney A. Murray Hydroelectric Station. The complex also includes a lock and dam structure, inflow and outflow channels, an Old River closure structure, main-line levee extensions, and bank stabilization along the Red and Atchafalaya rivers. ORLSS was completed in 1958, along with the Overbank Structure, to prevent a natural cutoff (i.e., avulsion forming from the Mississippi River into the Atchafalaya River). The Auxiliary Structure was constructed (ca. 1986) to aid in reducing the flow of water through the existing structures and to allow USACE to maintain the distribution of flow. ORLSS and the Overbank work together with the Auxiliary and Sidney A. Murray Hydroelectric Station (ca. 1990) to maintain a 30 percent combined-flow diversion of the Mississippi and Atchafalaya rivers.

Figure 1. Site location map of the Old River Control Complex (ORCC) (modified from Heath et al. 2015).



1.3.1 Geologic setting

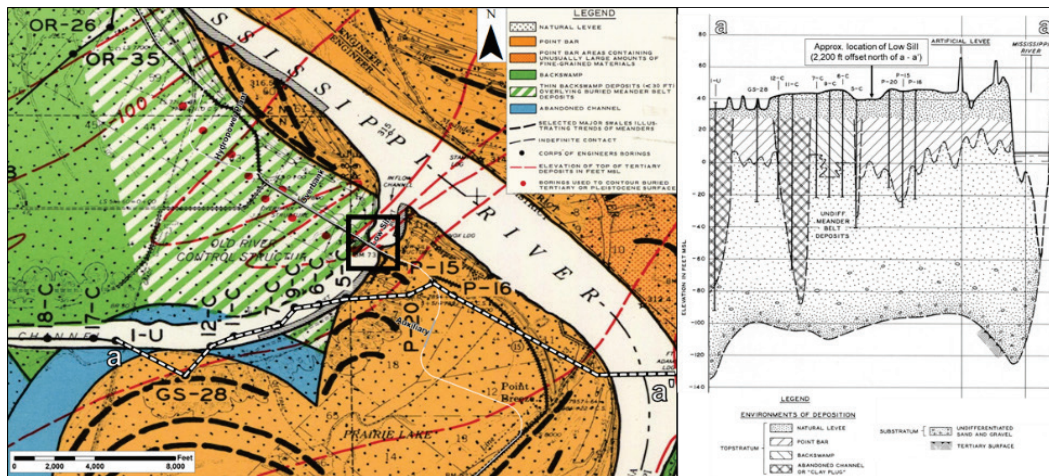
The following section presents a generalized geologic summary based on a more detailed summary of geologic studies conducted at ORCC (Breland et

al. 2021*) The study area is located along the east-central border of Louisiana (Figure 2). The surficial geology of the ORCC area consists mainly of four depositional environments common to the Lower Mississippi River Valley, backswamp, natural levee, point bar, and abandoned channel deposits as identified by Fisk (1947) and Saucier (1969, 1994), which comprise the topstratum. Backswamp and abandoned channel deposits are primarily composed of plastic clay with a higher moisture content, while point bar and natural levee deposits are composed of a mixture of sand, silt, and clay. The shallow, subsurface materials of the right abutment, which are 6.1 m (20.0 ft) thick, consist mostly of clay, associated with a backswamp deposit, while the left abutment consists of a heterogeneous mixture of silt, silty sand, clay, and sand strata associated with point bar deposits.

The foundation geological materials underlying both inflow and outflow channels of ORLSS consist chiefly of alternating beds of silt (ML) and silty sand (SM) with occasional silty clay (CL) and sand (SP) strata (information courtesy of MVN). The exact location of the transition in depositional environment from backswamp deposits on the right abutment to point bar deposits on the left abutment is unknown. During construction, the inflow channel of ORLSS was excavated down to a designed elevation of -1.5 m (-5.0 ft). Material overlying this datum is likely that of relatively recent siltation brought into the inflow channel since construction. A 3.0-m (10-ft)-thick, highly plastic clay (CH) layer underlies the alternating strata. This CH layer gradually becomes thin to absent approximately 38 m (125 ft) from the channel centerline and 335 m (1,100 ft) upstream of the weir. The CH layer extends 152 m (500 ft) downstream from the weir in the outflow channel and was not encountered in a soil boring 305 m (1,000 ft) downstream from the weir. These fine-grained deposits of the topstratum overlie poorly graded, fine-grained substratum sands (SP) at an elevation of -12 m (-40 ft) on the right abutment to -18 m (-60 ft) on the left abutment. The finer sands grade downward into coarser-grained sands and gravels near the Tertiary Period (approximately 66 to 2.6 million years ago) contact at around -36.6 m (-120 ft) elevation.

*Breland, B., L. A. Walshire, M. K. Corcoran, J. R. Kelley, J. E. Simms, D. W. Harrelson, and M. Zakikhani. 2021. *Old River Control Complex (ORCC) Low Sill: A literature synthesis*. ERDC/GSL draft in preparation. Vicksburg, MS: U.S. Army Engineer Research and Development Center.

Figure 2. General geologic settings (Saucier 1969).



1.3.2 Old River Low Sill Structure (ORLSS)

ORLSS is a steel pile-founded, reinforced-concrete structure with eleven 13.4-m (44-ft)-wide, steel-gated bays separated by reinforced-concrete monoliths. Gates 5-7 are low-flow bays while gates 1-4 and 8-11 are high-flow bays. Both inflow and outflow channels at ORLSS were constructed to convey water from the Mississippi River through ORLSS at a design flow capacity of 8,495 m³/s (300,000 ft³/s). The inflow channel is 305 m (1,000 ft) wide and includes a 0.5-m (1.5-ft)-thick concrete apron, which extends 30.5 m (100 ft) upstream of the weir axis, and a large, stone riprap wingwall on the left abutment. The outflow channel is 180.5 m (592 ft) wide and includes a stilling basin, which consists of derrick stone, riprap, and a drainage blanket. Revetment, comprised of an articulated concrete mattress, is present along the banks of both inflow and outflow channels. There are three rows of sheet piles located along different areas of the structure. One row is located at the upstream edge of the gate bays down to an elevation of -11 m (-36 ft). Another row is at the upstream edge of the stilling basin down to an elevation of -12.2 m (-40 ft) in the low-flow bays and -8.2 m (-27 ft) in the high-flow bays. The last is at the downstream edge of the stilling basin down to an elevation of -12.8 m (-42 ft) in the low-flow bays and -7.6 m (-25 ft) in the high-flow bays.

A scour hole developed near the left abutment of ORLSS from an eddy current during a flood on the Mississippi River in 1973. Heavy rains along the Mississippi River Valley brought enough water in the flood to inundate 48,562.3 km² (12 million acres) of land (Chin et al. 1975). The peak discharge of the Mississippi River during the flood at Tarbert Landing,

which is approximately 11 km (7 mi) downstream from ORLSS, was 42,418.6 m³/s (1,498,000 ft³/s) at a peak stage of 18.1 m (59.3 ft) on 13 May (USACE 1974). For comparison, the peak streamflow at Baton Rouge was 39,105.6 m³/s (1,381,000 ft³/s) in 1973 while the 2011 discharge was at 40,776.3 m³/s (1,440,000 ft³/s) (USGS 2020). ORLSS had a discharge of 14,045.2 m³/s (496,000 ft³/s) during the flood of 1973 (USACE 1974). At Knox Landing, located 1.6 km (1 mi) downstream from ORLSS on the Mississippi River, the flood of 1973 lasted 95 days above a bank-full stage of 15.5 m (51 ft) (USACE 1974).

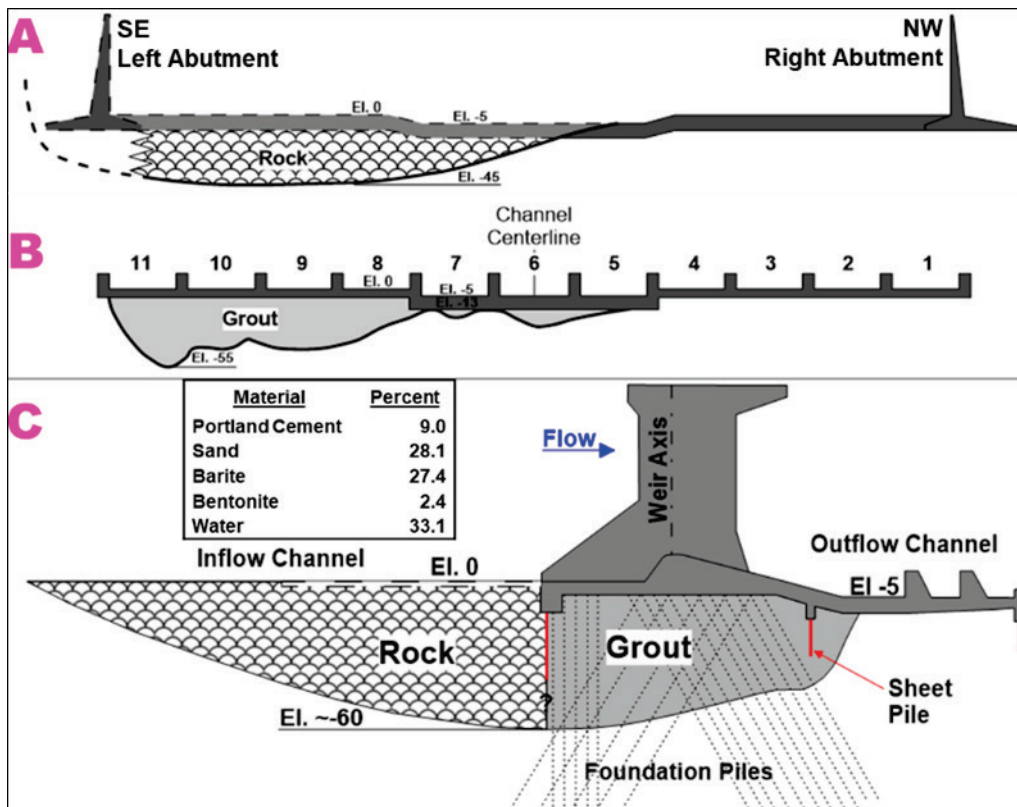
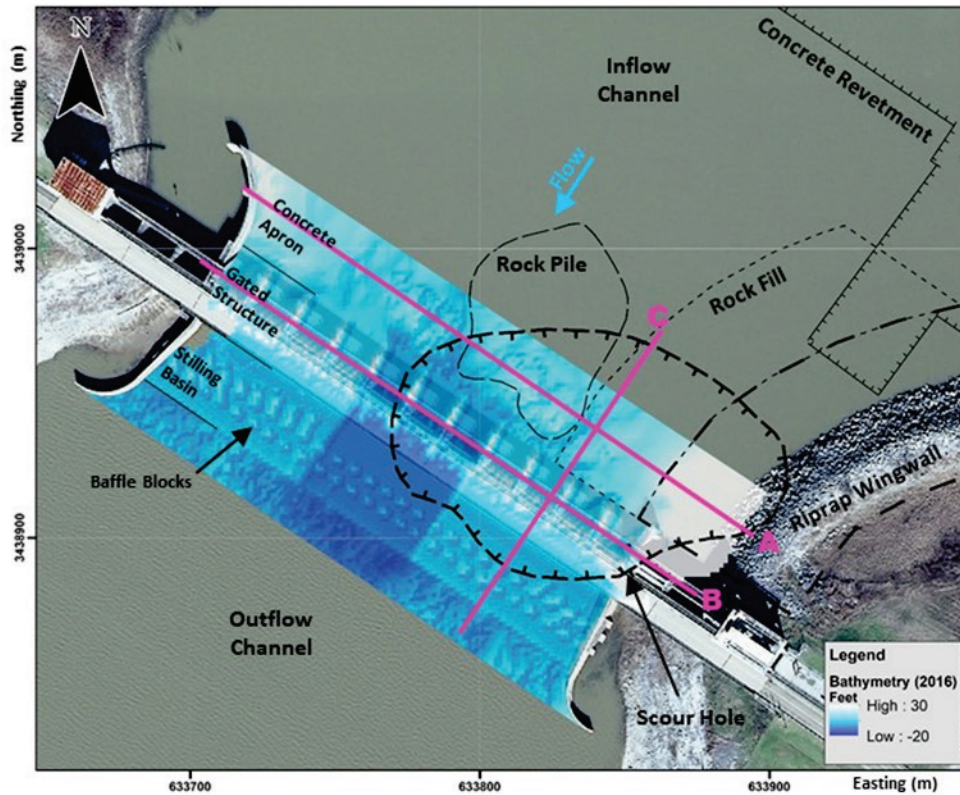
The scour hole that developed during the flood of 1973 resulted in collapse of the left abutment wingwall, partial collapse of the concrete apron, and significant removal of foundation material. Borehole data, range-line measurement, and scaled drawings were used to approximate both the horizontal and vertical extents of the grouted scour hole (information courtesy of MVN; Wilson 1978). The dimensions of the scour hole were estimated to be 91.5 m (300 ft) in diameter and extended vertically down to around -18.3 m (-60 ft) in elevation. These approximations were used to determine the survey geometry for the waterborne geophysical data collection conducted by ERDC. Figure 3 provides an illustrative view of the features of ORLSS described previously, including the area of the scoured foundation.

The emergency remediation efforts performed on ORLSS, following the development of the scour hole, included riprap placement to prevent further scouring and grouting. The rock was temporarily placed in a pile out in the inflow channel and was to be relocated to fill in various gaps created by the scour. This rock was described as type “A” stone with the following specifications: (1) no piece was to exceed 8 tons, (2) no more than 10 percent by weight were to weigh less than 1 ton, and (3) at least 50 percent by weight were to weigh 3 tons or more (information courtesy of MVN). Rock was sourced from quarries located in Kentucky and Missouri. Limited documentation exists that describes the composition of this rock, but it is thought to be mostly limestone, based on the regional geology of the area from where it was sourced. This rock was also to be used to construct the riprap wingwall on the left abutment to replace the collapsed concrete wingwall.

Grouting operations used a self-leveling, highly pumpable grout mixture consisting of sand, bentonite, barite, water, and Portland cement. A

sanded, low-cement content grout mixture was used for most of the remediated scour hole. The material percentages for the bulk-fill grout mixture are provided in the inset table in Figure 3 (cross section C). Two other grout mixtures were used but comprised a smaller portion of the overall remediated scour hole volume. One was a non-sanded, medium-cement content mixture; this slurry mixture would incorporate the muck (siltation) material that had built up at the bottom of the scour hole to prevent dilution of the bulk-fill mixture. The other mixture was a non-sanded, high-cement mixture with a high compressive strength as a capping mix to bond the bulk-fill grout mix to the base of the structure.

Figure 3. Schematic drawings of ORLSS (courtesy of MVN). Elevations are in feet.



1.3.3 Physical site properties

Physical properties of each material at the site are critical, not only for selection of the geophysical methods used for investigation but also for interpretation of the resulting data. The primary materials of ORLSS, each having geophysical responses that are relevant to this survey, are water, various grout mixtures, riprap, river sediment, and the underlying subsurface conditions that have been described previously in this report. The subsurface geology were the primary targets of the 2018 land-based geophysical investigation (Simms et al. 2021) and showed measurable changes in geophysical (seismic and ERT) response.

ERT surveys have been demonstrated as an effective geophysical technique in the evaluation of grouted regions (Komine 2000; Oh 2012). These previous studies indicate that low resistivity is typically associated with grout mixtures and that high resistivity is generally associated with native soils. Oh (2012) indicates that an increasing resistivity would be observed with increasing void space.

The electrical resistivity of cement and grout, an important parameter for interpretation of the ERT data, can vary greatly, depending on relative amounts of each grout mixture component. Electrical grout-monitoring devices were used to measure the differences in electrical response to determine grout levels during the remediation efforts. The calibration observations from these devices (Wilson 1978; Ainsworth 1979) are as follows: 10-in. (full-scale) deflection in air, 5-in. (half-scale) deflection in water, 1-in. deflection in grout, 3- to 4-in. deflection in muck (siltation), and 1.5- to 3-in. deflection in water contaminated with cement. The electrical response is provided in a qualitative sense but provides an indication of the grout's electrical response. Because water is more conductive than air, and the grout's deflection was lower than water, the electrical response of the grout would be very conductive. Wilson (1978) states that check borings, after curing of the grout, indicate an absence of open cavities or muck in the grout. However, no additional observations of the grout's electrical response were noted following emplacement and hardening. It is likely that the grout's electrical properties could have changed following the hardening process. Thus, the electrical resistivity of the grout underlying ORLSS is uncertain in a quantitative sense. Despite this uncertainty, a reasonable assumption is that a relatively low electrical resistivity might be observed from the grouted mass based on the composition of the mixtures. Materials in the grout mixtures known to

have lower resistivities, such as barite, bentonite, and water, constitute approximately 63 percent of the bulk-fill mixture. UngROUTED zones that might occur within the grout would exhibit a higher resistivity in contrast to intact grout. It is likely that these zones would contain either water, river sediments, or other material (not associated with the grout) rather than air. Despite the low likelihood of occurrence, an air-filled void was not discounted during observation and interpretation of the geophysical data. Although check borings indicated an absence of open cavities or muck in the grout (Wilson 1978), borehole data are typically limited spatially and may not detect lateral variability of subsurface features. Table 1 shows some nominal resistivity values for common materials applicable to the site.

The rock that comprises the riprap wingwall will also produce a response in the resistivity data. This could also hold true for the rock pile area in the inflow channel if any rock remains, but it may exhibit a different geophysical signature than the wingwall. The presence of riprap in the scour complicates efforts in the delineation of the grout based on the wide range of resistivities that limestone can exhibit. Additionally, the man-emplaced materials could yield similar resistivities to those of the natural sediments.

Table 1. Nominal electrical resistivity values for common materials (Telford et al. 1990; Johnson et al. 2017).

Materials	Nominal resistivity, Ω -m
Air	$10^9 - 10^{15}$
Limestone	100 - 10,000
Alluvium and sand	10 - 800
Fresh water	10 - 100
Clay	1 - 100
Barite	39.37

1.3.4 Previous geophysical surveys

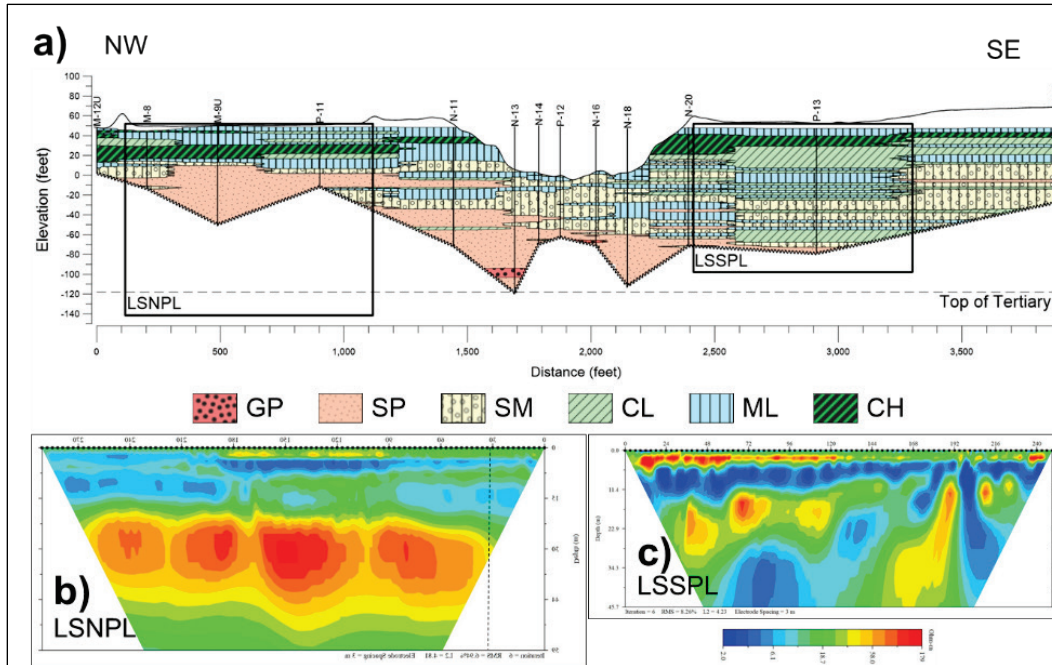
Land-based geophysical surveys using ERT and seismic refraction were previously conducted proximal to both the left and right abutments of ORLSS. Figure 4a illustrates a section view of the horizontal and vertical extents of the land-based resistivity survey measurements along with their relationship with the subsurface geology. These surveys found a subsurface geology that resembles a layered geometry on the right abutment side. The geological layers are clay-rich from backswamp deposits. Conversely,

surveys on the left abutment show more complex features in the subsurface. The resistivity cross section for Line LSNPL, acquired on the right abutment (Figure 4b), shows features that are interpreted as clays with electrical resistivities of about 15 ohm-meters (Ω -m) or less (blues) and sand with electrical resistivities in excess of 50 Ω -m (yellow and red colors). These values may change for sediments underlying the river, as those may have higher fluid content; the electrical properties of the fluids may be different in the two environments. Nonetheless, this provides useful background for interpreting the marine data sets.

The northwest end of line LSSPL (Figure 4c) is proximal to the riprap wingwall and exhibited higher resistivities relative to sands in the deeper subsurface. Drawings from USACE (courtesy of MVN) show that areas of emplaced stone near the left abutment wingwall coincide with the more resistive zones (red colors). Therefore, these results were used to aid in understanding ERT results for emplaced rock and natural subsurface materials in the waterborne ERT surveys. According to the land surveys, the resistivity values for clay range between 2 and 10 Ω -m, for silty sand range between 10 and 30 Ω -m, and for sand range between 30 and >150 Ω -m. During the time of the land-based surveys, the river elevation ranged between 14 and 14.8 m (46.2 and 48.5 ft). Therefore, the land-based data sets represent geophysical responses for saturated conditions in the subsurface. These land-based data should have comparable geophysical resistivity and seismic values to those for natural materials in the marine measurements.

Results of the seismic land surveys conducted in 2018 were complex because of the occurrence of low-velocity layers underlying higher velocity layers and strong lateral velocity contrasts that are presumably associated with transitions in soil type between different depositional environments. It is anticipated that the lateral velocity transitions associated with point bar deposits on the left abutment continued into the pre-scour channel and, at some point in the sediments beneath the pre-scour channel, transitioned into a layered structure typical of the backswamp deposits observed on the right abutment of the channel. Because the structure indicated by the land seismic surveys on the left abutment side is so complex, the interpretation of both seismic and resistivity features in the marine data becomes more difficult to distinguish pre-scour from post-scour effects where both can involve sharp lateral transitions in geophysical properties.

Figure 4. Interpreted ERT sections from land surveys: (a) geologic cross section of ORLSS with outline of ERT profiles, (b) ERT line LSNPL parallel to levee embankment on the upstream side near the right abutment, and (c) LSSPL parallel to levee embankment on upstream side near the left abutment.



2 Geophysical Methods

Multiple geophysical methods are generally deployed to address questions like those of concern at ORLSS usually for two reasons. First, different methods can define different physical properties of the materials of concern and by comparing these properties, a better interpretation can be reached. This is exemplified in the land-based seismic and resistivity data that were acquired at ORLSS. Second, because the physical properties in the area of concern are not fully known, geophysicists cannot be certain as to which method will provide the most useful information. By deploying multiple methods, there is a higher likelihood that the geophysical survey will be as effective as possible.

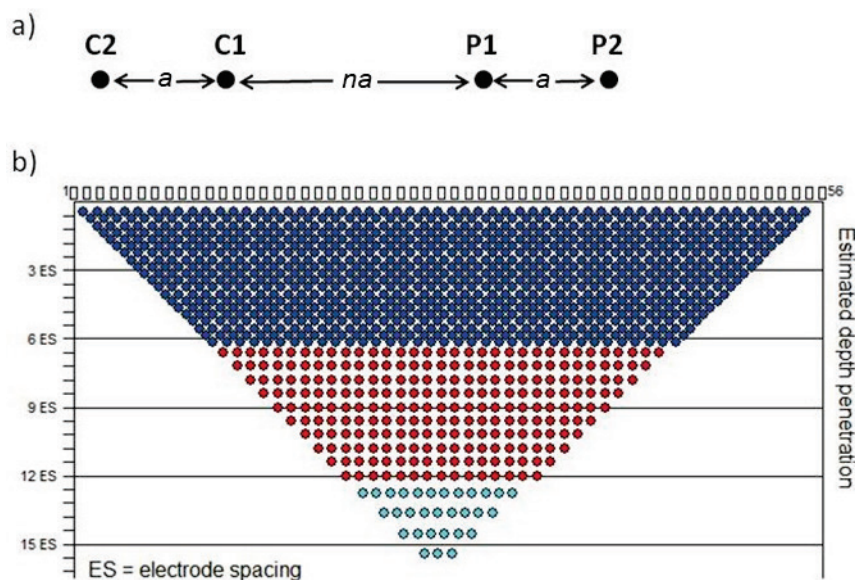
2.1 Electrical resistivity tomography (ERT)

An ERT survey measures how well electrical current flows through the subsurface. An ERT survey is typically conducted by using a linear array of electrodes in contact with a known surface. A current is injected through a pair of electrodes (C1 and C2) that is transmitted into the subsurface where the potential difference, or voltage, is measured between a pair of potential electrodes (P1 and P2). Between the C1 and C2 electrodes, the injected current flows in a hemispherical pattern that will increase in radius with increasing spacing between the potential and current electrodes. The apparent resistivity, in ohm-meters ($\Omega\text{-m}$), can be computed by knowing the current injected into the ground, the electrode geometry, and the measured potential difference. The apparent resistivity data are used to construct a subsurface resistivity distribution that most closely correlates with the subsurface geology through a computational process known as inversion. The inversion method determines the best estimates for computed apparent resistivity values from the measured apparent resistivity values.

Resistivity is the inverse of conductivity and is a property of subsurface materials that can vary by several orders of magnitude. Some of the major factors that influence measured resistivity values are material type, porosity, water content, water salinity, and temperature. In general, unconsolidated material, such as soil, will be less resistive than rock, and clays will be less resistive than sand. Porous material will exhibit a higher resistivity if the void space contains air. The inclusion of water in pore spaces will cause a lower resistivity relative to the material's unsaturated bulk resistivity.

The waterborne survey used merged electrode configurations that consisted of dipole-dipole and strong gradient electrode configurations. The dipole-dipole configuration, shown in Figure 5a, uses four electrodes linearly arranged to acquire a single measurement, with the two current electrodes (left side) and two potential electrodes (right side) equally spaced, a , but separated by a multiple, na , of the current (or potential) electrode spacing. By increasing the spacing between the current and the potential electrode pairs and/or the two current (potential) electrodes, both lateral and vertical information about the subsurface is obtained. In this manner, it is possible to obtain a 2-D profile image of the subsurface. Because of the nature of measurements using an increasing electrode spacing, the number of measurements at depth decreases as the electrode spacing increases. Thus, the subsurface area imaged is similar to that of an inverted triangle. The dots in Figure 5b show pseudo-depth locations of resistivity measurements for given electrode spacings. The dipole-dipole electrode configuration was supplemented with additional measurements from a strong gradient array, which uses two current electrodes at both ends of the potential electrodes to collect measurements. The strong gradient configuration produces a strong signal that is suited for conductive environments.

Figure 5. Idealized diagram of a dipole-dipole electrical resistivity configuration. (a) By using different values for a and n , 2-D coverage of the subsurface is obtained (b). In (b), the rectangles along the surface represent electrodes (in this example there are 56), and the dots in the subsurface represent the pseudo-location of a measurement. For a given number of electrodes, and as the electrode spacing increases, the number of measurements at depth decreases.

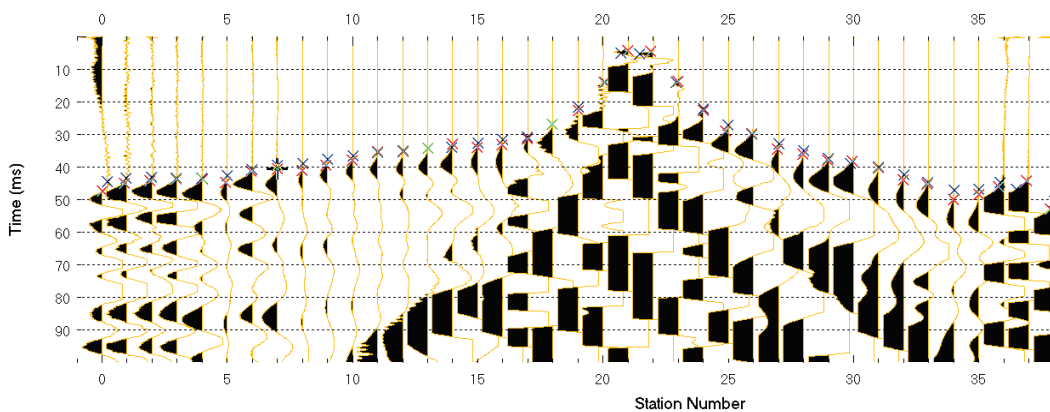


2.2 Seismic refraction and reflection

There are several seismic methods that can be used for shallow site characterization, from which a selection is made based on the problem of interest, depth range, and geologic properties of the site. The limitations for marine seismic surveys are typically greater than for land-based surveys in procedural options, acquisition, and positional accuracy. In addition, the contrast in physical properties of the targets can be difficult to anticipate. Marine data acquisition uses hydrophones (instead of geophones, which are used for land-based operations) that are deployed on a cable with fixed separation and towed behind a boat. There are several options for use as a source of seismic energy, with an airgun being one of the most common. In an airgun, a pneumatic chamber is pressurized with compressed air from scuba tanks. When fired, a solenoid is triggered that releases air into a firing chamber, which in turn causes a piston to move, producing a pulse of acoustic (i.e., seismic) energy underwater.

Seismic refraction methods involve analysis of the travel times from a seismic energy source to each sensor (hydrophone) in a linear array. Collection of seismic measurements at a series of source separations within the hydrophone array enables a cross-sectional image of seismic velocities to be produced for a vertical plane beneath the geophone array. The first step in seismic refraction analysis is to measure the travel times for every source “shot point” and every sensor position for those shot points (Figure 6). In marine deployments, seismic refraction acquisition and processing are designed to determine only the seismic P-wave velocities. A marine seismic survey requires the hydrophone array to be deployed at a certain offset distance from the source, which is dictated by the water depth and desired depth of investigation. Greater offset distances result in deeper depths of investigation but at the expense of resolution. After measuring the travel times, various analysis methods are available, ranging from methods that determine layered model solutions to “tomographic” solutions that allow more lateral variation in the seismic velocities. These velocities are characteristic of certain rocks or soils and vary depending on the distribution of rock and soil units in the subsurface. When seismic and resistivity cross sections are compared, the changes in rock or soil types can often be determined with greater confidence.

Figure 6. Idealized diagram of travel times of first-arriving seismic waves indicated by “x” in the top portion of the figure that can be compiled for all shot points.



Seismic reflection methods, if conducted as the primary goal of a survey, require a different acquisition procedure than seismic refraction methods. In general, the goal of seismic reflection analysis is to enhance seismic waves that reflect from sub-horizontal layers beneath the survey lines, associated with changes in the lithologic makeup of the layers. If the travel times for waves at small source-receiver separation are consistent with (but not equal to) travel times for waves at larger source-receiver separations from the same interface, the data can be processed in such a way that, after corrections for offset, the two can be overlain so as to enhance reflected waves and mask energy that is not reflected. A processed seismic reflection section can yield a cross section that maps lithologic interfaces beneath the survey line. Seismic reflections, if observed in a seismic refraction data set, can be analyzed and yield useful information about subsurface lithologic interfaces.

3 Field Operations

Waterborne geophysical data were collected on both the inflow and outflow channels of ORLSS between 2 and 11 December 2019. The resistivity data were acquired 2-6 December, and the seismic data were acquired 9-11 December. Data were acquired using two 18-ft SeaArk boats (Figure 7) operated by ORCC personnel. The primary boat housed the geophysical equipment and geophysical crew, and the secondary boat was used to assist in positioning and aligning the cables. Both boats were used to position each resistivity survey line as stationary as possible during the data collection (approximately 10 min per line). The seismic survey was conducted by using one boat to tow the hydrophone array in a predetermined grid.

Figure 7. SeaArk boat used for data acquisition at ORLSS.



3.1 Weather conditions

During the resistivity data collection, weather patterns were favorable but during the seismic data collection, the weather was less favorable with conditions including rain and wind. Climatic conditions during data collection are provided in Table 2 based on weather data acquired from the National Climatic Data Center (NCDC) of the National Oceanic and Atmospheric Administration (NOAA) weather station located at the Baton Rouge Metro Airport (-91.1469° , 30.5372°).

Little to no precipitation occurred during the resistivity data acquisition. Rainfall can influence the conductivity of the water and thus the resistivity survey results. Wind speeds and direction influence

the water current direction, which can cause relatively more curvilinear survey lines. However, this was mitigated through the use of two boats to keep tension on the resistivity cable and to maintain straight and consistent line bearing, to the extent possible.

Weather conditions can also affect seismic data. Wind can lower the accuracy with which the boat and tow cable can maintain position along a line. Both wind and rain can contribute to an increase in noise levels on the hydrophones, although this can generally be overcome by using a more powerful seismic source.

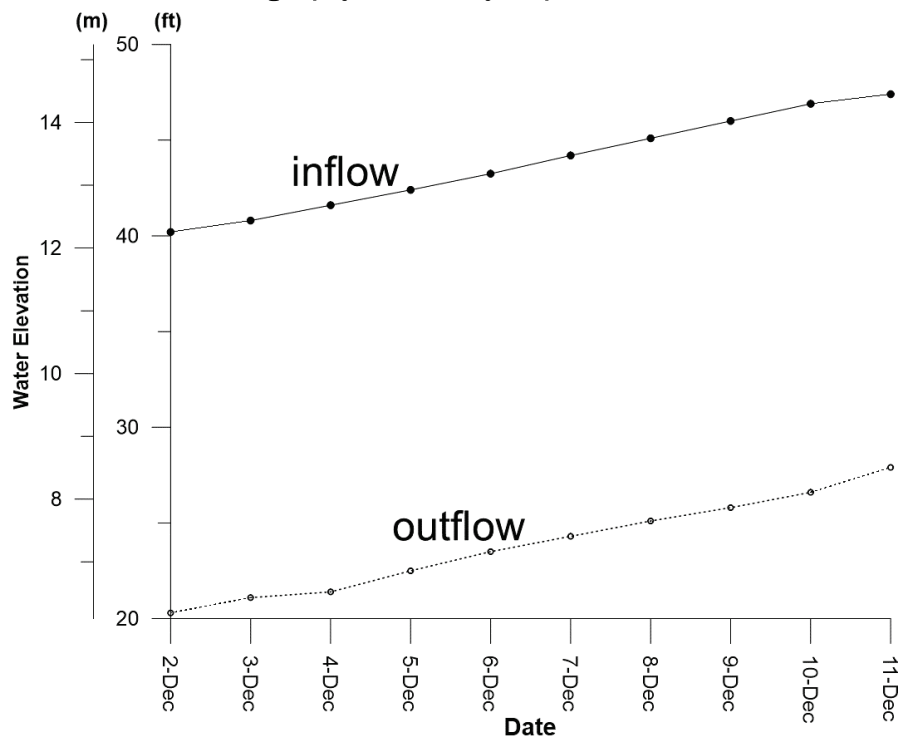
Table 2. Weather conditions during data collection period (NOAA 2019).

Day	Rainfall (in.)	Wind speed (mph)				
		Max	Avg	Azimuthal Wind Direction	Max Gust Speed	Azimuthal Gust Direction
2-Dec.	0	15	6.4	360	24	310
3-Dec.	0	12	2.6	220	13	220
4-Dec.	0	9	1.8	350	13	30
5-Dec.	0	15	5.8	150	19	140
6-Dec.	0.01	17	6.4	240	22	250
7-Dec.	0	15	6.9	20	20	10
8-Dec.	0	9	4.3	140	12	150
9-Dec.	0.01	23	10.2	220	31	210
10-Dec.	1.54	22	12.3	20	32	10
11-Dec.	0	20	10.8	20	26	30

3.2 River elevation and bathymetry

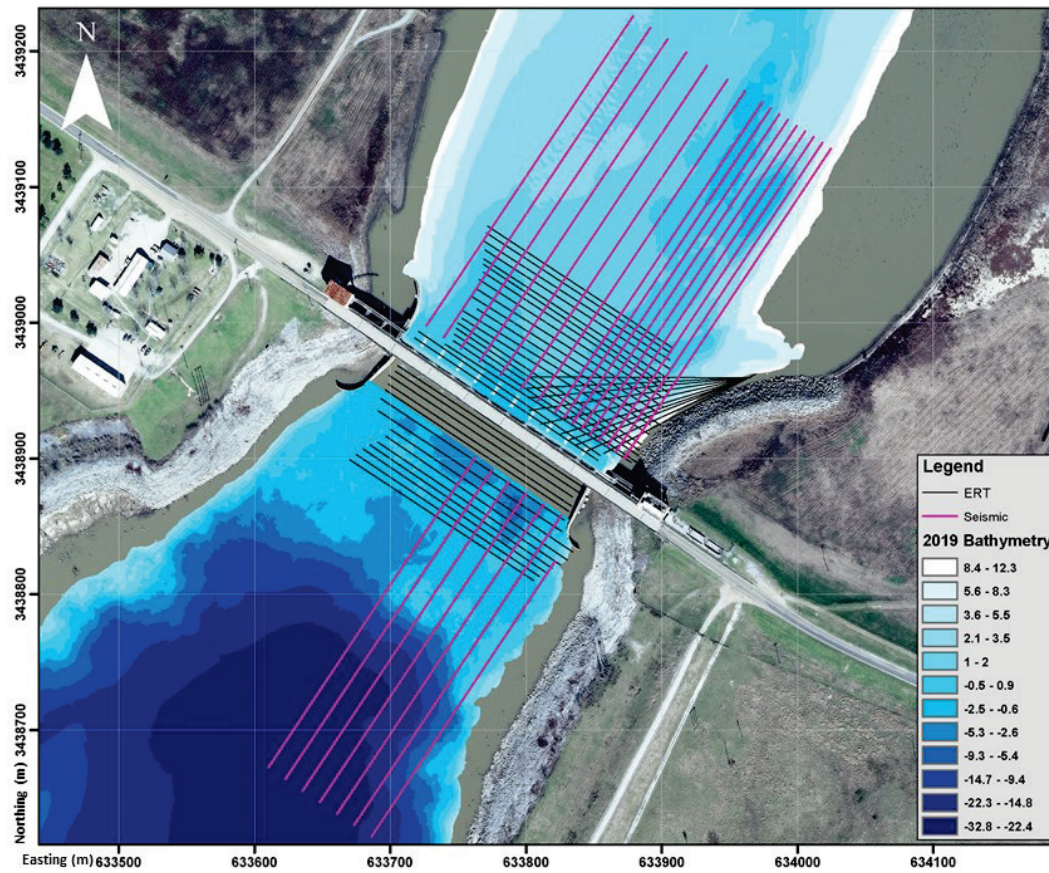
River elevations of both inflow and outflow channels were acquired from the daily readings provided by the ORLSS project office. Figure 8 provides the water elevations, with respect to mean sea level (MSL), of both inflow and outflow channels during the time of the waterborne geophysical collection. Water elevation in the inflow channel ranged between 12.3 and 14.4 m (40.2 and 47.4 ft). Water elevation in the outflow channel ranged between 6.2 and 8.5 m (20.3 and 27.9 ft).

Figure 8. Plot of river elevation, in meters and feet, during the waterborne geophysical survey acquisition.



A bathymetry survey conducted in December 2019 (Figure 9) shows that the inflow channel gradually deepens from a bathymetric elevation of about +12.2 m (+40 ft) along the shore to about 0 to +2 m (0 to +6.6 ft) near the center of the channel and adjacent to the structure. The bathymetry of the outflow channel shows steeper slopes along the shoreline that deepen to about 2 to 5 m (6.6 to 16.4 ft) in elevation proximal to the stilling basin. About 152.4 m (500 ft) downstream from the structure, the outflow channel deepens sharply to about -30 m (-100 ft) below MSL. The bathymetric data on both the inflow and outflow channels of ORLSS were used to determine the depth of the water column during the data collection with respect to the corresponding channel gage readings (Figure 8).

Figure 9. Bathymetry of the site, in meters with respect to MSL, from December 2019 (provided by MVN) and location of geophysical survey lines. Seismic lines are shown in red, and resistivity lines are in black.



4 Data Acquisition and Processing

4.1 Electrical resistivity data acquisition and processing

Electrical resistivity (ER) data were acquired by using a SuperSting™ (SS) R8 control unit and electrode switch box, manufactured by Advanced Geosciences Inc. (AGI) and powered by two 12-V deep-cycle marine batteries. This is an eight-channel system, meaning eight readings (i.e., potential electrode pairs) are acquired simultaneously while a current is applied to two other electrodes. A single marine cable layout with 28 electrodes spaced at 6 m (19.7 ft) was used, giving a total line length of 162 m (534.6 feet). The cable has a 50 m (164 ft) lead-in to allow sufficient distance between the boat and the first electrode to avoid interference. The control unit is pre-programmed to acquire data with several combinations of electrodes within the 28-electrode array, in such a way that both dipole-dipole and strong gradient data sets are acquired. Measurement time to acquire a single survey line was approximately 10 min, which does not include time to position the electrode cable. The SS system was operated in “boost mode,” which uses a second 12-V battery that enables the instrument to acquire data at a higher signal-to-noise ratio. Based on the general assumption that the depth of investigation for ERT data is approximately 20 percent of the electrode spread length, which in this case is 162 m (531.5 ft), the estimated depth of investigation would be 32 m (107 ft). The minimum size of a target detectable by an ERT survey is typically less than half the electrode spacing, which in this case is 3 m (9.9 ft). Targets that are small and deep cannot be as easily detected as shallower, larger targets. The rule of thumb is that the target cannot be detected if its size is less than a quarter of its depth.

Two Trimble GeoXH 6000s, one of which has centimeter precision, were used to collect Global Positioning Satellite (GPS) data at each end of the resistivity cable during the data collection. High-visibility electrical tape was used to mark distance measurements on the resistivity cable, and these were used to determine the positions of both the first and last electrodes on the cable. Additionally, the azimuthal bearing of each survey line was taken with a compass. These measurement data were used conjunctively to calculate both the start and end points of each survey line, following postprocessing of GPS data. Equipment used for resistivity data acquisition, as described above, is shown in Figure 10.

The resistivity data were processed by using EarthImager 2-D resistivity inversion software. Prior to inversion, the processing steps included removing noisy data (i.e., negative resistivity values and spikes), selecting the number of iterations, and setting error reduction boundaries and root mean square (RMS) error thresholds. The inversion output is a 2-D color plot of resistivity with respect to depth. A blue-to-red color scale is used for the 2-D profiles that represent lower to higher resistivity values, respectively. Not all profiles are presented at the same color scale; therefore, it is important to observe the magnitudes on the scale bar rather than looking only at the high and low colors.

Figure 10. SuperSting R8/IP system, GPS, and cable used in ERT data acquisition.



4.2 Seismic data acquisition and processing

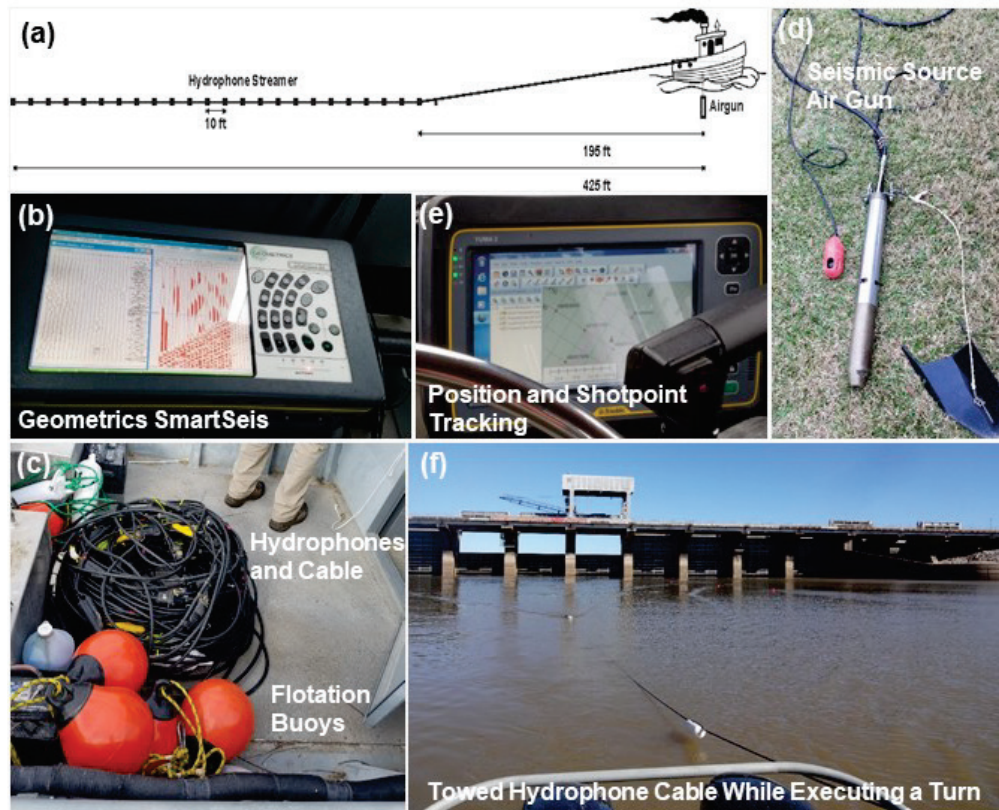
The hydrophone streamer consisted of 24 Geospace MP-25 10-Hz hydrophones spaced 3 m (10 ft) apart. Seismic data were acquired using a

shot offset (distance between seismic source and closest hydrophone) of 59.5 m (195 ft) for a total streamer length of 129.6 m (425 ft) (Figure 11a). Seismic refraction data were recorded with a Geometrics Smartseis ST seismograph (Figure 11b) connected to the 24-channel hydrophone streamer (Figure 11c). The hydrophone streamer was towed behind the boat approximately 0.9 m (3 ft) below the water surface. The seismic source was a Bolt airgun (Figure 11d) with a 327.7 cm³ (20 in³) chamber pressurized to 10.3 MPa (1,500 psi). The airgun was mounted on the port side of the boat and towed at a depth of approximately 0.9 m (3 ft) below the water surface.

During acquisition, a computer tablet with GlobalMapper software was used to track the position of the boat to aid the boat pilot in steering along each survey line and to indicate shot locations (Figure 11e). Positional coordinates were provided by a Hemisphere AtlasLink differential GPS with submeter accuracy. The boat position and hydrophone cable position deviated from the planned survey line locations due to wind and current by an estimated average error of ± 6 m (± 20 ft). Because the cable was towed a fixed distance behind the boat, the distance between the airgun and the closest hydrophone was constant.

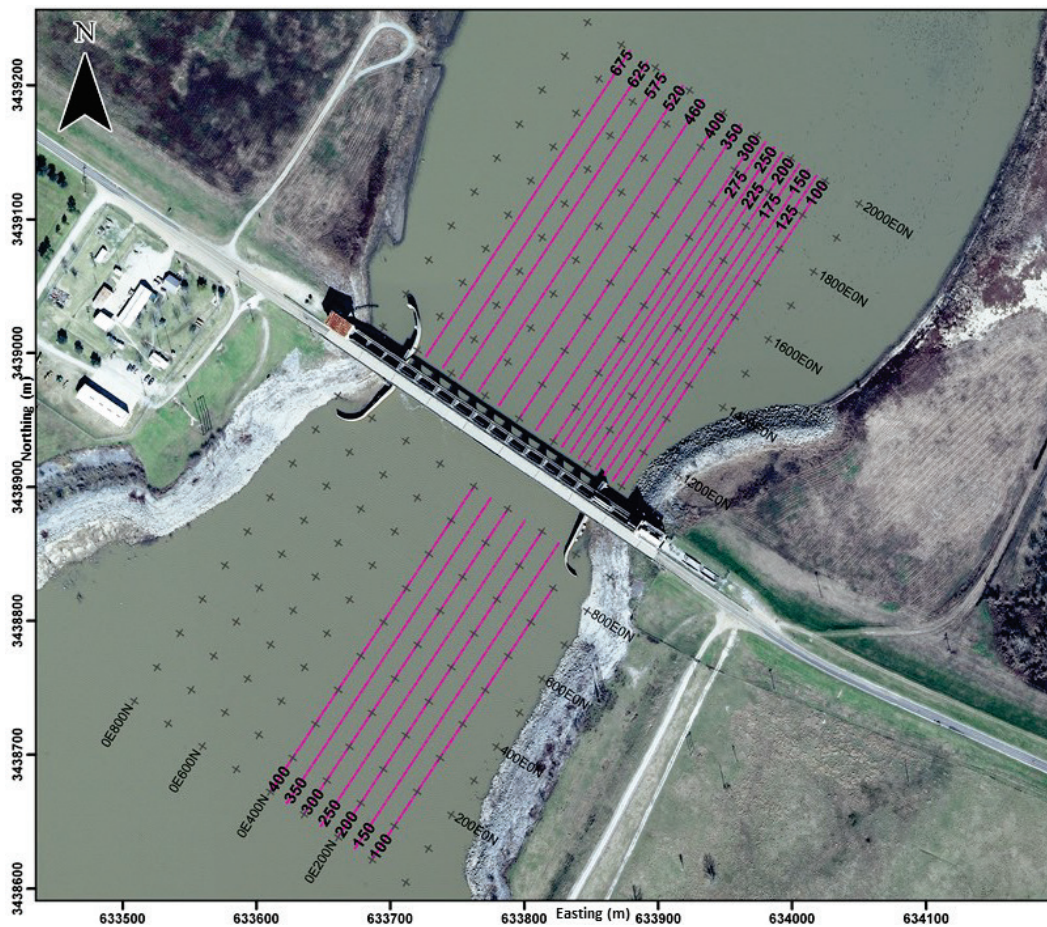
When the end of a line was reached, the boat would turn around in the area outside of the survey area (when at the end of the grid farthest from the structure) or as efficiently as possible (when close to ORLSS) and would begin acquiring data on the adjacent line once the hydrophone cable was relatively straight (Figure 11f). Thus, when the boat was outbound, data acquisition would begin when the boat was about 152 m (500 ft) from ORLSS and, when inbound, the last shot would be acquired when the boat was within about 15 m (50 ft) of the structure. Two passes in opposite directions were made along each survey line to provide both forward and reverse shot points for the refraction analysis.

Figure 11. Equipment used for seismic survey acquisition: (a) seismic data acquisition configuration, (b) Geometrics SmartSeis used for data recording, (c) hydrophones and cable attached to flotation buoys, (d) airgun used as the seismic source with a control fin and hydrophone, (e) tracking system used to maintain acquisition geometry of prescribed survey layout, and (f) hydrophone cable being towed behind the boat (white floats) after making a turn near the structure. Orange floats on the cable that have not yet turned and are still moving toward the structure can be seen closer to the structure.



Shots were acquired at 30.5-m (100-ft) intervals along prescribed survey lines (Figure 12) as the boat moved down the survey lines at a speed of approximately 3.7 to 5.6 km/h (2.3 to 3.5 mph). The data were sampled at a rate of 0.125 ms with a maximum range of 200 ms.

Figure 12. Marine seismic refraction survey navigation plan and acquired survey lines (magenta).

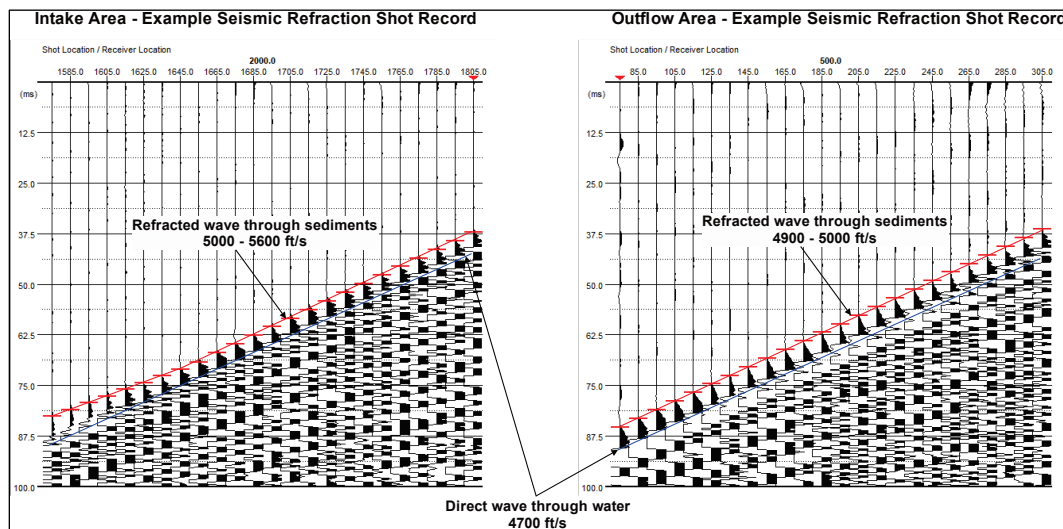


Because the seismic wave must travel through the water column before reaching the bottom sediments and because the seismic waves from the bottom sediment are not recorded as “first arrivals” for hydrophones that are within 76.2 m (250 ft) of the shot point, it is not possible for seismic refraction analysis to image the sub-bottom within 76.2-91.5 m (250-300 ft) of the ends of the lines. This is explained in greater detail in Appendix B. It significantly reduces the portion of the scoured area that can be imaged with seismic refraction methods.

The seismic data files were organized by line number into separate directories for seismic refraction analysis. The files were imported into Geogiga DWTOMO v9.15 software. The shot and hydrophone geometries were entered for each line, and the shot records were individually analyzed for first arriving energy (direct or refracted). A frequency bandpass filter of 100-800 Hz was applied to the data. Seismic data quality exhibited coherent first arrivals in each shot record, as indicated by the examples

provided in Figure 13. The travel-time of the first arriving energy was manually picked and saved in the Geogiga ASCII file for each survey line. The direct P-wave through the water column is evident as a higher-frequency signal with a constant velocity of 1,433 m/s (4,700 ft/s) (Figure 13). Refracted P-waves through the bottom sediments have slightly higher P-wave velocities ranging between 1,463 and 2,012 m/s (4,800 and 6,600 ft/s), with an average velocity of 1,615 m/s (5,300 ft/s).

Figure 13. Example seismic shot records and travel-time picks for both inflow and outflow channels.



The seismic data were processed for seismic reflections by using the Geogiga Reflector module of the Geogiga package, version 9.0. The data were first frequency filtered by using a bandwidth of 50-800 Hz. Next, a semblance utility was used to assess stacking velocities, which were consistent with the velocities measured in the refraction analysis, about 1,463 m/s (4,800 ft/s). A normal moveout correction was then applied to each shot gather. This corrects for the lateral component of source-receiver separation so that reflections will appear flat-lying if the proper velocity is used and if the interface from which they are reflecting is horizontal and flat. Corrections are made for the lateral components of the raypath for each source/receiver pair (“normal moveout” or NMO) so that corrected traces provide a one-dimensional reflection response beneath the selected midpoint. The number of data traces from source/receiver pairs that are combined for a midpoint is referred to as the “fold.” A seismic reflection cross section is formed by aligning the stacked traces for a sequence of midpoints. Normally, seismic reflection sections will have a fold of at least 8

and sometimes as many as 48 traces for each midpoint. A more complete description of the seismic reflection profiling is provided in Appendix B.

The seismic data at ORLSS were acquired by using standard seismic refraction procedures, which are different from seismic reflection acquisition procedures. Because of this, only low-fold seismic reflection cross sections could be produced. The seismic-reflection cross sections at ORLSS have a fold of 1 or 2, meaning non-reflected waves are retained in the cross section and can confuse the interpretation if not properly recognized. Thus, it is important to use caution so that non-reflected waves are not misinterpreted as reflections. Despite this, because reflections could be seen in the raw data, they might provide additional information about ORLSS, so it was appropriate to perform seismic reflection analysis. A benefit of seismic reflection analysis is that, because of the geometry of the seismic reflection technique, it can image features that are within about 30.5 m (100 ft) of the end of the line (i.e., halfway between the shotpoint and nearest hydrophone).

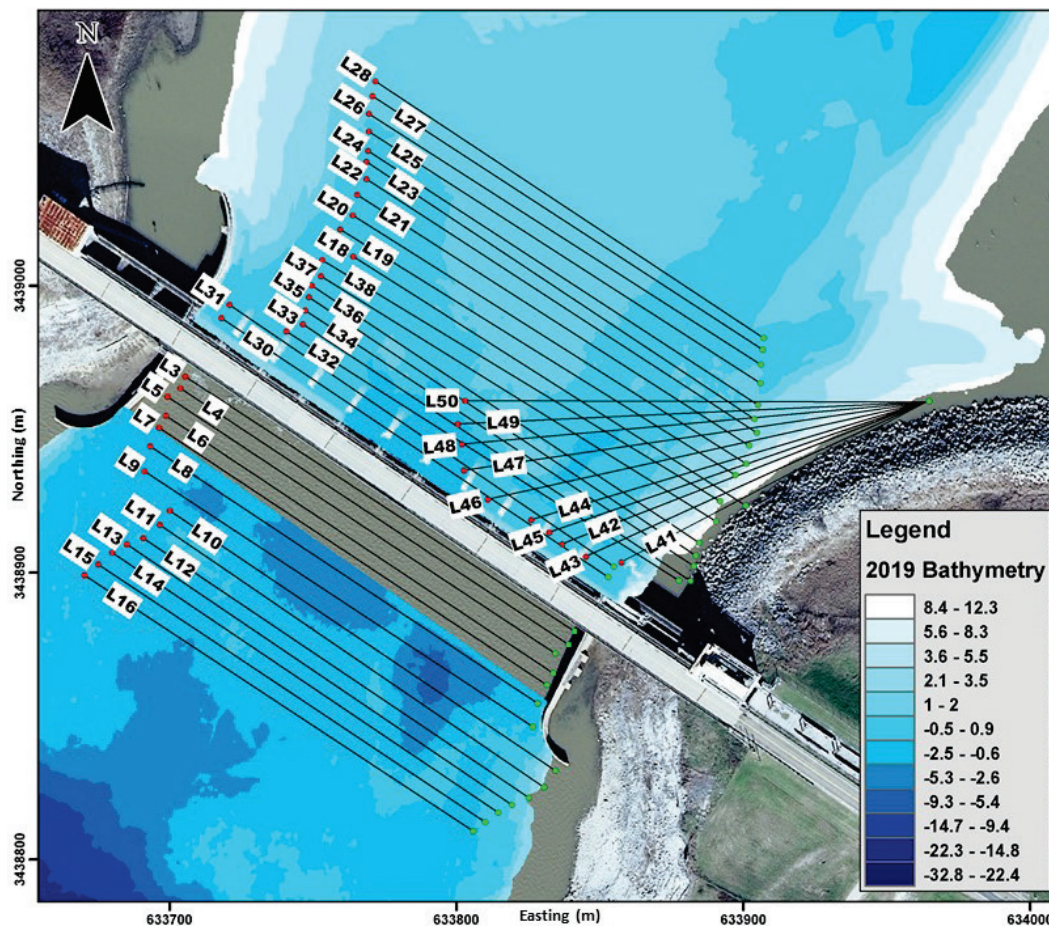
5 Results and Observations

In this report, depth refers to the linear vertical distance from a reference point, which in this case is the water surface. It is important to note that all profiles provided in this report are represented vertically in depth with 0 corresponding to the water-surface elevation at the time of data collection. In this report, elevation refers to the vertical measurement with respect to the MSL datum. The profiles are presented in depth rather than elevation because of the variance in the water-surface elevation, as seen in Figure 8. An elevation-to-depth conversion was applied to the bathymetric data and estimated scour hole vertical extents during the interpretation process.

5.1 Resistivity

ERT data were acquired along 44 lines, including 30 on the inflow side (Lines 18-28, 30-38, and 41-50) and 14 on the outflow side (Lines 3-16). Of the 30 ERT lines that were collected on the inflow side, 20 (Lines 18-28 and 30-38) were aligned parallel to the weir axis of ORLSS and are nominally parallel to one another. The remaining 10 lines (Lines 41-50) on the inflow side were part of a “fan” configuration and were acquired with one boat that maintained a nearly stationary position while the other boat moved from one gate to another along ORLSS. In this manner, both boats could maintain position throughout the data acquisition period, and a stable line could be acquired. Some survey lines had minor curvature during periods of moderate to high winds despite efforts to maintain a straight cable. However, errors induced by these variables are considered negligible based on maximum deviations from parallel of about 5 m (16.4 ft). The locations of the 44 ERT lines are shown in Figure 14.

Figure 14. Resistivity lines with bathymetric map (m, MSL). Green and red points indicate the start and end electrodes, respectively, for each line.



Initially, data were collected by using an SS R8 console connected to a single 12-V deep-cycle marine battery. Inspection of the data revealed lower signal-to-noise ratios at greater depths. To improve data quality, a second SS R8 console that had “boost mode” capability (to provide higher signal-to-noise performance for deep measurements) was used beginning with Line 20, and Line 20 data were acquired with both consoles (i.e., one with and one without “boost mode”). Both data sets for Line 20 were processed, and both showed RMS errors of less than 5 percent. The percent difference of the measured resistivity values between both processed versions of Line 20 was less than 5 percent. This indicates that the ERT data collected with and without boost mode are comparable and that boost mode was not necessary for acquiring high quality data at ORLSS. This result confirms that Lines 1-19, which were acquired without boost mode, are valid and that it was not necessary to repeat the measurements to achieve high data quality. The boost mode data console was used for Lines 21-50 as a preventive measure.

The inversion procedure for the majority of the ERT lines yielded RMS errors less than 5 percent. However, the presence of the reinforced concrete slabs and monoliths generated noise in the resistivity data when the array was within about 10 m (32.8 ft) of the structure. The inversion procedure was modified slightly for ERT lines L30, L31, L2, and L3, which were acquired closest to ORLSS on both inflow and outflow sides. The noisy data were removed to mitigate its effect on the ERT inversion results to produce more reliable sections. Despite the revised inversion parameters, Line 2 remained too noisy to be reliably included in the final data set. The depth of investigation varied from line to line but was generally about 30 to 35 m (98.4 to 114.8 ft), as expected.

ERT profiles are presented with a horizontal axis at the top in distance (m) and both left and right axes that indicate depth (m). ERT profiles from the inflow and outflow parallel layout are oriented in a southeast–northwest, or left abutment–right abutment, direction from left to right. The ERT profiles from the fan layout are oriented in a northeast-southwest direction from left to right. All ERT profiles are provided in Appendix A. The ERT profiles in Appendix A acquired in both the inflow and outflow channels are presented in sequence of distance from the weir axis of ORLSS. The ERT profiles from the fan layout in Appendix A are shown in sequence of the 28th electrode position (end of line) from the left abutment toward (but not reaching) the right abutment.

The following narrative describes the observations that were made based on the inversion results of the ERT data. Selected ERT profiles from the inflow, “fan,” and outflow data sets are presented in the body of this report, but the discussion also refers to ERT profiles that are given only in Appendix A. The ERT profiles presented in the body of this report have been annotated and provide the channel bottom, based on bathymetry, and represented by a dashed line for reference. Note that a truncation occurs in the dashed line, representing the channel bottom, because it is outside the data extents of the 2019 bathymetry.

5.2 Inflow parallel lines

The ERT profiles from the inflow channel, parallel to the weir axis of ORLSS, are represented by a blue-green-yellow-red linear color scale, in order from lower to higher resistivity. It is important to note that the line numbers are not sequential moving upstream from the structure. Lines L18-L28 were first acquired with L18 starting at the upstream end of the

right abutment wingwall with line numbers that sequentially progress with distance from ORLSS (L28 farthest up channel). Lines L30-L38 were acquired starting immediately adjacent to the concrete monoliths with line numbers that sequentially progress to the upstream end of the right abutment wingwall where Line L18 was positioned. Figure 15 shows the inversion results for lines L30, L18, L21, and L28. Water elevations during the time of this survey were at 12.7 m (41.6 ft) for lines L18-L28 and 12.9 m (42.4 ft) for lines L30-L38.

In general, resistivity values in these sections ranged between 1 and around 100 Ω -m, except for L30, as it exceeds 1,000 Ω -m. A relatively conductive layer (20 to 40 Ω -m) in the upper portions of the sections, that is typically 8 to 14 m (26.2 to 46 ft) thick, corresponds to the water column. Beneath the water column (subsurface materials), resistivity values vary from section to section.

L30, which was acquired closest to ORLSS, shows areas of high resistivity (200 to >1,000 Ω -m) with a lobate geometry that is coincident with the concrete monoliths. These lobate, resistive features do not persist in sections farther from the structure. The resistivity decreases rapidly to less than 5 Ω -m at a depth of 7 m (23 ft), which is likely caused by the steel in the structure.

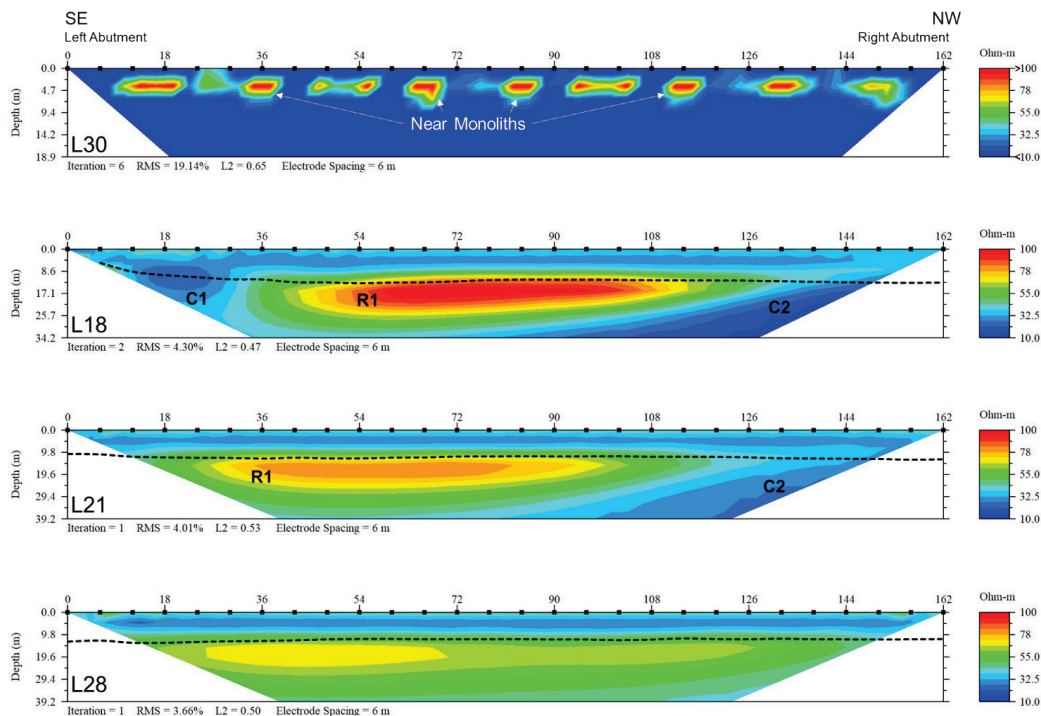
Discontinuous areas of higher resistivity (~200 Ω -m) are observed near positions 18 and 150 m in ERT lines L31 through L33 (Appendix A). This is likely caused by proximity to the left abutment riprap wingwall and the monolith. Lower resistivity values are observed beneath the channel bottom. The interface between the higher and lower resistivities exhibits a relatively planar geometry with the higher resistivity layer extending deeper progressively away from the structure.

An anomalous area of higher resistivity (feature R1) is observed in L18 (Figure 15) beneath the channel bottom between positions 54 and 108 m. ERT profiles near L18 toward ORLSS (L36 to L38, Appendix A) show a progressive increase in resistivity from 75 Ω -m to around 100 Ω -m that is coincident with the position of R1 in L18. This area of higher resistivity persists up channel through lines L36 to L21 and varies in lateral extent across each line between positions 36 to 108 m. This feature exhibits a decrease in resistivity and size at L21 and continues to decrease in resistivity and size with distance from the structure progressing towards L28.

An area of lower resistivity is observed at the eastern flank of the feature R1. This feature, annotated as C1, is most apparent on L18 between positions 12 and 30 m (Figure 15). It can also partially be seen on profiles L37, L38, and L19 (Appendix A).

The western portions of lines L37-L38 and L18-L23, approximately between positions 102 to 150 m, show areas of lower resistivity at a depth of 15 to 30 m (49.2 to 98.4 ft). This area of low resistivity, labeled C2, trends deeper eastward.

Figure 15. ERT profiles acquired in the inflow channel parallel to the weir axis. Dashed line represents the channel bottom.



5.3 Inflow fan lines

Additional ERT profiles from the inflow channel were collected in a “fan” layout to acquire ERT data more nearly perpendicular to ORLSS (Figure 14). Resistivity values from the inverted profiles are represented by a blue-green-yellow-red linear color scale, in order from lower to higher resistivity. From left to right, each line is orientated relatively northeast to southwest, or the edge of the riprap wingwall to a gate bay. Line numbers progress from L41, L43, L42, L45, L44, L46, L47, L48, L49, and L50 starting at gate 11 and proceeding to gate 7. Figure 16 provides ERT lines L41, L42, L44, and L49. Inflow water elevation at

the time of the fan survey was 13.2 m (43.25 ft). In general, the subsurface resistivity structure of the ERT profiles from the fan layout exhibit relatively high resistivities between 80 and 150 Ω -m that are more concentrated to the northeast (toward the riprap wingwall). The high resistivity is caused by influence of the riprap wingwall and decreases with distance from the riprap. Discontinuous areas of lower resistivity (\sim 30 to 40 Ω -m) are present to the southwest.

L41 shows an area of high resistivity (100 to 150 Ω -m) between positions 0 and 84 m (feature R2). The top of this feature (L41) is encountered near the water surface, which deepens to a depth of 3.7 m (12.1 ft) near position 84 m. The lateral extent of the resistive response from feature R2 gradually decreases from L41 to L50 (Figure 16 and Appendix A). The character of the resistive area of R2 appears to deepen with distance from position 0 m at the interface with the water column as profiles rotate away from gate 11.

On L42 (Figure 16), an area of lower resistivity (\sim 30–40 Ω -m) is encountered beneath the channel bottom. This feature is noted as C1 (likely corresponding to C1 as seen in the ERT profiles parallel to ORLSS) and is present on multiple ERT sections (L42, L45, L44, and L46) approximately between positions 78 and 126 m. The feature persists beneath the channel bottom to a depth of 30 to 35 m (98.4 to 114.8 ft) on L45 and L44. Somewhere between L46 and L47, feature C1 appears to decrease in vertical extent.

Between L47 and L50 (Figure 16 and Appendix A), approximately between positions 108 and 150 m, there is a progressive increase in resistivity between depths 9 and 21 m labeled as R1 (likely corresponding to R1 as seen in the ERT profiles parallel to ORLSS). This lateral increase in resistivity is coincident with the intersection of the estimated boundaries of the scoured area and rock pile in the forebay.

Figure 17 provides two three-dimensional (3-D) fence diagrams of select ERT profiles, showing one view looking north-northeast (left) and the other looking north (right). This figure illustrates the continuity of the features described above and their relationship with the rock pile, stone fill (i.e., rock fill) and the scour boundary. R1 progressively diminishes in resistivity once outside the boundary of the rock pile and with distance in the inflow channel from ORLSS. The conductive feature C1 is encountered within the estimated boundary of the scour hole, but resistive areas are

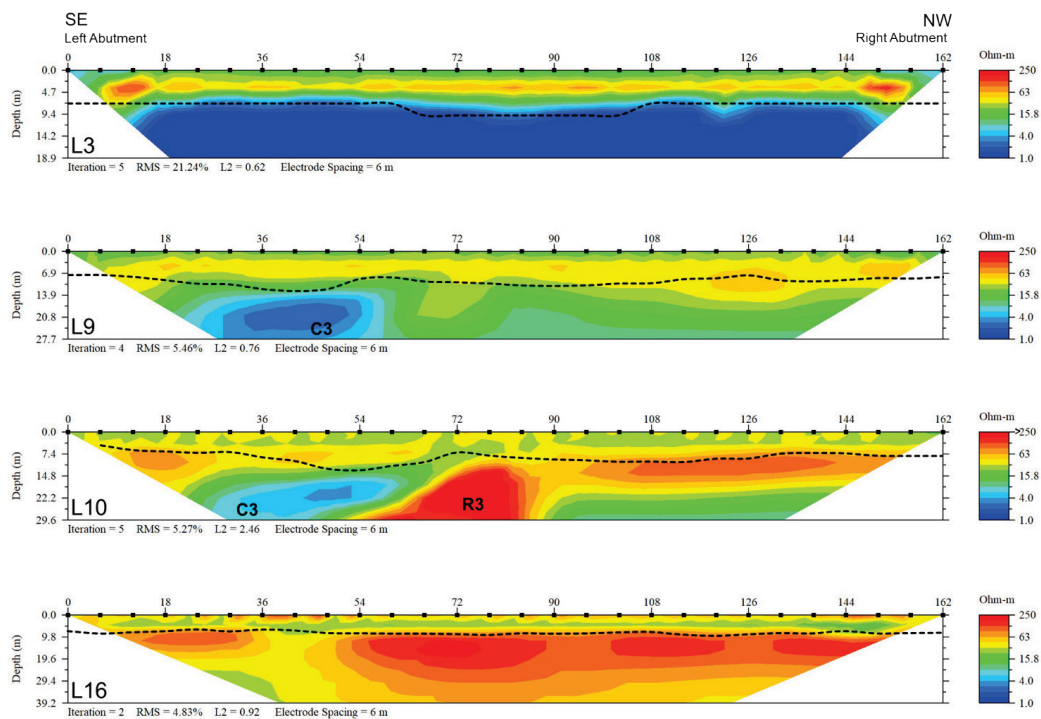
5.4 Outflow dataset

All outflow ERT lines are included in Appendix A. Figure 18 provides L3, L9, L10, and L16 to represent general features of the outflow data. Lines L3-L8 (Figure 14), which were collected over the stilling basin, are markedly different from the lines acquired farther from the structure. In general, the subsurface resistivity of Lines L3-L8 shows a layer of higher resistivity (50 to over 150 Ω -m) underlain by very low resistivity (less than 10 Ω -m) at a depth of 8-10 m (the steel at the top of the stilling basin). These lines exhibit decreasing resolution with depth once the top of the stilling basin is encountered. The high conductivity (i.e., low resistivity) of reinforcing steel in the stilling basin essentially served as a barrier to resistivity measurements at depths greater than 8 to 10 m (26.3 to 32.3 ft).

The character of the ERT lines changes beyond Line L8. Lines 9-16 exhibit a more heterogeneous resistivity character. The subsurface resistivity in L9 shows an area of low resistivity (less than 10 Ω -m), labeled C3 in Figure 18, between positions 24 and 60 m at a top depth of about 13 m. C3 is observed in an area having a slightly deeper water column. Bathymetric changes can influence the resistivity readings. However, this effect typically occurs when the vertical bathymetry changes are greater than the horizontal electrode spacing of the ERT survey. In this case, the change in the bathymetry of the channel bottom is less than the 6-m (19.7-ft) electrode spacing. Therefore, C3 does not appear to be an artifact caused by a change in the channel bottom. This low-resistivity feature is laterally persistent in the outflow lines past the flank of the stilling basin. The contrasting resistivity and geometry of feature C3 gradually dissipates with distance from the structure. C3 has similar resistive character to C1 in the inflow channel, but at this point we are unable to explain its cause/origin or any possible relationship to feature C1.

L10 exhibits an area of high resistivity (850 to over 1,000 Ω -m), labeled R3 on Figure 18, between electrode distances 66 and 84 m that flanks C3. The anomalously high resistivity of feature R3 persists in the adjacent profile L11 (Appendix A). ERT profiles southwest of L10 show relatively lower resistivities than feature R3, varying between 100 and 500 Ω -m, encountered at depths around 9 to 30 m (29.5 to 98.4 ft). These resistive areas appear more continuous along their profile (e.g., L16 in Figure 18 and L12-L15 in Appendix A).

Figure 18. ERT profiles from the outflow channel. Dashed line represents the channel bottom.



5.5 Seismic

The following section describes the observations made from 23 acquired seismic lines. The data were acquired using standard seismic refraction procedures and were analyzed by using refraction processing methods. In addition, because reflections were observed in the raw data set, the data were processed by using seismic reflection processing methods to understand the character of those features.

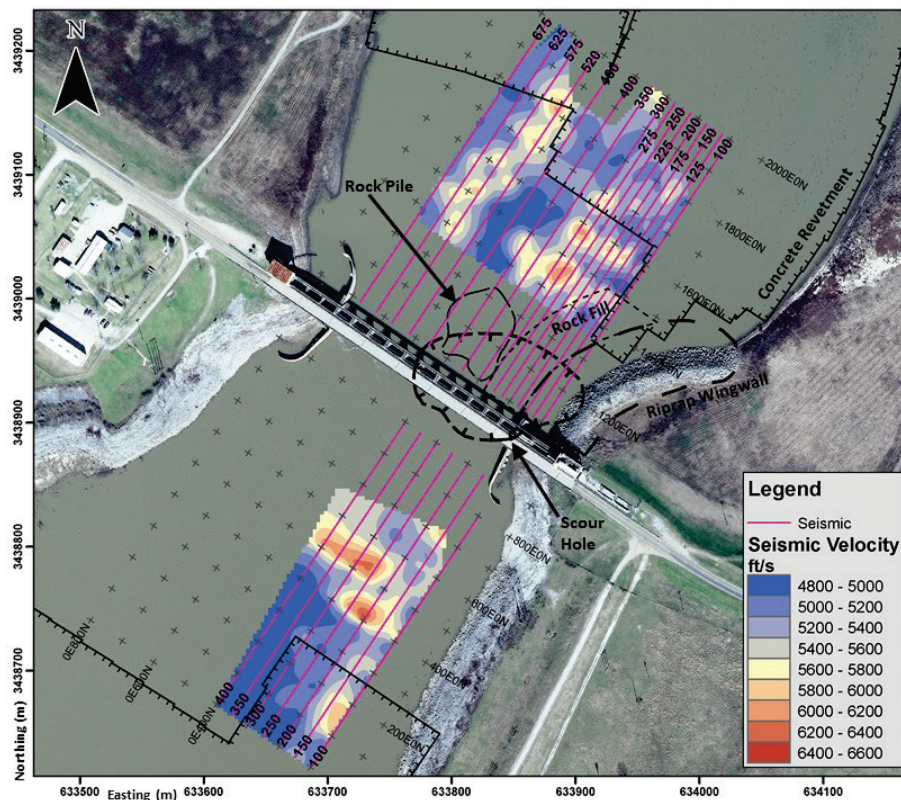
5.5.1 Seismic refraction

The goal of the seismic data was to provide cross-sectional images of changes in seismic velocity, similar to the electrical resistivity cross sections, as close to the ORLSS structure as possible. As discussed under the seismic processing section, because the apparent P-wave velocity of water and of the sediments is very close and there is little variation in the velocities along the survey lines, the seismic inversion could not produce a representative seismic refraction 2-D inversion. This means the team was unable to obtain seismic cross sections that penetrated into the bottom sediments yet was able to produce maps that showed only the sediment velocities of the uppermost sediments in the river bottom. Furthermore, as explained in

Appendix B, the area imaged is not as close to the ORLSS structure as desired because of the water column depth and low sediment velocities.

A plan view map of the shallow sediment velocity is shown in Figure 19. It was constructed by plotting the apparent P-wave velocity at the center of the hydrophone array for each shot. The map shows consistent line-to-line trends that could be related to sediment stiffness and its variability. Higher bottom velocities could be related to emplaced concrete mattresses (revetment). However, it is unlikely that the concrete revetment was detected by the seismic survey because it is probably not thick enough to be resolved. The velocities in Figure 19 do not correlate with the inflow channel bathymetry nor with locations of the concrete revetment. Lower velocities (4,800 to 5,400 ft/s) are observed within the area of concrete revetment, which could be caused by recent siltation (i.e., soft sediments). Low bottom velocities also could be associated with concentrations of sands and/or poorly compacted sediments (e.g., old scour fill materials), which could be related to the stratigraphic transition from backswamp deposits on the north side to point bar structural features on the south side. On the outflow channel side, lower seismic velocities correlate with a bathymetric low (-32.8 to -22.4 m) near the center of the channel, seen in Figure 9.

Figure 19. Apparent P-wave velocity of shallow sediment.



5.5.2 Seismic reflection

The following section describes the results of the seismic reflection analysis and resulting observations. Line numbers for the seismic reflection profiles correspond to those on the map provided in Figure 19, which also provides the relationship of the profiles to the scour boundary. Seismic reflection profiles are presented with a distance axis, in feet, at the top (“Reference Grid Location”) and a depth axis, in feet, at the left and in meters on the right. The channel bottom, derived from December 2019 bathymetric measurements (Figure 9), is overlain on each figure as a dashed blue line. The distance axis correlates to the positional data on Figure 19. All seismic reflection profiles are oriented in the southwest-to-northeast direction from left to right. It is important to note that all seismic reflection profiles in this report are presented with the water surface at a depth of 0 m (0 ft). The following presents a selected number of seismic profiles that represent the conditions at ORLSS. All seismic profiles, including a more comprehensive description on the processing steps, are provided in Appendix B.

Three selected seismic reflection profiles from the inflow channel side (Lines 150, 400, and 675) are provided in Figure 20. Reflections from the channel bottom (annotated by a dashed blue line on each seismic profile) exhibited consistent results with the bathymetry. Repeating groups of sub-horizontal reflections (M1, M2, M3, M4, and M5), each with an apparent group thickness of about 6 m (20 ft), occur at depth increments of about 15 m (50 ft). These sub-horizontal reflections are observed in all three sections. These are multiples of reflections from the bottom of the channel, as described in Appendix B. In some of the stacked sections, as many as five multiple reflections (M1, M2, M3, M4, and M5) can be seen.

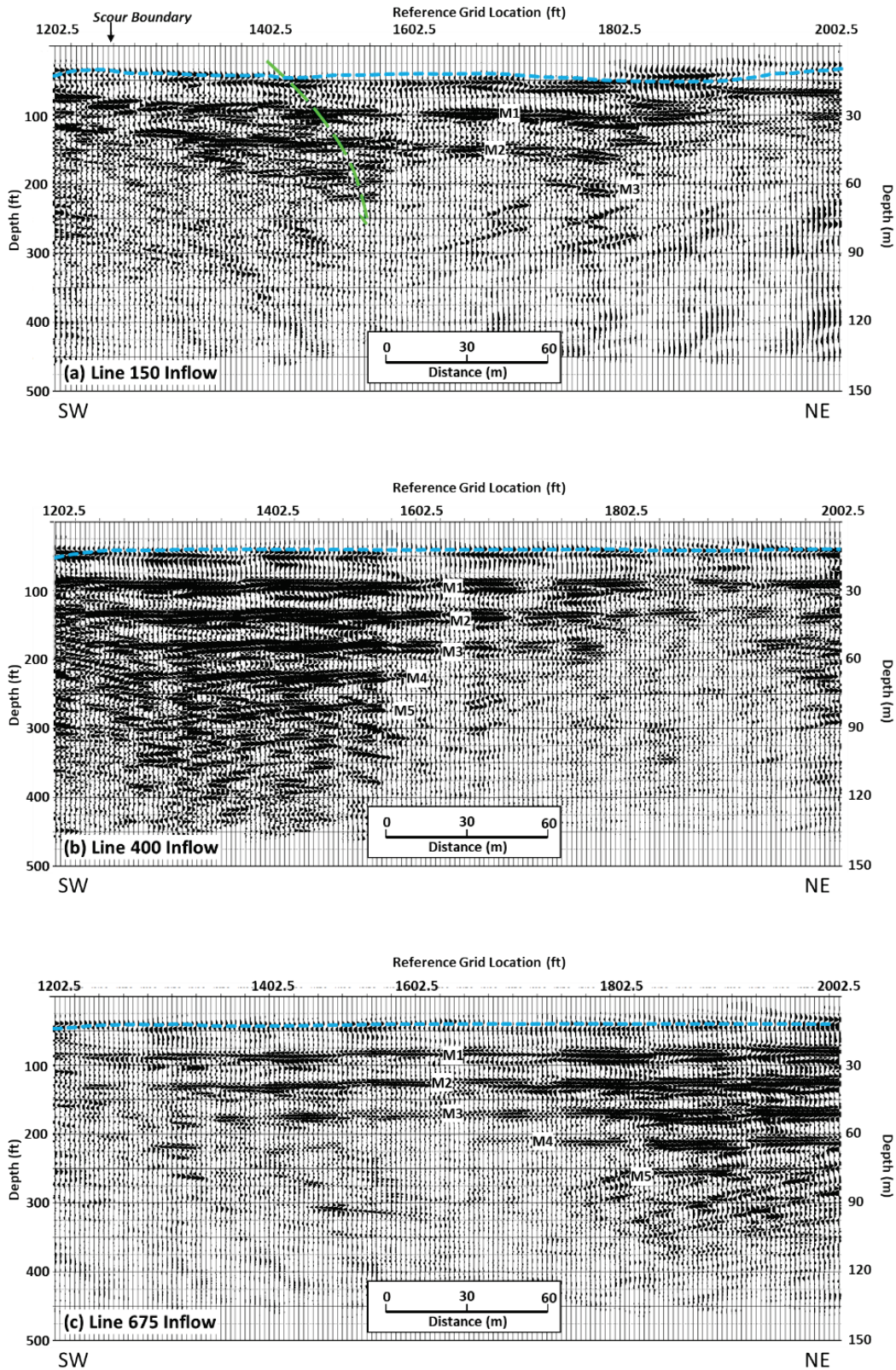
The estimated boundary of the scour (from Figure 3) extends to approximately Reference Grid Location 1260 on Line 150, as indicated on Figure 20a. The scour boundary does not intersect the other two profiles in Figure 20 (Lines 400 and 675). The primary reflections are weak in the scour portion of Line 150 and are not indicative of any variations associated with the scour. Multiples in this portion of Line 150 are not continuous, as they are in Lines 400 and 675. The channel bottom multiples on Line 150 appear to be disturbed between Reference Grid Locations 1,200 and 1,400 ft (roughly bounded by the green dashed line). This disturbed area extends beyond the estimated scour boundary from Figure 3. In this disturbed area, there are more lateral offsets in the

multiples, which are probably enhancements of lateral breaks in the channel bottom reflections. There are also more numerous and irregular reflections between the sets of multiples in the disturbed region of Line 150 than on Lines 400 and 675. On Lines 400 and 675, Figure 20b and Figure 20c, the multiples are more continuous and have fewer reflections between multiples. On closer inspection of the full set of seismic reflection cross sections shown in Appendix B, the disturbed nature of reflections seen in the scour portion of Figure 20a is not consistent from line to line, even though the lines are spaced only 8 m (25 ft) apart. Because of this, researchers are unable to conclude that this disturbed feature is representative of any actual structural feature of the filled scour.

Three selected stacked seismic reflection profiles from the outflow channel side of ORLSS (Lines 150, 300, and 400) are provided in Figure 21. As with Figure 20, the channel-bottom bathymetry is overlain on each profile as a dashed blue line. The primary reflections, including the deepening of the channel-bottom surface on the left (southwest) side of the profiles, correlate with the bathymetry. In some cases, the primary channel-bottom reflections are obscure (e.g., between Reference Grid Locations 400 and 550 of Figure 21b and c). These areas of weak primary reflections generally correlate with places where the bottom surface is shallow or where there is a transition from shallow to deeper water. Shallow reflections can be obscured due to low angles of reflection or effects related to the normal moveout correction (see NMO discussion in Data Acquisition and Processing section). Where the channel bottom is steeper, the weak primary reflections can be associated with low reflection angles or rough bottom interfaces. Rough interfaces cause interfering reflections that add together to produce a weak response.

These outflow sections also show multiple reflections (M1, M2, M3, and M4). There are generally fewer multiples on the southwest ends of the profiles than are seen on the inflow side because of the greater water depth. On all outflow sections (Figure 21), there are many diffractions. Several of these are labeled “D” just above each apex of each one, with tails extending downward in both directions from the apex. These diffractions, which resemble an inverted “V,” emanate from the channel bottom or a channel-bottom multiple indicating either rough channel-bottom topography or localized heterogeneity in the shallow channel bottom, located at each apex.

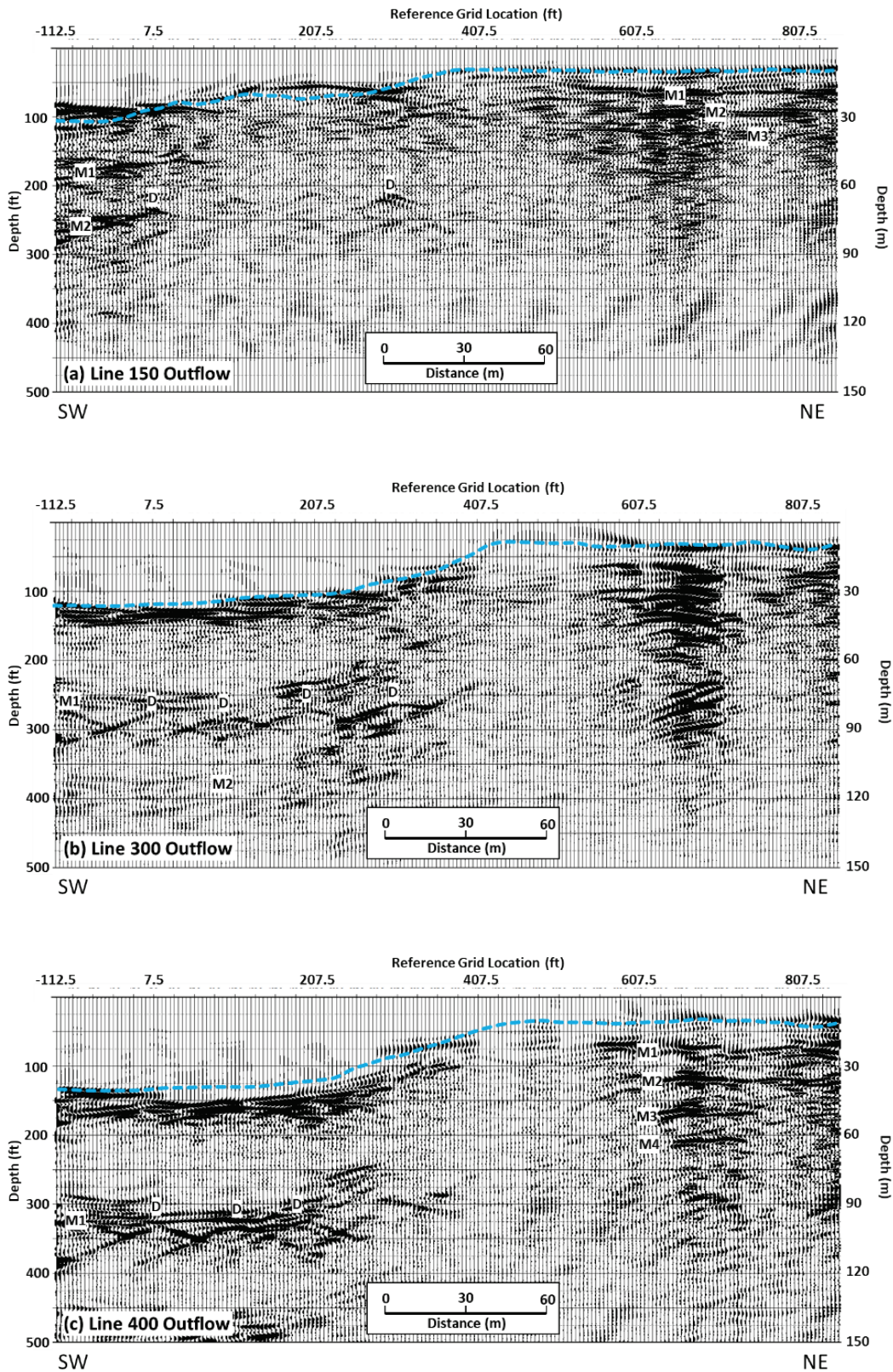
Figure 20. Stacked sections for three lines on the inflow side of ORLSS: (a) line 150 (green dashed line of approximate disturbed area), (b) line 400, and (c) line 675. The blue dashed line represents the channel bottom.



To remove the artifacts at these points, the depth section can be “migrated,” a procedure that should collapse the diffractions to a point at the apex. Examples of migrated profiles for Lines 300 and 400 (Figure 21b and Figure 21c) are provided in Appendix B (Figure B9).

For the stacked seismic reflection sections in the inflow channel (Figure 20) and outflow channel (Figure 21), it is evident that multiple reflections dominate the deeper response and mask reflections that might otherwise be observed from deeper sediment interfaces. While this is unfortunate, it was important to analyze the reflected waves in the seismic data to assess possible information that might be important in understanding the site.

Figure 21. Stacked depth sections for three lines from the outflow channel of ORLSS: (a) line 150, (b) line 300, and (c) line 400. Blue dashed line represents the channel bottom.



6 Discussion

The interpretation of the geophysical data sets is difficult because of the complicated history of the site, the diversity of in-situ naturally emplaced materials and numerous human-emplaced materials (i.e., soil, riprap) and interference associated with the structure (e.g., steel, grout, concrete). The following factors were considered in the interpretation.

1. As described previously, a transition in depositional environment from a layered backswamp stratigraphic environment on the right abutment side to a laterally discontinuous point bar deposit on the left abutment side occurs in 3-D space, presumably beneath the channel. Geophysically, this would indicate a transition from predominantly 2-D horizontally stratified high/low resistivity units to an environment with 3-D changes, both lateral and vertical with a wide range of resistivity values. The stratigraphic environment transition may have dictated the location of the scour (e.g., if sands were easily scoured and limited to the area near the left abutment). The complex stratigraphy can complicate the problem of distinguishing between fine-grained topstratum deposits and barite- or clay-based grouts and similarly between man-emplaced limestone and sands/silts emplaced by the river after the scour repair.
2. The resistivity associated with naturally emplaced materials (e.g., clays, silts, or sands) overlaps those associated with some materials used to construct the structure (concrete, limestone riprap) and man-emplaced materials used to remediate the scour event (limestone riprap, various types of grout).
3. The historical record is incomplete. Boundaries of features, such as the rock pile (Figure 3), are not available in detail; the disposition of the blocks in the rock pile is not fully understood (e.g., Where was this rock emplaced, and was it used to construct the riprap wing wall and/or to fill the scour?).
4. The behavioral interaction between the grout and the emplaced rock is not fully understood. Was the flow of grout limited to the volume beneath ORLSS, in proximity to the piles, or did it move tens of meters into the emplaced riprap that was used to fill the scour? Is the material currently in place in the scour hole filled with a mixture of stream sediment with the riprap or grout with the riprap? To what elevations (upper and lower bound) would the grout have penetrated?

5. The excavated limits of the inflow channel were designed at -1.5 m (-5 ft) elevation relative to sea level, which, based on water elevations at the time of the survey, would be at an approximate depth of 14 m (45.9 ft) relative to the water surface (as shown on the resistivity cross sections). However, water flowing from the Mississippi River is likely to rework the inflow channel bottom sediments. The extent of these processes and spatiotemporal changes is beyond the scope of this geophysical effort but were considered in the interpretation of the data.
6. The subsurface resistivity from the results of the land-based geophysical investigation adjacent to both left and right abutments provided an indication of the electrical response of the subsurface soils and was used to correlate to the waterborne ERT profiles. Without the land-based data, the interpretation of the waterborne geophysical data would have been more difficult and would have resulted in greater uncertainty.
7. Both the natural and anthropogenic features of ORLSS at and below the sub-bottom have not been static through time. Factors, such as rock removal/emplacement, remediated scour hole, repairs that required additional placement of steel, revetment, and bathymetric changes, have implications in the interpretation of the geophysical response, thus requiring consideration of the four-dimensional aspects (i.e., temporal changes) in addition to the 3-D character of the subsurface, both natural and anthropogenic, and their corresponding anisotropy.

6.1 Interpretation of ERT survey

6.1.1 General statements

The waterborne ERT survey achieved a depth of investigation between 30 to 39 m (98.4 to 127.9 ft) relative to the water surface, which varied according to line. Relative to sea level, the water-surface elevation ranged from 12.3 to 13.2 m (40.2 to 43.25 ft) in the inflow channel and 6.2 to 7.2 m (20.3 to 23.5 ft) in the outflow channel during the ERT survey. The scour hole reached an estimated maximum vertical extent of about -18.3 m relative to sea level. This means that the base of the scour hole lies at a depth of 30.0 to 31.5 m relative to the water surface. Thus, the ERT survey depth of investigation (30.0 to 39.0 m) exceeded the bottom of the scour hole datum. However, because resolution decreases with depth, it is difficult to draw conclusions about the structure near the bottom of

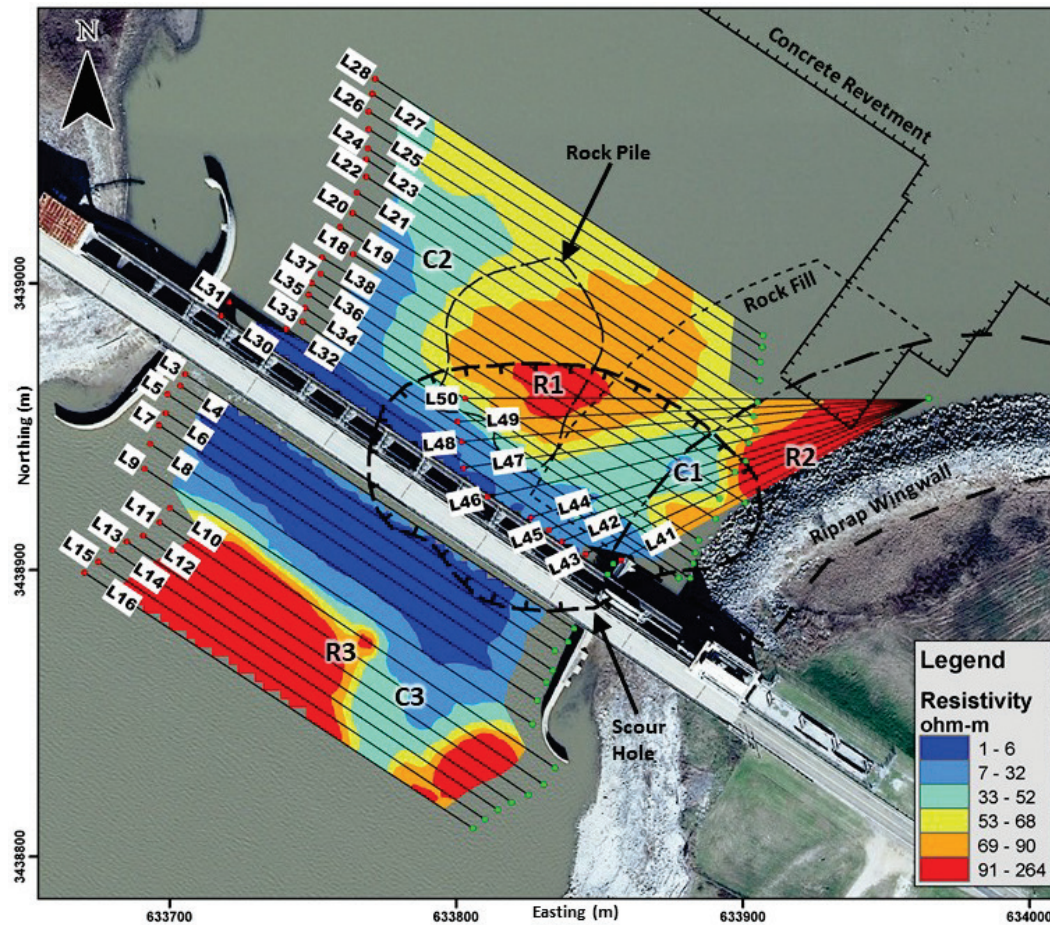
the scour. ERT lines acquired closest to ORLSS were noisy, caused by the proximity of steel and reinforced concrete.

Figure 22 provides a synopsis of features observed in the ERT data from both inflow and outflow channels, in addition to the diagrammatic outlines of components of ORLSS presented earlier in Figure 3. The contour map overlain with the features, represented by the blue-green-yellow-red color scale, is an average of the resistivity values between the channel-bottom surface and 6 m (19.7 ft) below. Key features in this figure are the following.

1. A high-resistivity feature, with resistivities shown as orange and red, in the center of the channel that largely corresponds with the location of a rock pile that was emplaced in the inflow channel and indicated as feature R1 in the individual ERT lines.
2. A high-resistivity feature, located in and around the location of the former left wingwall, now a riprap wingwall, associated with the limestone blocks of the wingwall. This feature is labeled R2 in the individual ERT lines.
3. A low-resistivity zone centered between the two resistive features R1 and R2 (labeled C1 in the inflow channel) and largely coinciding with the mapped location of the scour hole. Here, the lower resistivity is attributed to the conductivity of the solidified grout mix, based on an assumption that some of the grout penetrated beyond the structure and into gaps between blocks of limestone used to fill the scour hole.
4. A low-resistivity zone on the right abutment side (C2) at a depth of about 15 to 30 m that trends deeper eastward. The resistivity, depth encountered, and proximity to backswamp clay deposits on the right abutment side (as described earlier in Geologic Setting and Previous Geophysical Surveys) suggest that the conductive character of C2 could be associated with these backswamp clay deposits.
5. A low-resistivity feature in the outflow channel (C3) observed at the edge of the stilling basin that appears to dissipate with distance from the stilling basin.
6. A high-resistivity feature in the outflow channel (R3) observed at the edge of the stilling basin and adjacent to C3.

In the remainder of this section, details of this interpretation are provided with a focus on anomalies in the individual lines.

Figure 22. Plan view of interpreted ERT results overlain with feature boundaries. Resistivity values are an average of the resistivity values between the channel-bottom surface and 6 m below.



6.1.2 Sub-bottom sediments

The subsurface resistivity ($\sim 50\text{--}70\ \Omega\text{-m}$) in L28 (Figure 15), which was acquired farthest from ORLSS in the inflow channel, shows a more continuous trend with resistivity values that are comparable to the subsurface resistivity of the soils from the land-based survey. Therefore, L28 is interpreted to be representative of the channel-bottom sediments absent of any rock (riprap) and/or grout.

The less-resistive feature (C2) observed in the western portions of L37, L38, and L18–L23 exhibits a deepening trend toward the centerline of the inflow channel. These areas of lower resistivity in the deeper portions of the ERT profiles that become progressively shallower westward are interpreted as saturated sediments beneath the channel bottom. The westward deepening trend of feature C2 compares to geologic cross sections that show a similar

geometrical trend in ML and SM strata¹. Additionally, the subsurface resistivity values of the silty sand from the land survey on the right abutment side are comparable to those of feature C2.

Based on the land surveys and geologic mapping, it is interpreted that a transition in depositional environment occurs somewhere in the inflow channel. The deposits near the right abutment consists primarily of backswamp clays overlying sands, whereas the soils adjacent to the left abutment are a more heterogeneous mixture of silts, clays, and sands from point bar deposition. The greater heterogeneity of onshore soil strata near the left abutment was considered during the interpretation of the marine geophysical data. An understanding of the geometry of depositional environments, their soil characteristics, and the electrical response of these soils is necessary for differentiating electrical responses generated by emplaced materials (i.e., grout).

6.1.3 Left abutment riprap wingwall

The ERT lines from the fan layout (Figure 16) exhibit resistive near-surface readings, noted as R2, that were influenced by the riprap wingwall from the start of each line to about position 84 m. This resistive feature from the riprap wingwall shows a southwesterly deepening trend in its resistive character, which coincides with the limits of the designed wingwall (information courtesy of MVN). The riprap wingwall was designed at a 1:2 slope from the crest to its toe at an elevation of 0 m (relative to sea level). This slope is expressed by the transition from a planar to an oblique trend in the interface between the resistive areas of the riprap and the conductive water column. In ERT profiles, such as L41, the riprap surface appears mostly planar. This is because the bearing of L41 is relatively perpendicular to slope direction.

Comparison of the waterborne ERT lines and the land-based ERT survey shows that the resistivity values of areas with likely riprap are not much higher than the SP sands in the natural sediments. This is because the spaces between riprap blocks are filled in with either water, grout, or native material between stone blocks, therefore, exhibiting a less resistive response than intact solid limestone.

Interestingly, the base of the resistive area of the riprap wingwall deepens from around 13 m (42.7 ft) in L41, 18.5 m (60.7 ft) in L42, and 21 m (68.9 ft) in L44. This implies that the deeper portions of this

resistive character of the riprap wingwall exceed the designed elevation of the toe, which was at 0 m (0 ft) relative to sea level. The base of the resistive feature, which extends to 21 m (68.9 ft) in L49, would be at about -7.8 m (-25.6 ft) below sea level or 7.8 m (25.6 ft) below the designed riprap wingwall toe. This could possibly be associated with riprap placed near the wingwall toe to remediate the scour area.

6.1.4 Resistivity trends associated with rock pile

Feature R1, shown in L18 on Figure 15, shows an anomalous, resistive area (75 to 100 Ω -m) that was also observed in lines L36 through L20 (Appendix A). The resistive character of feature R1 is coincident with the lateral extent of a rock pile (Figure 22) that was temporarily placed during the remediation efforts on ORLSS (information courtesy of MVN). ERT profiles show areas of higher resistivity in proximity to this rock pile, which appear to dissipate near the flanks of the illustrated extents of the rock pile. The resistive character of feature R1 gradually dissipates with distance from the rock pile extents toward the Mississippi River. Less resistive responses (50 to 70 Ω -m) that are more continuous are encountered in the most distal ERT lines (e.g., L28) where feature R1 was not encountered. ERT lines L49 and L50 from the fan layout show a trend of increasing resistivity between positions 108 m and 144 m, which corresponds to the more resistive feature R1 on L49 (Figure 16). This is also coincident with the extent of the rock pile in diagrams of the forebay. It is likely that some of the rock from the original rock pile still exists in the inflow channel despite the efforts to relocate the rock to more strategic areas related to the scour (information courtesy of MVN). It is possible that as much rock was relocated as feasibly possible, and the remainder was graded with the channel bottom.

6.1.5 Resistivity trends associated with the estimated scour area

The conductive (i.e., low resistivity) feature (C1) observed on L18 between positions 12 and 30 m (Figure 15) is within the estimated lateral extents of the scoured area. This conductive feature is observed to have a resistivity of around ~20 – 30 Ω -m beneath the channel bottom. Based on these estimated lateral extents, the scoured area should extend approximately 90 m (295.3 ft) along L18, but feature C1 does not extend to this distance in the resistivity profiles (i.e., the boundaries of feature C1 do not coincide with the presumed boundaries of the scour). L37, L38, and L19 seem to image a portion of this feature at positions 36, 24, and

18 m, respectively. Also, based on mapped areas of the scour hole (Walshire 2021^{*}), there is a relatively deeper section of the scoured area at 10 m south of position 11 m on L18. The resistivity of this feature is less than 30 Ω -m, whereas the sediments underlying the channel bottom should be more resistive, based on comparison with L28.

Feature C1, as shown in L42 and L44 from Figure 16, exhibits a zone of low resistivity, interpreted as a portion of the scour hole where electrically conductive grout penetrated the riprap fill. The less-resistive character of feature C1 dissipates between L46 and L47. The general area where this conductive feature is encountered in the fan lines is coincident with the conductive feature (C1) that is observed on L18. The extent of this conductive feature in the inflow channel is within a portion of the estimated extent of the scoured area. However, the conductive feature does not appear to persist throughout the entire scour hole area. The conductive feature C1 is interpreted as grout fill based on the spatial association of the conductive anomaly within the scoured area, the lateral changes in the character of C1, contrasting resistivity to the limestone blocks of the riprap wingwall, and contrasting resistivity to the sub-bottom sediments. As stated earlier, the electrical properties of these sub-bottom sediments could overlap with grout. However, the areas laterally surrounding C1 that are more resistive, in addition to the resistivity of the sub-bottom sediments on L28, suggest that it is unlikely this conductive area (C1) is caused by conductive sediments (e.g., clay and silt). Also, the conductive character of C1, as well as the resistive character of bounding features, such as R1, suggests that the scour hole does not consist of a uniform body of grout or rock. Instead, it is interpreted that there are portions where the riprap has been grouted and portions where the voids (i.e., pore spaces between riprap blocks) are filled with some combination of river sediment and/or water. The localized character of C1 supports an interpretation that it is caused by a conductive grout filling the spaces between resistive limestone riprap blocks. These coincident patterns indicate that L18, L42, L45, L44, and L46 imaged the grout in a portion of the scour hole. Comparison of the ERT profiles in Figure 16, the resistivity map in Figure 22, and cross sections of the scour hole shows that the less-

^{*} Walshire, L. A. 2021. *Stability analysis of Old River Low Sill Structure*. ERDC/GSL draft in preparation. Vicksburg, MS: U.S. Army Engineer Research and Development Center.

resistive areas (C1) are most common near the deepest portions of the scoured area (near gates 9-11, see Figure 3).

As described above in the section Old River Low Sill Structure (ORLSS) and shown in Figure 3, the historical documentation illustrates that the scoured area on the inflow channel side was filled with riprap to prevent further scouring. Grouting operations were conducted in borings from the top of the structure that were adjacent to a sheet pile wall located at the upstream edge of the gate bays. The grout mixture used for remediation efforts was a self-leveling, fluid-like grout, which would spread laterally until the scour was filled or encountered a barrier. The sheet pile wall at the upstream edge of the gate bays truncates at an elevation of -11 m (-36 ft) and would have impeded the flow of grout into the forebay. However, if the lateral extent of the scour hole flanked the sheet pile wall at gate 11, then grout could have infiltrated the scoured forebay area.

Based on the ERT profiles, the research team's interpretation is that the remediated scour hole is not a uniform mass of rock or grout. Gaps between limestone riprap blocks in a portion of the scoured area are filled with grout, while in other portions the gaps may be filled with some combination of river sediment and/or water. The most resistive responses in the inflow channel are from the riprap wingwall. Large gaps between the riprap blocks were filled (at least at shallow depths) mostly with water at the time of the survey. The averaged resistivity response of the riprap and water is dominated by the more resistive riprap. Elsewhere, the area interpreted as the remains of the rock pile has an electrical response that is slightly less resistive than the riprap wingwall. This is likely a result of a combination of water, sediment, and the reduced quantity of rock relative to the wingwall. As described earlier, this rock may be slightly smaller, as the larger riprap in the rock pile would have been relocated to more strategic portions of the scoured volume while the remaining smaller rock sizes might have been graded into the channel-bottom sediments. It is important to note that this interpretation is an assumption of the procedures in relocating the riprap from the rock pile. The electrical response of the area interpreted as grout is less resistive than the areas of riprap and channel-bottom sediments. The electrical response of the subsurface in ERT profiles that are most distal from ORLSS is slightly more resistive than the response in the grouted area. The conductive response is most apparent in areas where the scour was the deepest.

Based on the ERT inversion results and their interpretation, there is no evidence to support the presence of large air-filled voids (>3 m in diameter). It is likely that any former void zones within the grout would be filled with either water, other material not associated with the grout (e.g., unconsolidated material and/or sediment), or a combination. Considering that a water-filled cavity would have a low contrasting resistivity compared to the rest of the grout, the ERT data do not suggest the presence of any large water-filled cavities (>3 m in diameter). It is possible that smaller water/sediment-filled zones (<3 m) within the grouted area could be present but not detectable using the survey parameters employed.

6.1.6 Outflow channel and stilling basin

ERT lines from the portion of the outflow channel that are closest to ORLSS (L3-L8, Figure 18 and Appendix A) show an area of low resistivity beneath the water column. This is likely caused by the presence of the reinforced concrete in the stilling basin. L8 was collected near the edge of the stilling basin and represents a transition of the ERT survey from the concrete in the stilling basin into the outflow channel.

ERT lines acquired farther from the stilling basin (L10-L16, Figure 18 and Appendix A) exhibit high resistivities that generally vary between 100 and 500 Ω -m. These more resistive areas are likely caused by the presence of riprap in the outflow channel. The trends in resistivity observed from feature C3 (unrelated to C1 on the inflow channel) (Figure 18 and Figure 22) occur beneath the bottom of the channel and are not related to the bathymetric low. C3 was observed to have a resistivity that was less than 10 Ω -m while C1 had a resistivity about 20–30 Ω -m. C3 was encountered outside of the estimated boundaries of the scour hole. The lower resistivity of C3, when compared to C1, combined with the occurrence of C3 outside of the estimated scour hole boundary, indicates that C3 and C1 are unrelated. One possibility is that C3 could be a conductive area of clay, but this is highly speculative given the absence of ground-truthed data (i.e., borings) for this feature.

R3 is an area of anomalously high resistivity (850 to over 1,000 Ω -m) adjacent to the conductive C3 feature seen on L10. In other ERT profiles, the resistivity ranges between 100 and 500 Ω -m but appears more continuous. These resistive areas are likely representative of the electrical response of large riprap in the outflow channel. This interpretation could explain the wide range of resistivities observed in the outflow channel.

6.2 Interpretation of seismic survey

The shallow sediment along the channel bottom exhibited both high and low seismic velocities that may be associated with sediment stiffness. Typically, higher seismic velocities will occur in stiffer sediments and lower seismic velocities in softer sediments because of the degree of compaction. Therefore, the association of seismic velocity with relative stiffness can often be roughly correlated to erosion resistance. This correlation is applicable only to areas where primary reflections penetrated the water column. As described earlier, lower seismic velocities correlated with the bathymetric low near the center of the channel. This indicates that the velocities represent the change in channel depth with no seismic energy reaching the shallow sediments of the channel bottom, thus rendering correlations of seismic velocity with sediment stiffness irrelevant in areas where the water depth exceeds the seismic signal penetration. The seismic data, where they provided information relevant to the scour feature, do not reveal any features that are not apparent from the resistivity data and have lower resolution than the resistivity data. The area where seismic refraction provided shallow sediment properties is upstream from the scour feature. This is because there is a small contrast in seismic velocity between the water and the shallow sediments, which results in minimal signal penetration into the materials beneath the channel bottom. In addition, the geometry of both inflow and outflow channels allowed inadequate space in which the boat could maneuver to acquire data near ORLSS. Seismic reflection profiles derived from the seismic refraction data lacked the redundancy (stacking) that is needed to clearly delineate features within the scour and surrounding structural features. These profiles show disturbed areas within the scour but show no interpretable structural features within the scour. Specifically, there is a clear disruption of the channel bottom in the inflow cross section for Line 150. This disruption was observed from the difference in the character of multiples. Lines 400 and 675 showed multiples that were relatively subparallel and evenly spaced. The multiples in Line 150 were more irregularly spaced with numerous chaotic reflections in between sets of multiples. This disruption on Line 150 extends farther upstream from ORLSS (perhaps to about Local Grid Y=1450 on Figure 19) than indicated in the mapped scour area, which shows the scour extending only to about Y=1250 in the Local Grid coordinates. Because of the limitations in the seismic data described earlier, relating, or interpreting this disruption of multiples from this seismic data as part of the scour area would be highly speculative.

7 Conclusions

The goal of this project was to provide more detailed information about the 3-D character of the remediated scour hole that occurred in 1973, with emphasis on identifying voids and/or water/material-filled zones that might exist within the filled scour. Ideally, it would have been beneficial if geophysical data could have imaged the portion of the scour beneath ORLSS. However, because of the high concentration of steel piles (which exhibit high seismic velocities and high electrical conductivity) within that volume, no geophysical methods based on seismic or electrical methods could be used to address that volume. Therefore, the task of the geophysical team was to provide as much information as possible regarding the portion of the remediated scour that is adjacent to ORLSS. The results of the waterborne geophysical surveys were interpreted through comparative analysis with previously collected land-based geophysical surveys, construction drawings, geologic cross sections, associated bathymetry, and plans from the remediation efforts.

The seismic data revealed the presence of both high and low velocities in the shallow sediments that might be associated with stiffness of the sub-bottom channel sediments in areas where the seismic energy penetrated beneath the water column. Seismic data were less effective than the resistivity data because the velocity of the shallow sediment was close to the velocity of the water. Because of this, the distance from the source at which seismic waves from the shallow sediment reached hydrophones sooner than waves traveling through the water was much greater than it would have been if the shallow sediment velocity had been greater. Unfortunately, this resulted in having most of the area that could be imaged with the seismic method upstream from the scour hole.

The resistivity measurements provide some important insights into the 3-D character of the remediated scour volume. These insights from the results and the interpretation of the waterborne geophysical survey will provide a deeper understanding of the subsurface properties at ORLSS for geotechnical modeling efforts.

1. Preliminary understanding of the remediated scour volume was oversimplified. The team anticipated that the geophysical data would reveal a contrast in physical properties that would correspond to the estimated scour boundaries and that the material within the scour

- volume would have higher electrical resistivity (if controlled by limestone blocks) or lower resistivity (if controlled by an electrically conductive grout) when compared with surrounding sedimentary materials. Voids within the grout volume would be recognized as subtle changes in resistivity within that volume.
2. Studies of documents related to the scour volume remediation revealed additional complications and uncertainties. First, because the grout was inserted primarily under the ORLSS structure, the extent to which it migrated into the volume adjacent to the ORLSS structure was not known. Second, the size of the riprap used to fill the scour volume is not fully known and its geologic origin is less certain. It is believed to be limestone of type “A” stone; that is, (1) no piece was to exceed 8 tons, (2) no more than 10 percent by weight were to weigh less than 1 ton, and (3) at least 50 percent by weight were to weigh 3 tons or more. This rock may have been moved into the scour volume from a large, recently identified “rock pile” (Figure 3) that overlapped the scour volume and extended to its north and west.
 3. The resistivity data indicate a low-resistivity volume within part of the scour volume. This is interpreted to be a portion of the scour hole where an electrically conductive grout, which was inserted beneath the ORLSS structure, infiltrated into the riprap blocks that were placed prior to grouting operations in the scour volume, and may serve as a matrix to the riprap blocks.
 4. There are portions of the scour volume that are not electrically conductive. This could indicate that there are portions of the scour volume (in the area adjacent to the ORLSS structure) that were not penetrated by an electrically conductive grout and, therefore, are presumed to consist of ungrouted riprap blocks. Figure 23 outlines estimated boundaries of various areas based on interpretation of the resistivity data. The boundaries between the grouted and the ungrouted portions of the scour hole are only roughly defined, as resistivity tends to show a gradual transition from low values (in the grouted portion of the scour volume) to higher values (in the ungrouted portion).
 5. Figure 24 is a 3-D representation of the resistivity response of the inflow channel at a depth of 21.7 m (71.2 ft) below the water surface (9 m [29.5 ft] below sea level) with contours of the estimated scour boundaries and depth contours. The deepest portion of the scour is located adjacent to the structure where the resistivity measurements were influenced by the monoliths, and meaningful data were not acquired. The lower resistivity anomaly C1 extends from the edge of the deepest scour area to the

northeast, following the deeper portions of the scour contours. This anomalous area corresponds to the area labeled “Mostly Grout” in Figure 23. The more resistive anomaly R1 is located on the outer edge of the scour boundary, whereas R2 is located outside of the scour area. These resistive features likely represent areas of riprap with sediment fill (R1) and ungrouted riprap along the wingwall (R2). The feature C2 is likely associated with backswamp deposits.

Figure 23. Interpreted areas derived from the geophysical survey.

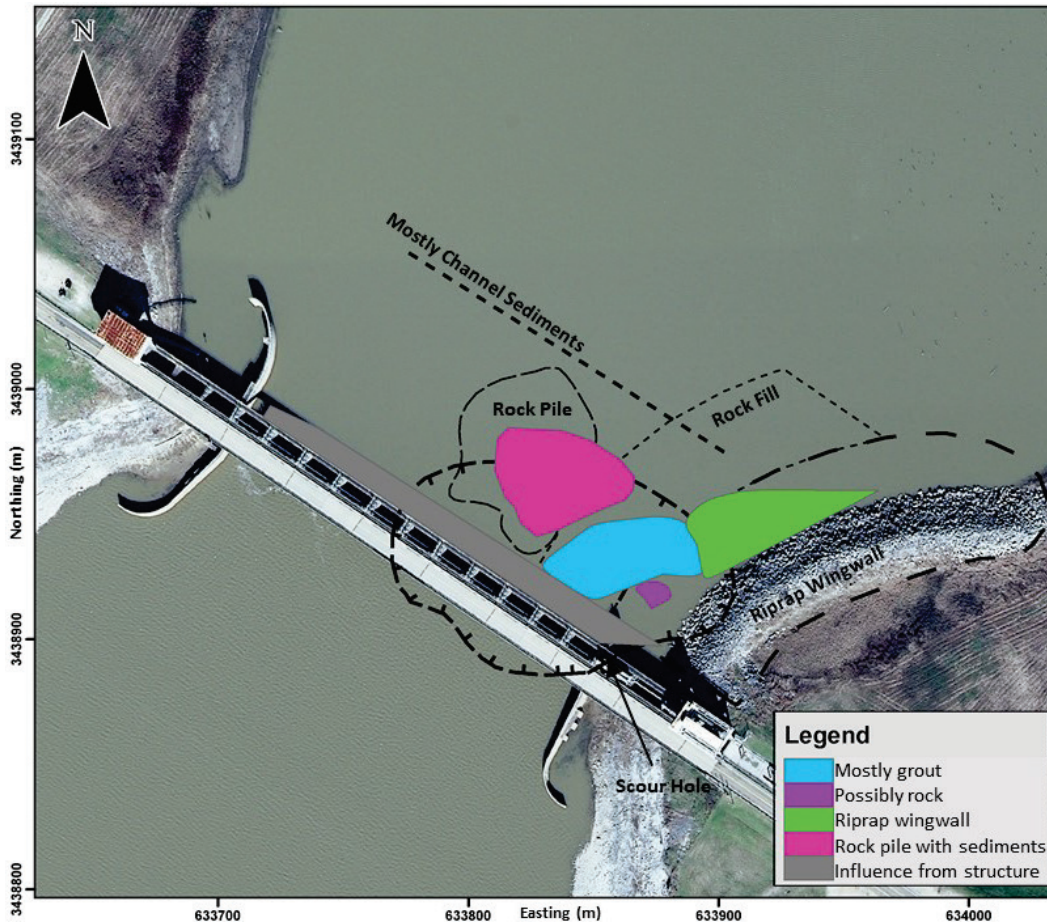
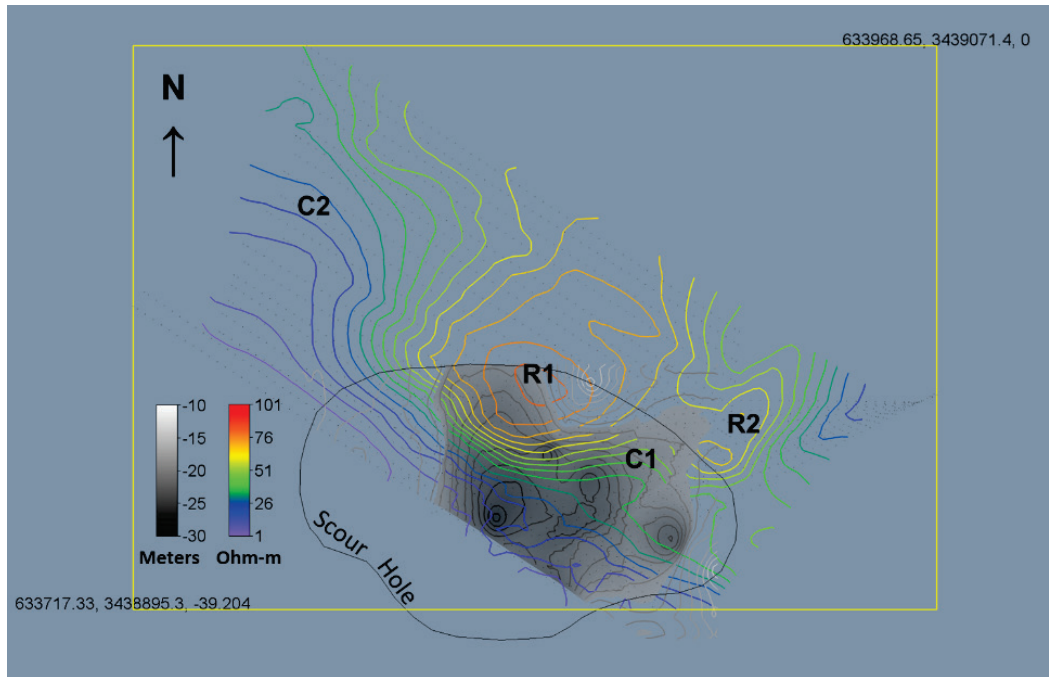


Figure 24. Contours of resistivity in a horizontal plane at 9m below sea level, 21.7m below water surface, shown in color. Gray-scale contours show estimated depth for the deeper part of the scour in meters relative to water surface. The boundary of the estimated scour is shown, and the four resistivity features R1, R2, C1, and C2 are labeled.



6. Areas where sediment has filled space between riprap blocks likely would have a resistivity response that is low but is higher than that of a grout-filled area (based on electrical conductivity measurements made at the time of the remediation effort). Should the lower resistivity, ungrouted portions of the scour volume be considered areas where voids are more likely to occur? This might depend on what features constitute a void that would be of concern at ORLSS. Where the riprap blocks are grouted, the grout is assumed to serve as a matrix to the blocks so that (when the space between blocks is fully filled) there would be no voids of concern in this volume. Within the ungrouted portion of the scour hole, it is likely that much of the space between riprap blocks has been filled with river sediment. Natural emplacement of the riprap blocks would control the size of these river sediment volumes, which would seem intuitively to be smaller than the size of the riprap blocks.
7. The electrical resistivity data provide a basis for selecting locations where cored samples could be collected to better understand the current condition of the filled scour hole. By selecting locations within the low-resistivity and high-resistivity portions of the scour hole, an

enhanced understanding of the scour could be achieved. The resistivity data provide a much better basis for selecting such locations than would be available in the absence of those data.

The results and interpretation derived from these results provide a greater understanding of the subsurface properties of ORLSS that will be integrated into future efforts in analysis related to its stability. The waterborne geophysical data could also serve as a decision tool for prioritizing borehole placement to ground-truth the grout characteristics.

Recommendations for future efforts that could expand on the waterborne geophysical data include (1) forward modeling and sensitivity analysis of varying resistivity values and geometries to simulate hypothetical water/material-filled zones, (2) investigating applicability atypical of formation factor to empirically derive an approximate porosity from the electrical resistivity tomographic (ERT) data, (3) making laboratory-based measurements on replicated and simulated grout mixtures to correlate the resistivity to compressive strength, and (4) conducting borehole-based geophysical analysis.

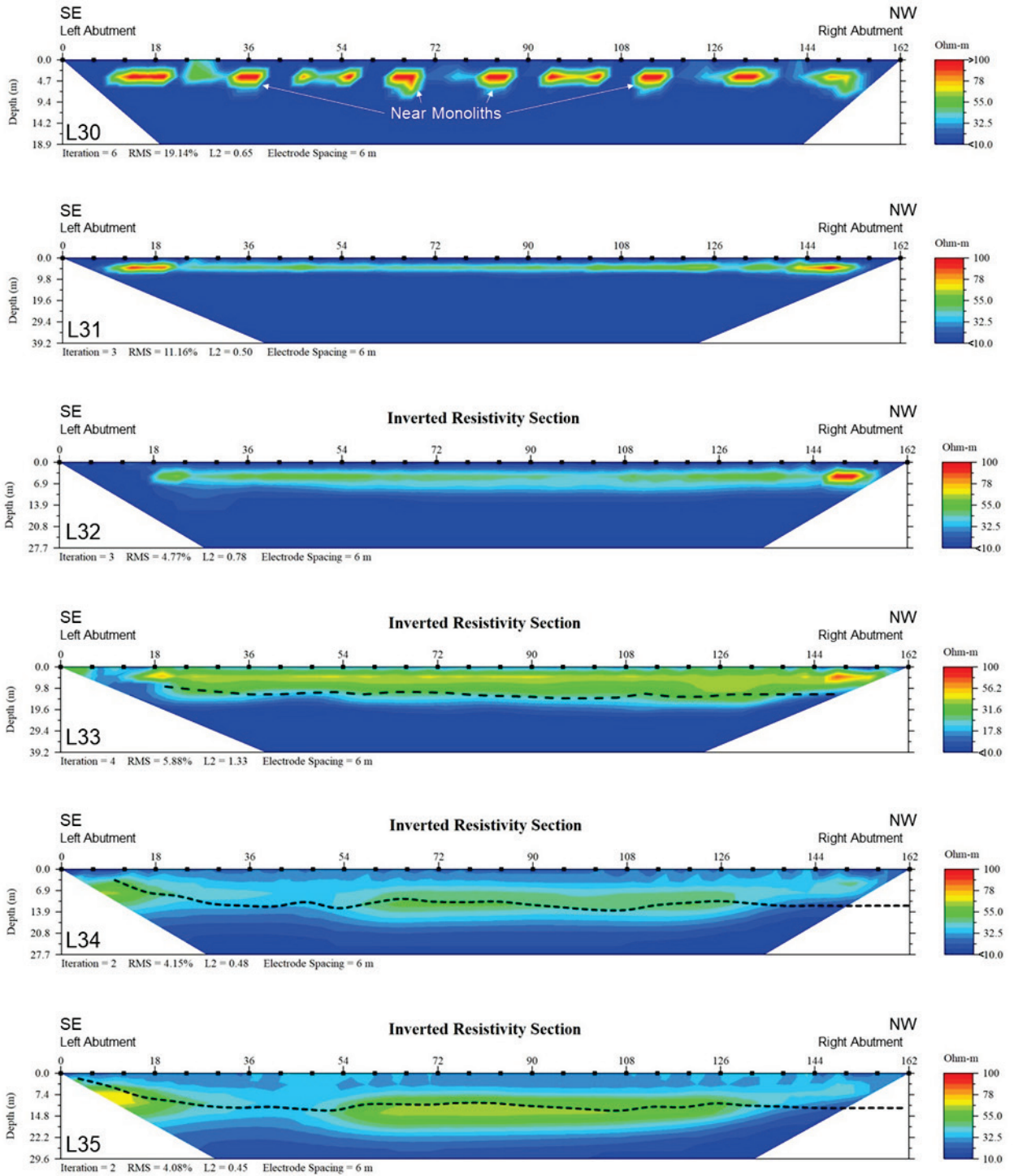
References

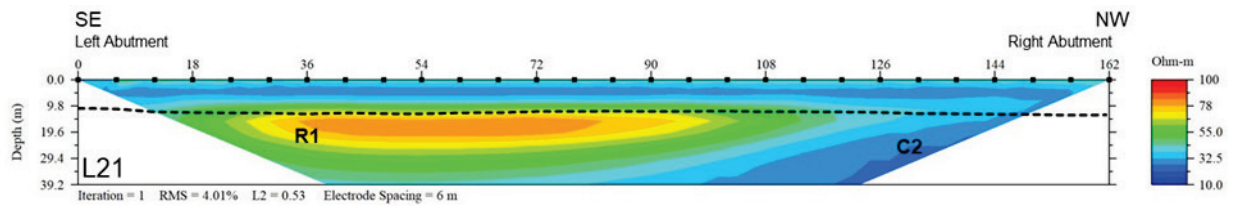
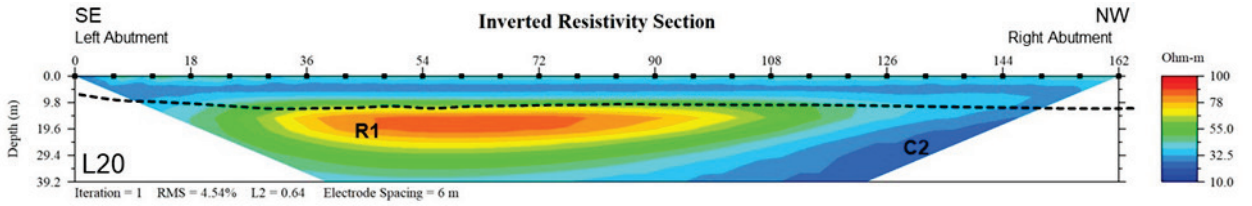
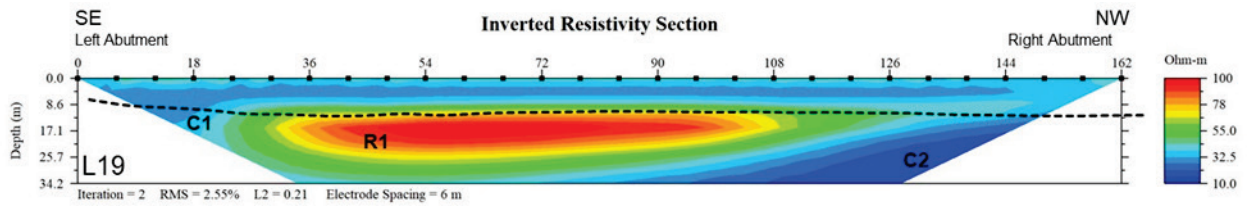
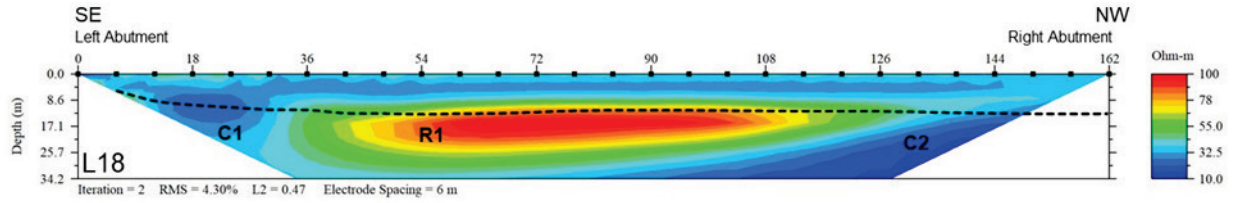
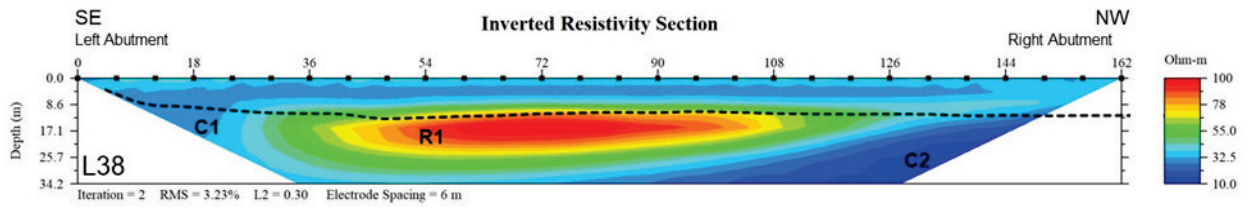
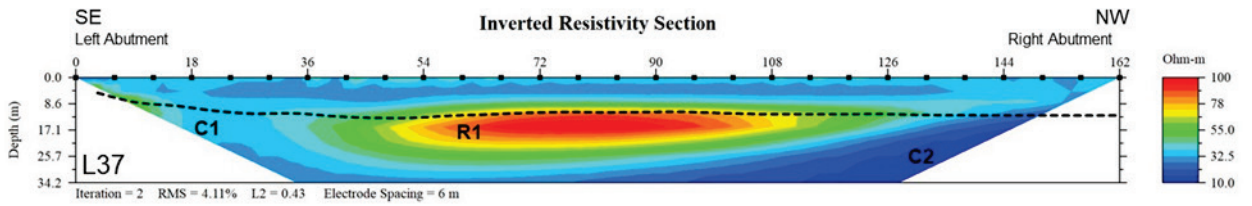
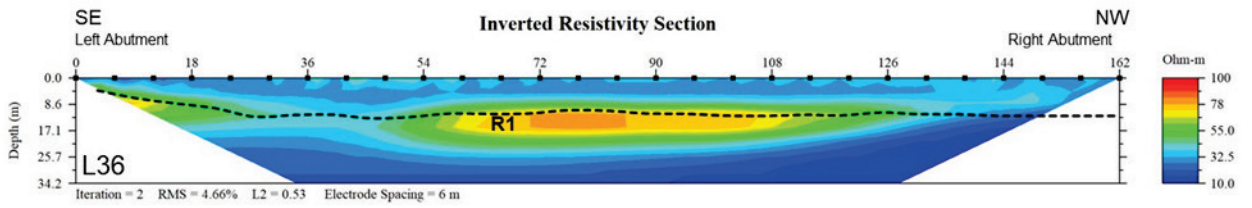
- Ainsworth, D. L. 1979. *Grouting instrumentation, Old River Low Sill Control Structure*. Miscellaneous Paper SL-79-23. Vicksburg, MS: U.S. Army Engineer Waterways Experiment Station.
- Chin, E. H. J. Skelton, and H. P. Guy. 1975. *The 1973 Mississippi River basin flood: compilation and analyses of meteorologic, streamflow, and sediment data*. U.S. Geological Survey Professional Paper 937. Reston, VA: U.S. Geological Survey.
- Fisk, H. N. 1947. *Fine-grained alluvial deposits and their effects on Mississippi River activity*. Vicksburg, MS: Mississippi River Commission, U.S. Army Engineer Waterways Experiment Station.
- Heath, R. E., G. L. Brown, C. D. Little, T. C. Pratt, J. J. Ratcliff, D. D. Abraham, D. Perkey, N. B. Ganesh, K. Martin, and D. P. May. 2015. *Old River Control Complex sedimentation investigation*. ERDC/CHL TR-15-8. Vicksburg, MS: U.S. Army Engineer Research and Development Center.
- Johnson, C. A., N. M. Piatak, and M. M. Miller. 2017. *Barite (Barium) - Critical mineral resources of the United States—Economic and environmental geology and prospects for future supply*. Reston, VA: U.S. Geological Survey.
- Komine, H. 2000. Evaluation of chemical grouted region by resistivity tomography. *Ground Improvement* 4:177-189.
- National Oceanic and Atmospheric Administration (NOAA). 2019. National Climatic Data Center. <http://www.ncdc.noaa.gov>.
- Oh, S. 2012. Safety assessment of dams by analysis of the electrical properties of the embankment material. *Engineering Geology* 129:76-90.
- Saucier, R. T. 1969. *Geological investigation of Mississippi River area Artonish to Donaldsonville, LA*. Technical Report S-69-4. Artonish Plates A and B. Vicksburg, MS: U.S. Army Engineer Waterways Experiment Station.
- Saucier, R. T. 1994. *Geomorphology and quaternary geologic history of the Lower Mississippi Valley*. Vol. I and II. Vicksburg, MS: U.S. Army Engineer Waterways Experiment Station.
- Simms, J. E., B. R. Breland, and W. E. Doll. 2021. *Geophysical investigation to assess condition of grouted scour hole, land-based and water-borne GPR surveys – interim report*. ERDC/GSL TR-21-30. Vicksburg, MS: Engineer Research and Development Center.
- Telford, W. M., L. P. Geldart, and R. E. Sheriff. 1990. *Applied geophysics*. Second Edition. Cambridge: Cambridge University Press.
- U. S. Army Corps of Engineers (USACE). 1974. *Flood of '73 post-flood report: U. S. Army Engineer District, New Orleans*. New Orleans: USACE.
- United States Geological Survey (USGS). 2020. National Water Information System; peak streamflow for the nation. <https://nwis.waterdata.usgs.gov/usa/nwis/peak>.

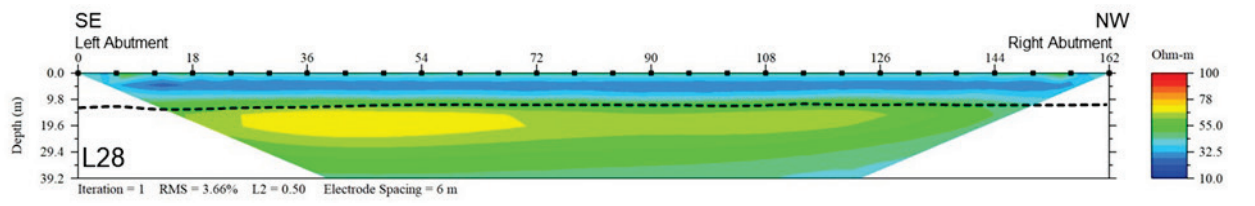
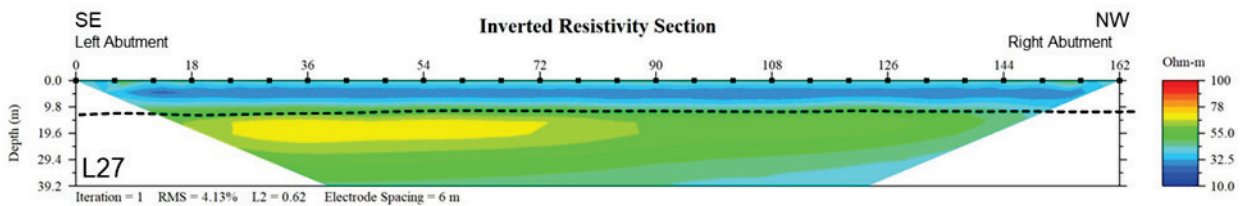
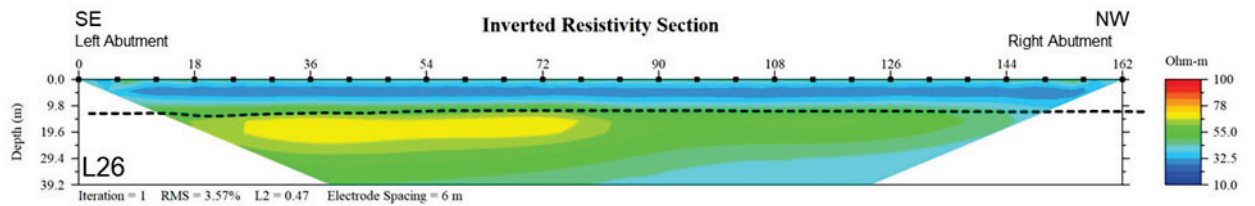
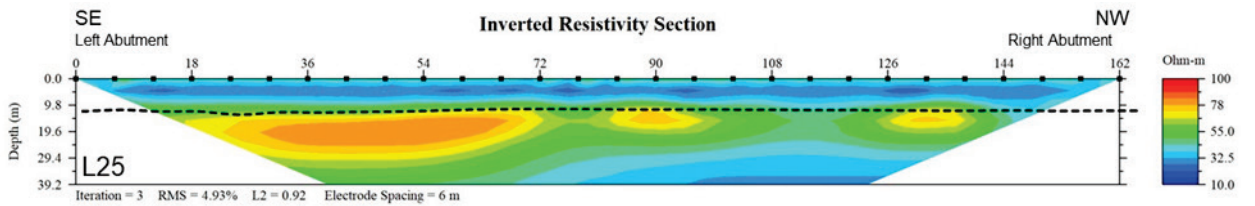
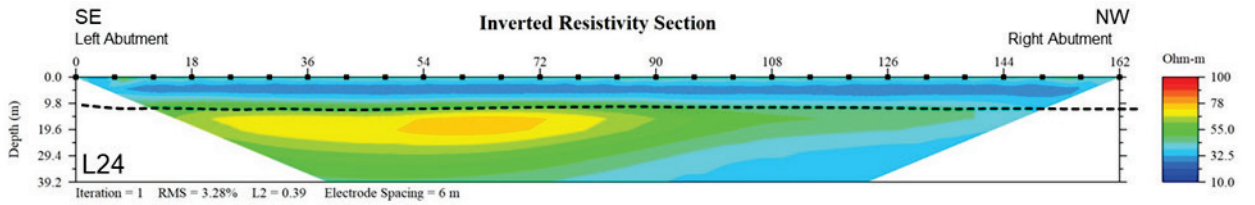
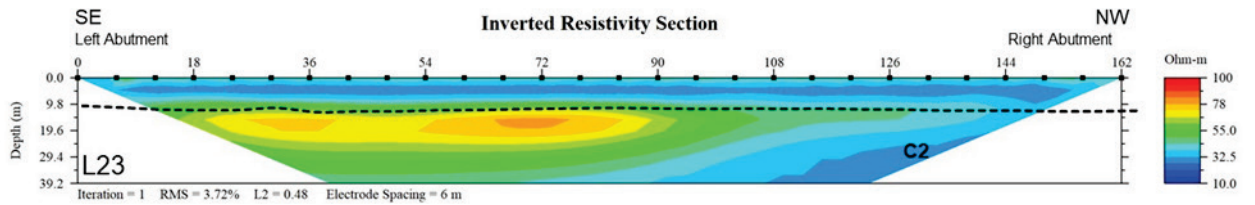
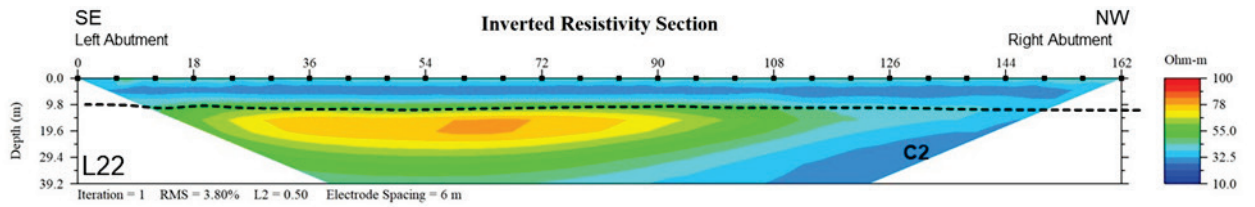
Wilson, H. K. 1978. *Grouting of scoured foundation Old River Low Sill Structure, Louisiana*. Miscellaneous Paper C-78-19. Vicksburg, MS: U.S. Army Engineer Waterways Experiment Station.

Appendix A: Inverted Resistivity Sections

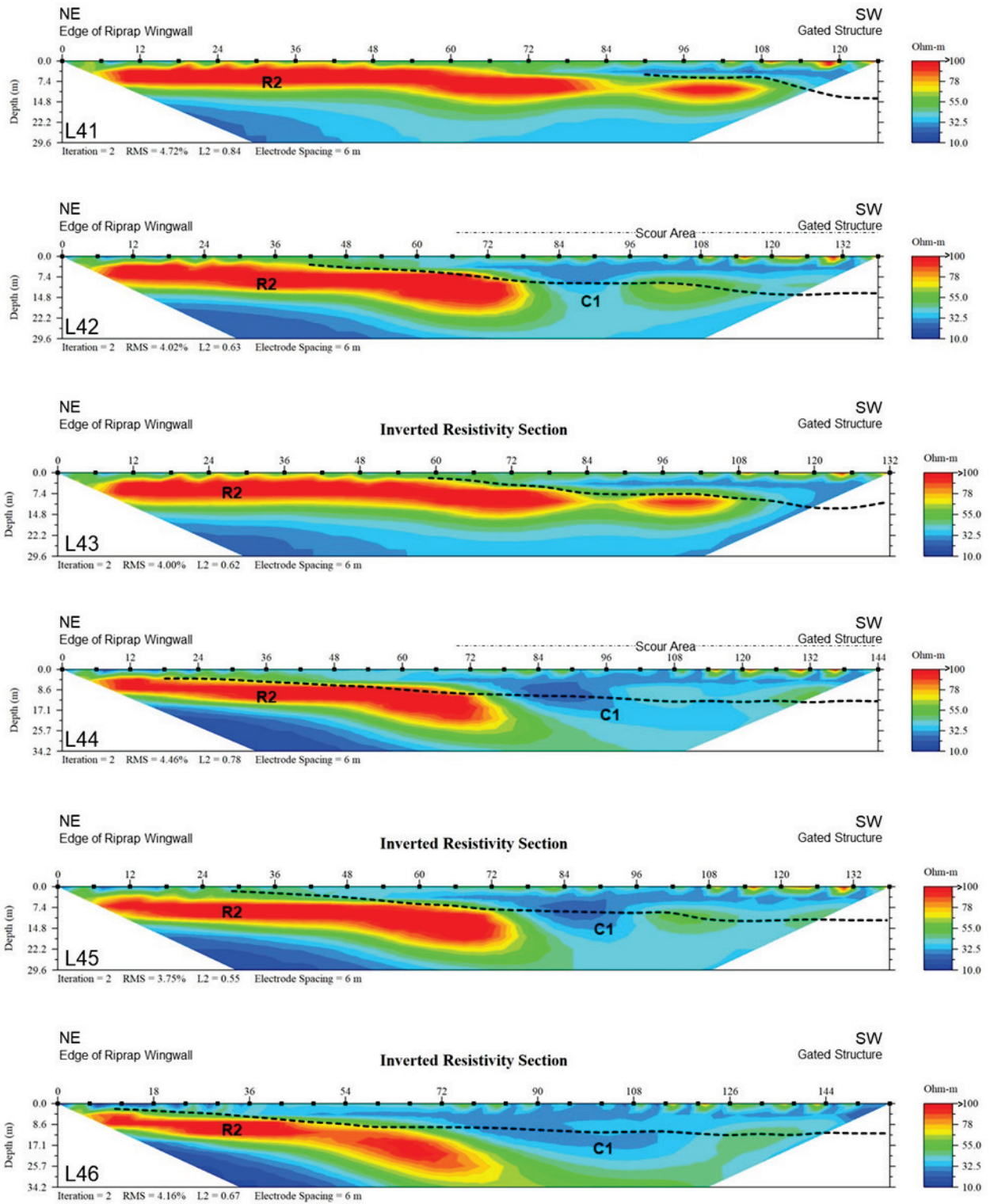
Inflow

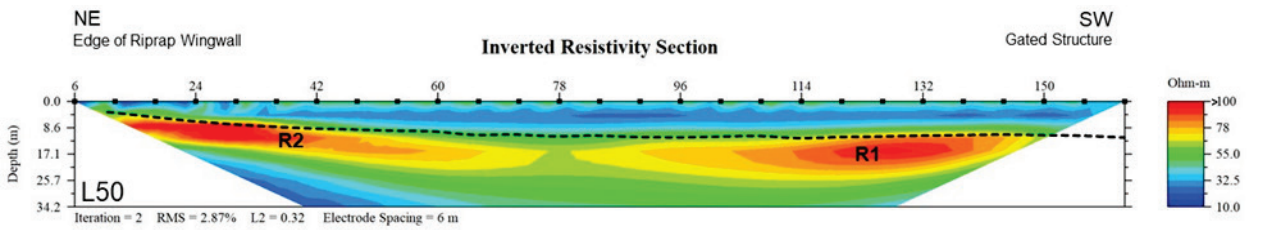
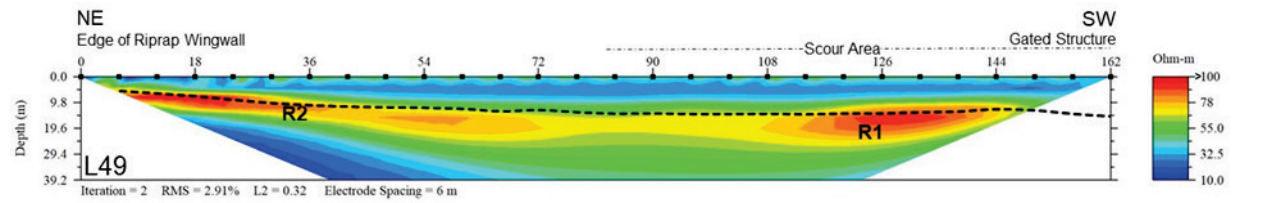
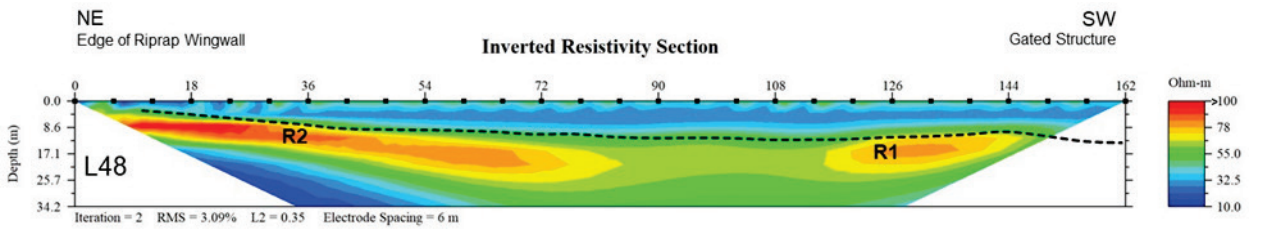
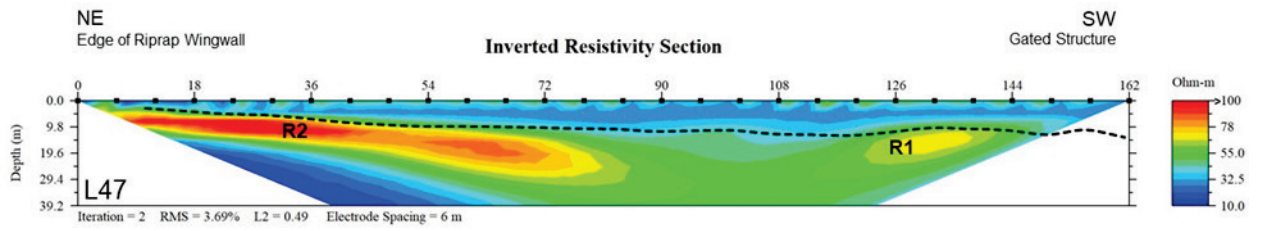




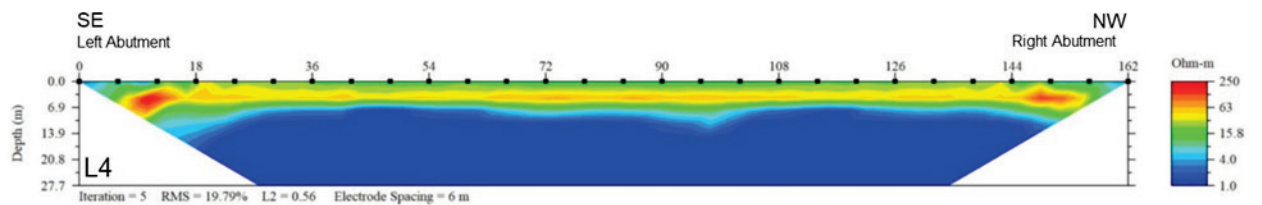
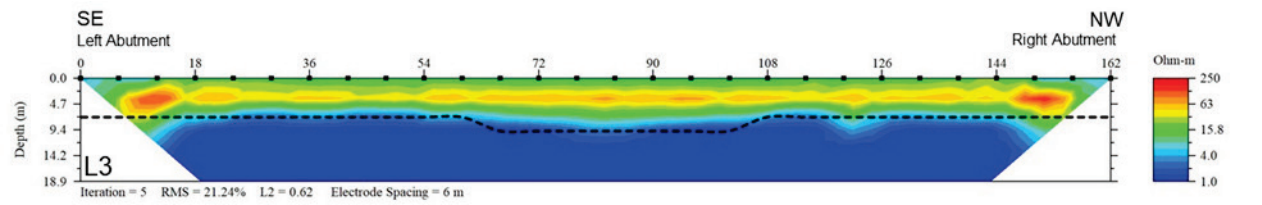


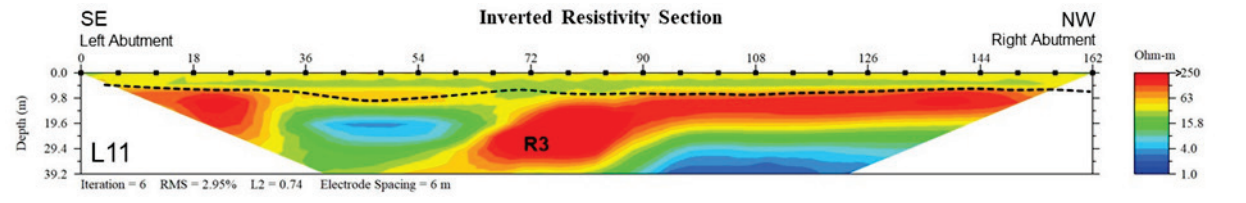
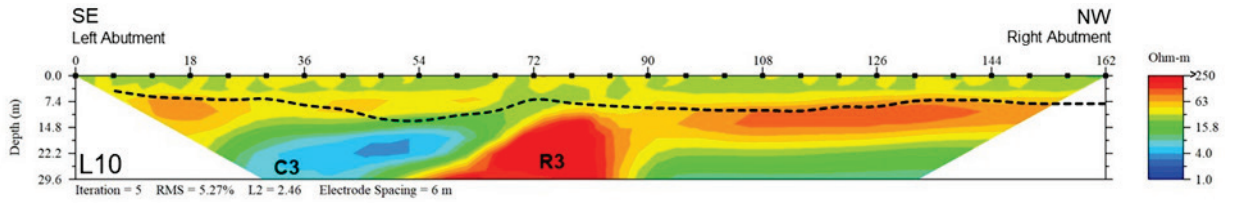
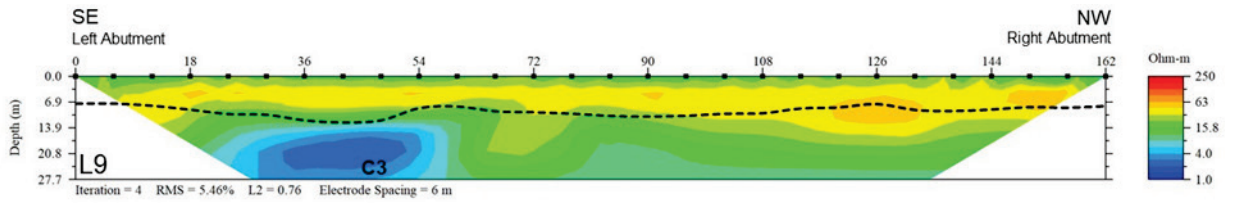
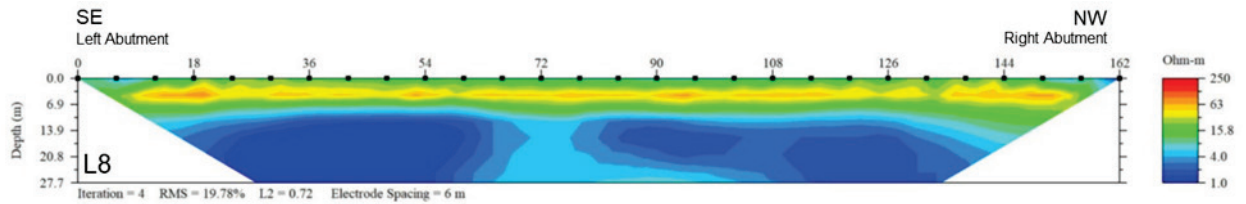
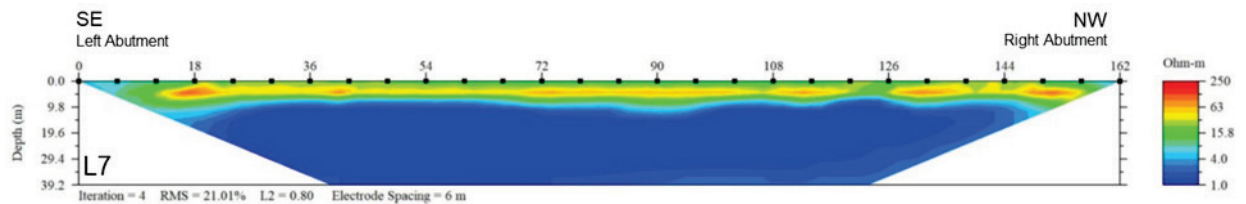
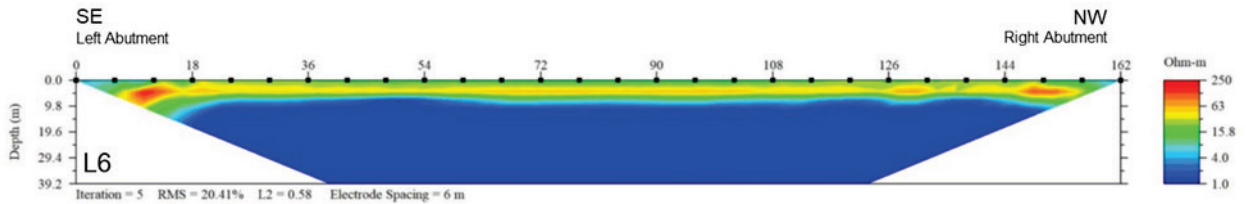
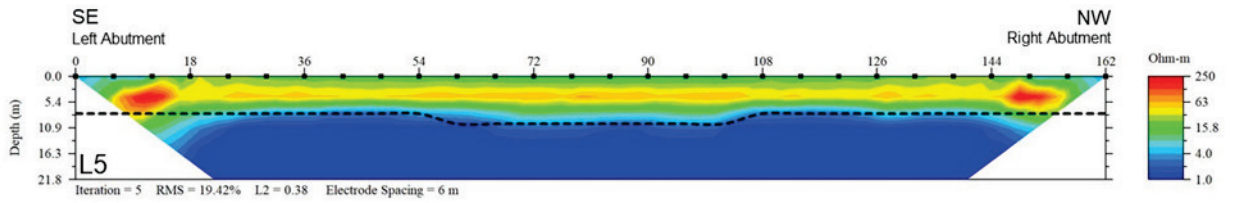
Inflow - Fan

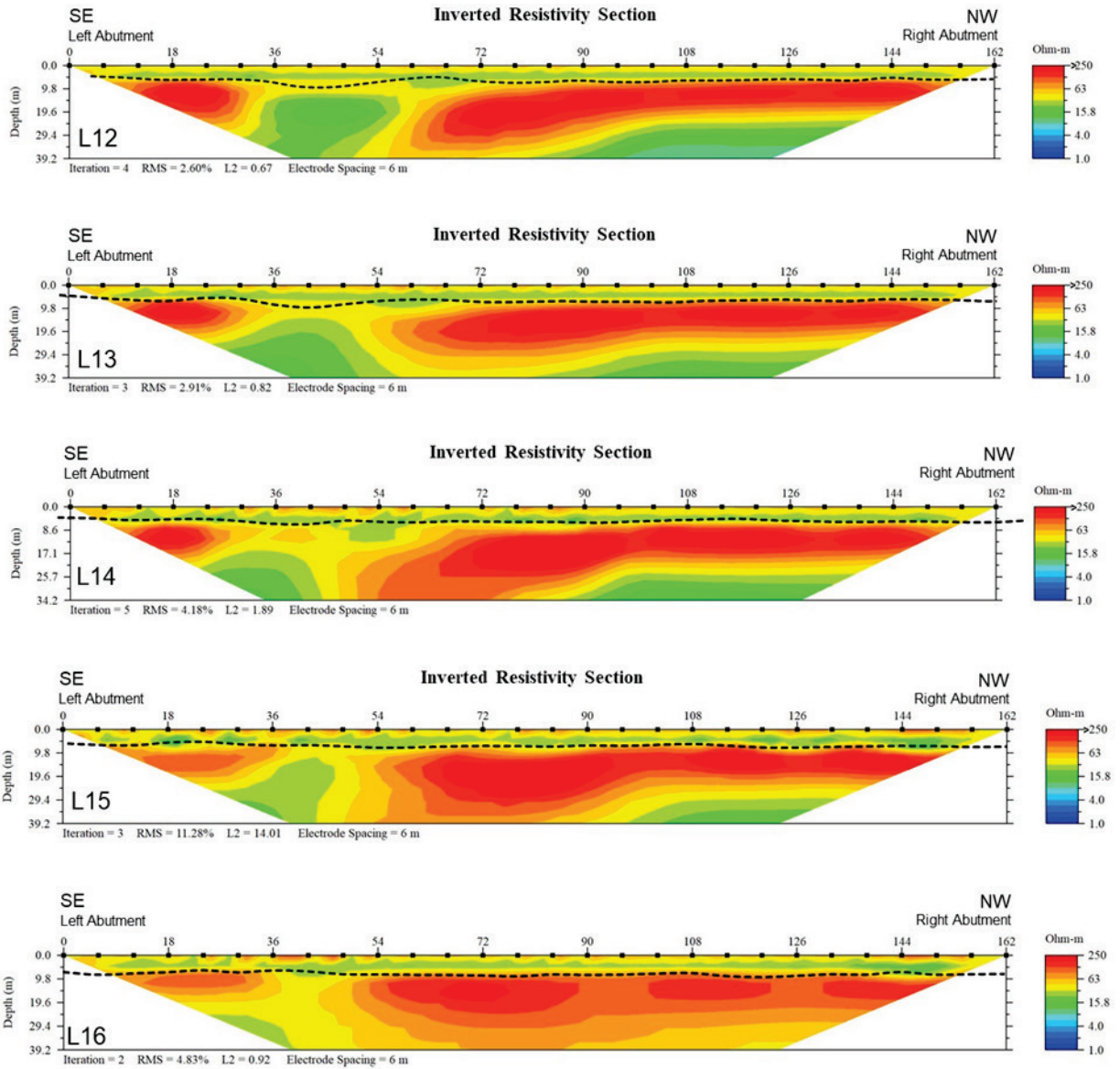




Outflow





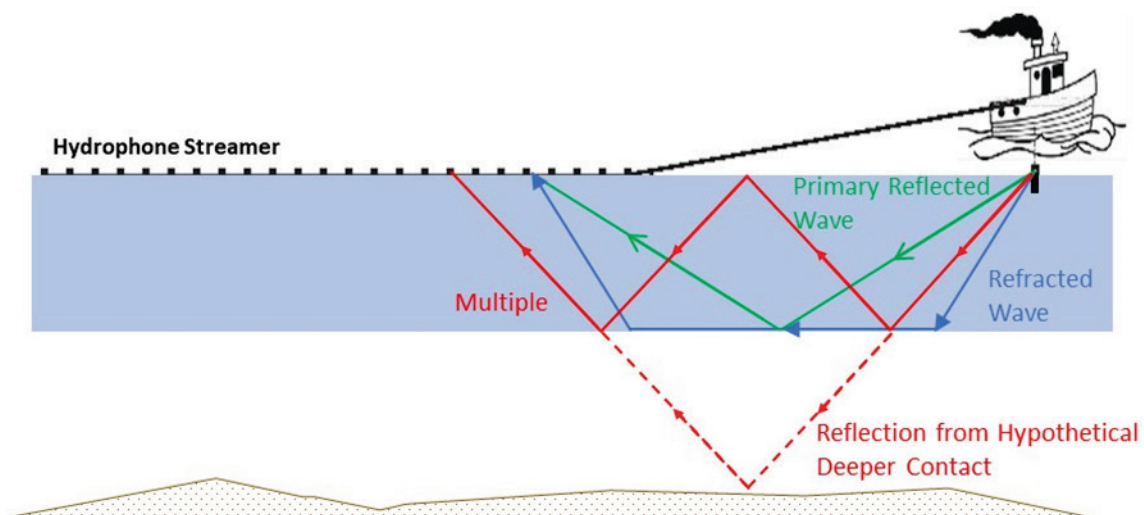


Appendix B: Seismic Data Processing

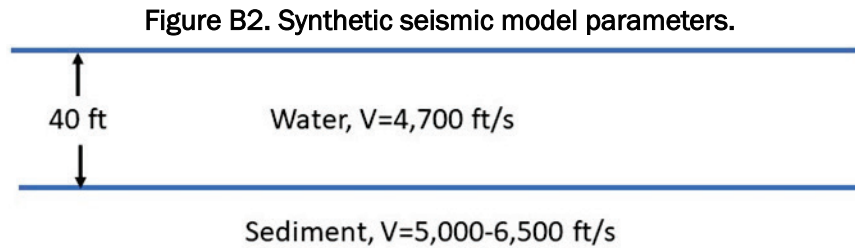
Marine seismic data were acquired at ORLSS by using field procedures designed to produce seismic velocity cross sections, similar to those generated in the land surveys at ORLSS (Simms et al. 2021) based on seismic refraction methods.

One primary difference between land and marine seismic refraction methods is that in a marine environment the seismic energy must pass through the water layer, so the water layer is imaged in addition to sub-bottom sediments and lithologic units. Whereas on land the rock and sediment velocities can be imaged near the seismic source, the marine environment imposes an offset distance from the source before any bottom sediment velocities can be determined. The refracted wave that passes through sub-bottom sediments is represented by the blue line in Figure B1. The velocity of sub-bottom sediments will not be measurable until this wave arrives at hydrophones before a direct wave that travels through the water, directly from the seismic source to the hydrophone.

Figure B1. Idealized diagram of raypaths for types of waves produced at ORLSS. The refracted wave is blue, the primary reflected wave is green, and a multiple reflected wave is solid red. The travel time for the multiple is the same as that for a primary reflection from greater depth with the brown representing a deeper geologic contact. A reflection from a hypothetical deeper contact is shown as a dashed red line, with the interface at twice the depth for simplicity; this assumes the same velocity in the water and the first geologic layers.

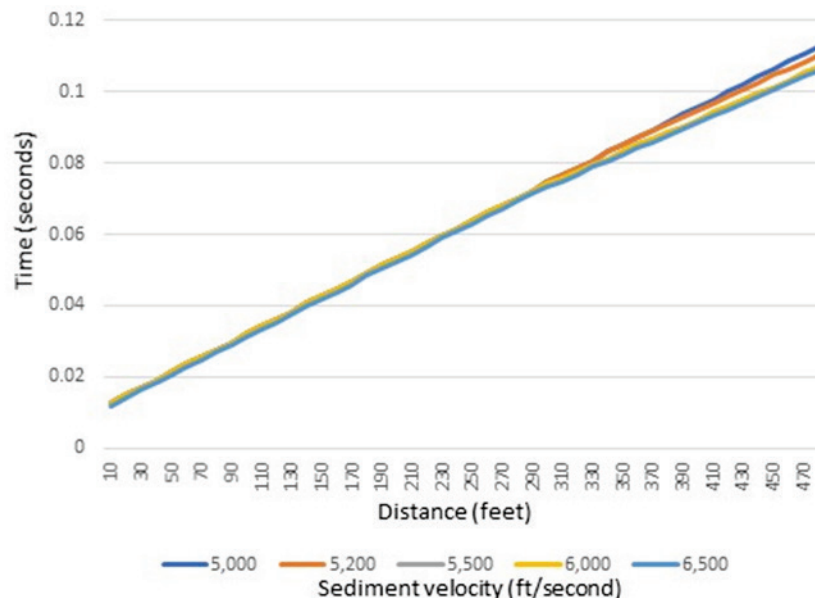


Synthetic seismic modeling was conducted to enhance understanding of the seismic data limitations. The modeling assumed a water layer, 40-ft thick, overlying a sediment layer of constant velocity. The water layer velocity was set at 4,700 ft/s, and the sediment layer velocity ranged from 5,000 ft/s to 6,500 ft/s (Figure B2). These values were selected after data acquisition was completed and represent actual conditions at ORLSS.



From this model, synthetic seismograms were computed by using the Geogiga software package. First arrival times were picked from these synthetic seismograms by using the same procedure described in the main text of this report. The first arrival times were tabulated for hydrophone offsets ranging from 0 to 480 ft and for sediment velocities of 5,000, 5,200, 5,500, 6,000, and 6,500 ft/s. Figure B3 shows the first arrival plots for all five selected sediment velocities on a single plot. This shows arrival times that would be observed if 48 hydrophones were deployed at distances of 0 to 480 ft from the seismic source.

Figure B3. Time-distance plot showing arrival times of seismic waves for five hypothetical bottom sediment velocities, based on the model in Figure B2.



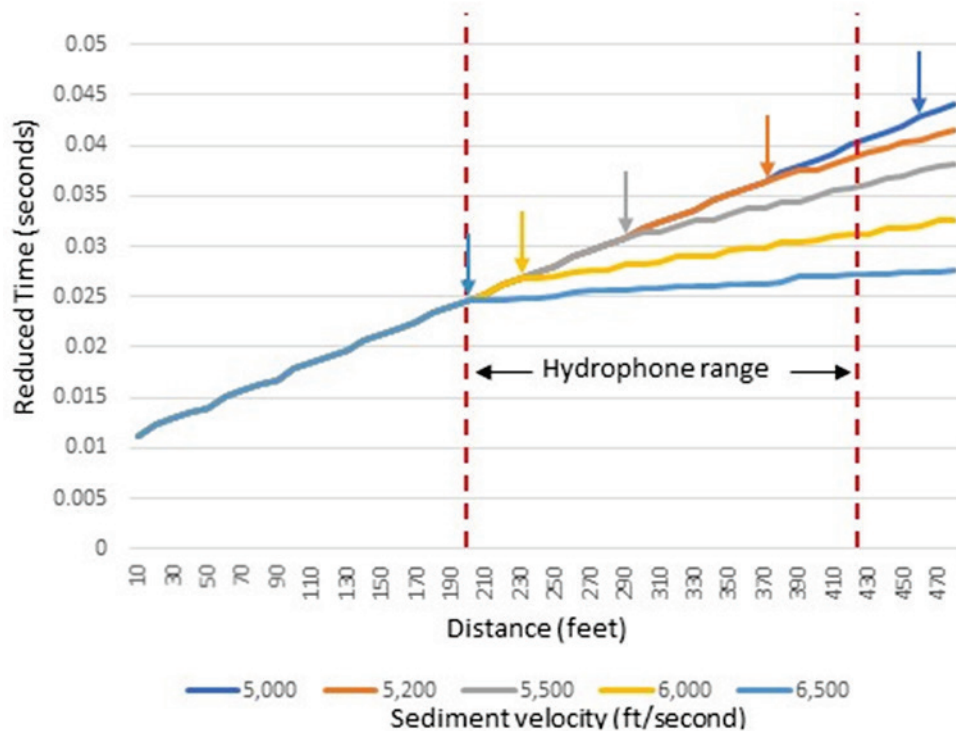
For distances out to at least 290 ft from the seismic source, the travel times for all five sediment velocities are identical. This is because it is faster for the seismic energy to pass through the upper portion of the water than to travel down to the sediment, along the sediment interface, and back up through the water column. There is little difference between the water velocity and sediment velocities and because of this, the first arriving wave will be through the water until reaching a large distance from the source. It is apparent from Figure B3 that the waves traveling through higher velocity sediments can arrive earlier than the water wave, beginning at about 300 ft from the seismic source.

It is difficult to recognize the details in Figure B3 because all five curves are so similar. To make it easier to observe subtle changes in velocity, geophysicists often plot the Reduced Time (TR) instead of Time (T) on the y-axis of such plots. The reduced time is simply

$$TR=T-(x/VR),$$

where VR is known as the reducing velocity. The reducing velocity can be any value but is typically chosen as a value slightly greater than the maximum velocity of layers at the site. In this case, a reducing velocity of 7,000 ft/s was used. Figure B4 shows a Reduced Time-Distance plot for the synthetic data set.

Figure B4. Reduced time-distance plot for the synthetic seismic refraction data.



This figure enhances the synthetic seismic data and shows several important features. Color-coded arrows are used to show the times at which the seismic waves that pass through the sediment layer arrive before the wave traveling through the water column for each of the five sediment velocities. This distance is known as the “crossover distance.” The range of distances, 59.4-129.5 m (195-425 ft), at which hydrophones were located relative to the seismic source is indicated within red dashed lines.

- From this figure, it is apparent that the first arrival curves are identical to one another between distances of 0 and about 61 m (0 and 200 ft). Beyond that distance, the crossover distances increase as sediment velocity decreases.
- At distances shorter than the crossover distance, the first arriving seismic energy is providing information only about the water velocity. No velocity information about the bottom sediments occurs for hydrophones closer than the crossover distance.
- When sediment velocities are close to the water velocity, as is the case for much of the ORLSS study, only the most distant hydrophones can provide information on bottom sediment velocity.

- In portions of the channel where the sediment is shallower than 12.1 m (40 ft), the crossover distance will be reduced; likewise, where the channel is deeper, the crossover distance is increased.
- The velocity of the sediments is measured as the slope in the time-distance curve (Figure B3); both the time-distance plot and the reduced time-distance plot (Figure B4) show that the slope changes with sediment velocity.

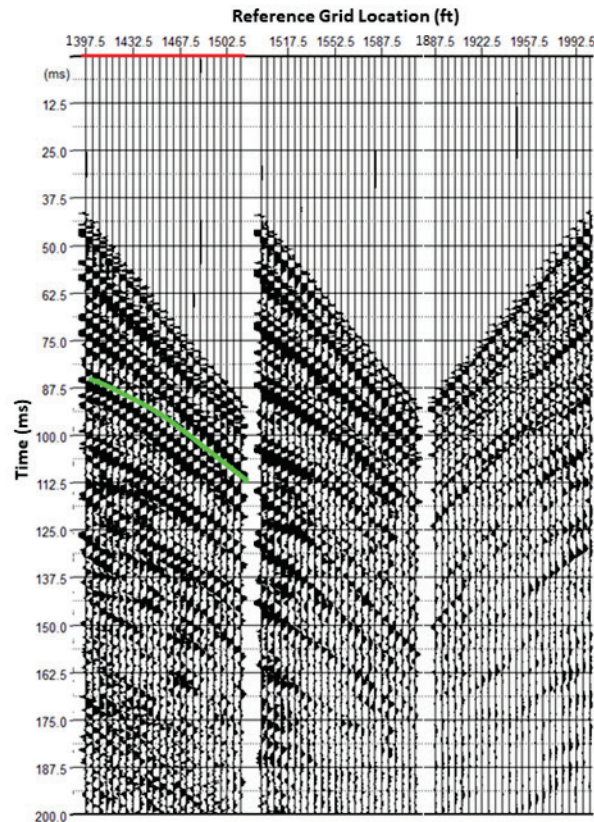
When sediment velocities are higher and when they change laterally along the seismic lines, there will be changes in slope in the portion of the time-distance plot beyond the crossover distance. By combining the time-distance plots for several shot points along the line, the sediment velocity, and even some changes in velocity with depth, can be determined along the line. Where sediment velocities are low such that only the last few hydrophones are encountering energy that has passed through the sediment layer, little information about the subsurface can be determined.

In summary, bottom sediment velocities were lower than anticipated at the onset of this project. Because of this, a longer offset from the source was required before sediment velocities could be measured, and so it was not possible to measure these velocities as close to the ORLSS structure as anticipated. In addition, as described in the body of the report, the low sediment velocities also precluded tomographic inversions that would have represented deeper portions of the sub-bottom and provided cross sections of bottom sediment velocities.

Seismic reflections

During acquisition, it was observed that some shots produced numerous seismic reflections, which could be hyperbolic wavefronts at arrival times later than the refracted “first breaks” (Figure B5). Raypaths for both refracted and reflected seismic waves are shown in the diagram in Figure B1. Seismic reflections were analyzed to determine whether they provided any additional information about the sediment interfaces in the vicinity of ORLSS that could be useful in assessing the subsurface structure.

Figure B5. Reflected seismic waves observed in three “shot gathers” during fieldwork on line 400N on the inflow side of ORLSS. One of the many reflections is highlighted in green on the left shot gather.



It is important to note that because the seismic data acquired at ORLSS were not acquired to detect seismic reflections, the data are not as robust as data that are acquired by using standard reflection acquisition procedures. Normally, seismic reflection data sets have a great deal of redundancy. The redundancy allows production of “stacked” seismic cross sections by compositing data from several shot-receiver pairs that are symmetric about a midpoint but with each pair at different offsets from the midpoint, and each of which contains reflections from several underlying interfaces. Corrections are made for the lateral components of the raypath for each source/receiver pair (“normal moveout” or NMO) so that corrected traces provide a one-dimensional reflection response beneath the selected midpoint. The number of data traces from source/receiver pairs that are combined for a midpoint is referred to as the “fold.” A seismic reflection cross section is formed by aligning the stacked traces for a sequence of midpoints. Normally, seismic reflection sections will have a fold of at least 8 and sometimes as many as 48 traces for each midpoint.

In the case of the reflections analyzed at ORLSS, typical fold is 1 or 2, which means that non-reflected waves are retained in the cross section and can confuse the interpretation if not properly recognized. Thus, it is important to use caution so that non-reflected waves are not misinterpreted as reflections.

Seismic data were processed for seismic reflections by using the Geogiga Reflector module of the Geogiga package, version 9.0. The files that were prepared for refraction analysis were used, and these files already had embedded source and receiver geometry. The data were first frequency filtered, using a bandwidth of 50-800 Hz. Next, a semblance utility was used to assess stacking velocities, which were consistent with the velocities measured in the refraction analysis, about 1,463 m/s (4,800 ft/s). The velocities were adjusted for each shotpoint to yield flat-lying reflections. This assumption was necessary because of the lack of fold in the data, so that there was no other basis for estimating velocities. An NMO correction was then applied to each shot gather. This corrects for the lateral component of source-receiver separation, so that reflections such as those in Figure B5 will appear flat-lying if the proper velocity is used and if the interface from which they are reflecting is horizontal and flat. An example of three shot gathers after applying the NMO correction is shown in Figure B6 for the same shots as shown in Figure B5. It is noteworthy that the post-NMO reflections do not have a constant arrival time across each of the shot gathers. They seem to dip slightly away from the shot. This is because either the velocity used for the NMO correction was too low or the reflecting surface was not horizontal. Because they dip in opposite directions that depend on which end of the shot gather the geophone was located (the shot was on the left for the two leftmost shot gathers and on the right for the third shot gather), it is likely that the velocity that was selected was too low. This can be adjusted through an iterative process until a consistent pattern results. Finally, after the NMO step has been completed, a stacked cross section can be produced for the line (Figure B7). These can be represented in terms of travel time (top, Figure B7); or, by applying the velocities used for the NMO correction, a depth section can be produced for the same line (bottom, Figure B7).

Figure B6. The shot gathers from Figure B5 after applying the NMO correction.

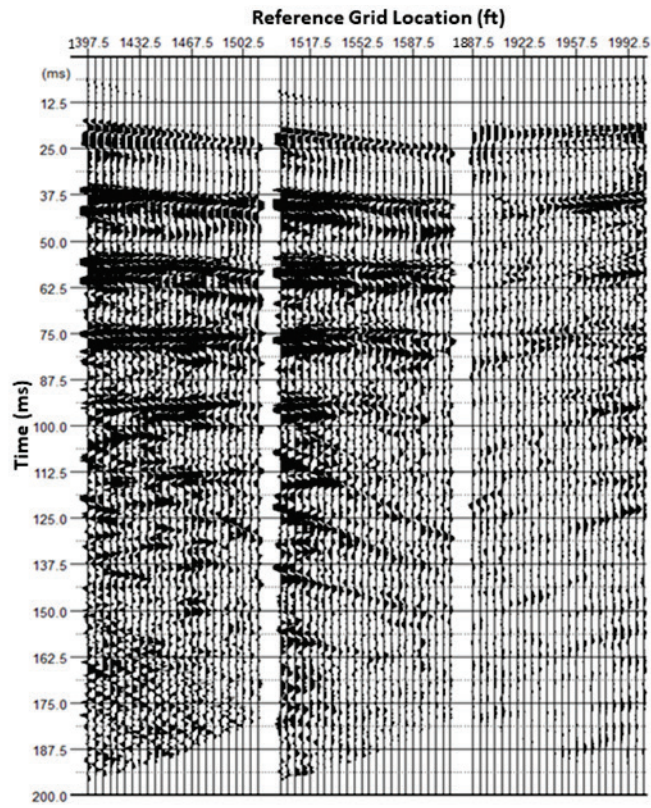
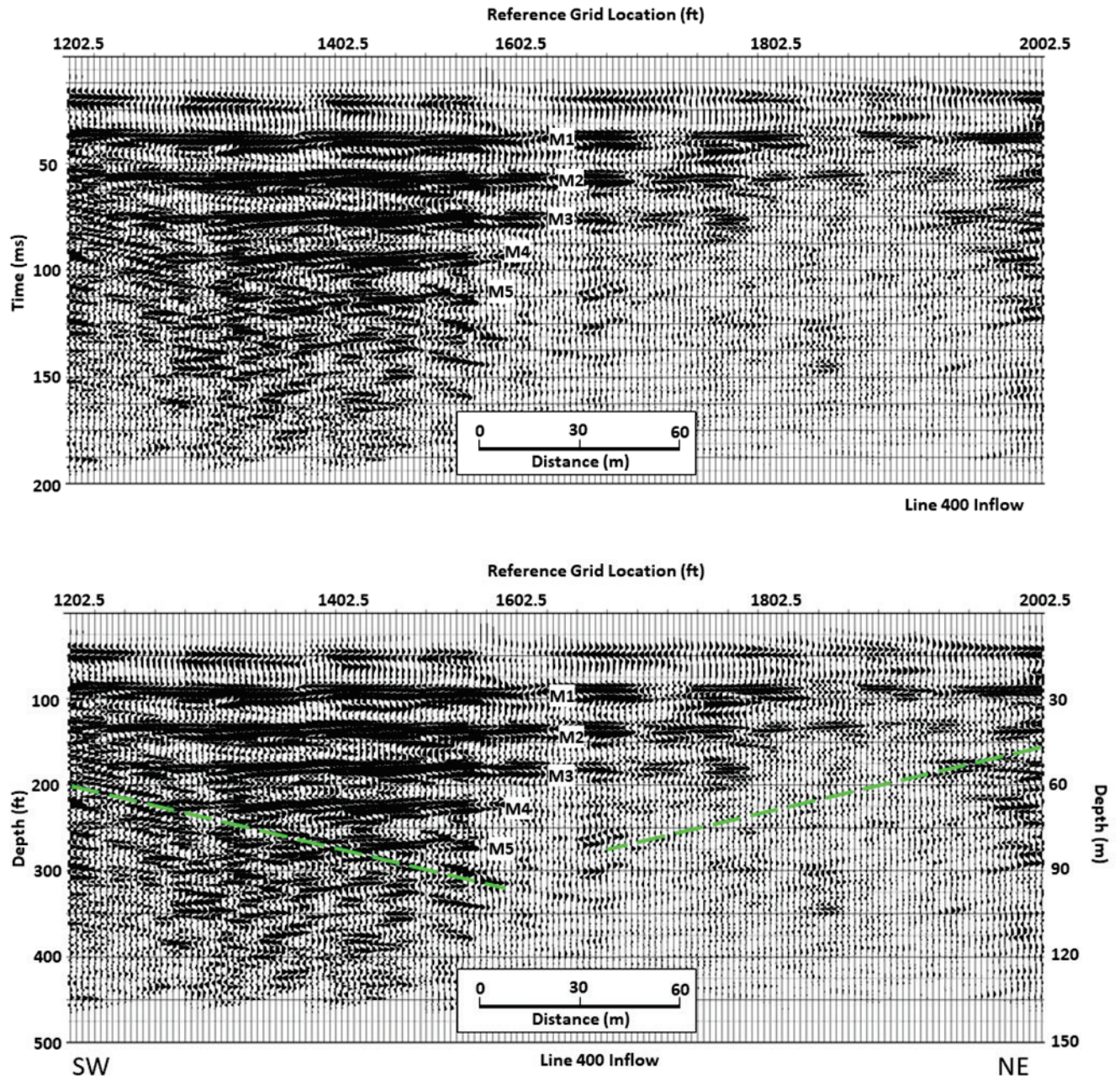


Figure B7. Stacked reflection section for Line 400 from the inflow channel of ORLSS, (top) in travel time and (bottom) in depth feet.



Because the first hydrophone was positioned 59.5 m (195 ft) from the airgun, the closest midpoint for any shot gather was 29.7 m (97.5 ft) from the airgun, and the most distant hydrophone yielded a midpoint that was 64.8 m (212.5 ft) from the airgun. The width of the subsurface represented by each shot gather is thus 35.1 m (115 ft). The positions of the midpoints relative to the local grid system (Figure 12 in the main report) are shown

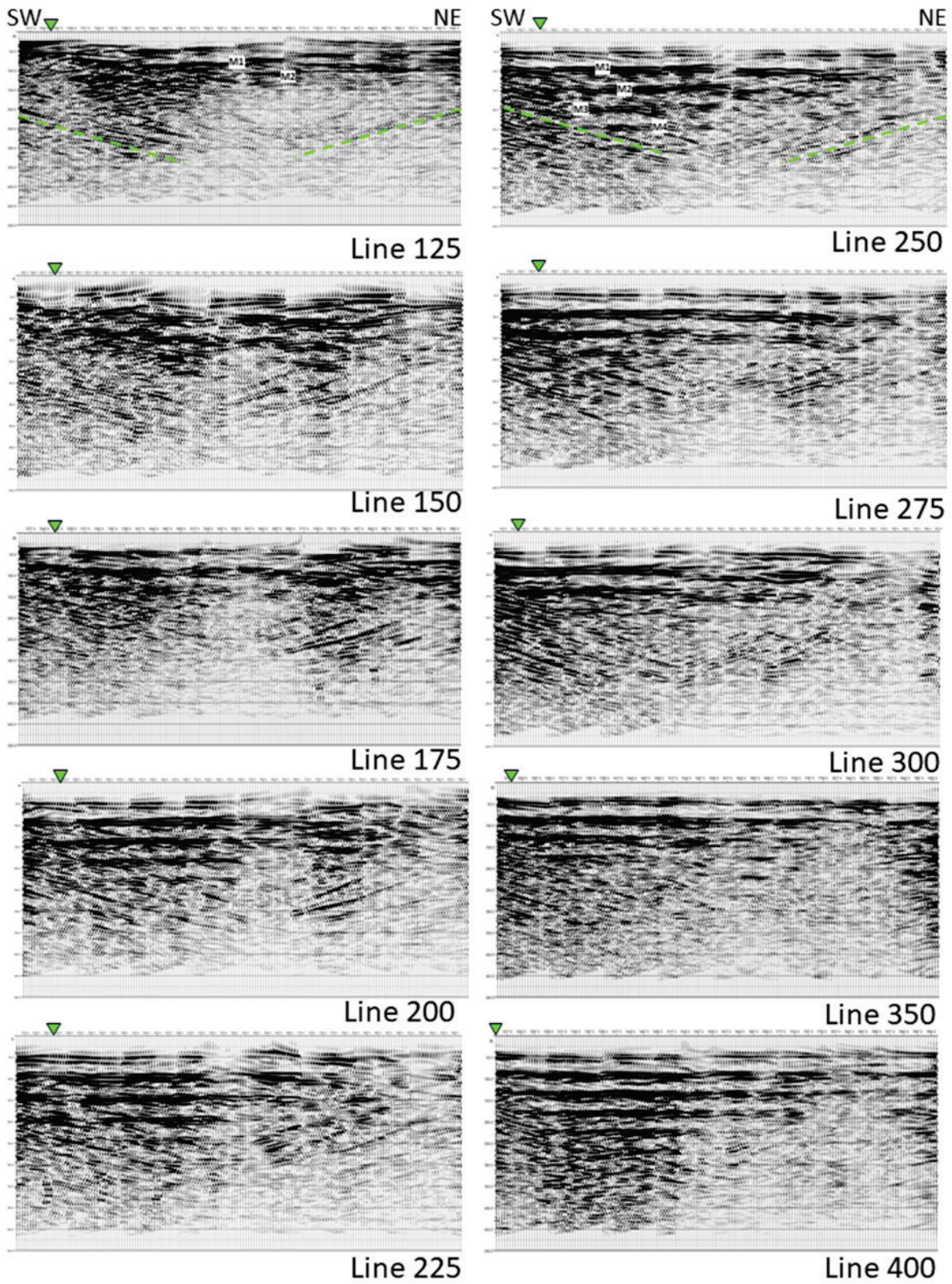
across the top of each shot gather. By combining data for each midpoint, the stacked cross sections shown in Figure B8 are produced.

Figure B8 includes stacked seismic reflection sections for Lines 125-400 on the inflow side of ORLSS. These lines are parallel and tightly spaced, 8 m (25 ft) apart for Lines 125-300. Each line represents the calculated seismic reflection response between grid lines 1200 and 2000 in the horizontal and approximately 152.4 m (500 ft) in depth. Thus, many features on the lines that are real could be expected to be similar or transitional between adjacent lines. Of course, the depth axis will contain features that are not actually at the depth shown in the figure but instead are artifacts of one kind or another. The actual portion of the data that could contain useable information is likely limited to 30.5-45.7 m (100-150 ft) depth or less. As noted in the body of this report, most lines show sets of 3-5 multiple reflections from the interface between the water column and the bottom sediments. These are often continuous from one end of each line to the other end. These are labeled as M1 through M5 on Figure B7 as examples. Each bottom multiple is a group of peaks, with the groups having an apparent thickness that ranges between about 5 and 15m (15 and 50 ft). The width of the group likely depends on the energy output of the source when the shot was acquired and the duration of the source “wavelet” (i.e., the total time duration of the transmitted signal from the airgun). The figures also have straight parallel lines that dip toward the center of the profile from both ends (parallel to the green dashed lines in Figure B7). These are artifacts called air waves, which represent energy traveling slowly through the air from the source. The fact that they converge toward the center of the profile from the ends is an indication that data were acquired when the boat was moving away from the ORLSS structure as well as when it was moving toward the ORLSS structure.

Some general observations can be made about the profiles in Figure B8. Multiples are labeled with M1...M3, and airwaves are indicated by dashed green lines on the top two images of the figure. Similar features occur in all images shown in Figure B8. Some lateral discontinuities in reflections or multiples occur at breaks between shot gathers, and these are related to an inability to precisely determine a velocity for the NMO correction. Lines 125-175 show more disruptions, or lateral breaks in the reflection multiples along their entire length, including breaks within shot gathers. The multiples are somewhat less continuous between lines 200-250. The outermost 20-25 percent portion of most

of the lines (nominally between reference grid locations 1800-2000) is weaker or more discontinuous than the portion closer to the ORLSS structure. For Lines 125, 150, and (to a lesser extent) 175, few to no multiples are observed between grid points 1200 and 1400, where the greatest scour is expected to occur. The clarity of the multiples improves gradationally from Line 175 to 400 such that at Line 400, they are largely undisturbed at the ORLSS (southwest) end of the line. This transition, in the extent of irregularity of the reflections and multiples, is probably related to irregular changes in the subsurface velocities and interference associated with diffractions from subsurface features, such as large riprap blocks. As noted above, depths on the seismic reflection sections should not be misconstrued to indicate actual depths. Lateral changes in the appearance over the entire depth range are more meaningful in these figures than any apparent changes with depth. The reflections are clearly responding to features within the remediated scour (edge of the scour is indicated by the green triangle at the top of each profile in Figure B8); however, because of the low fold and abundance of interference features, such as multiple reflections, the data are not as informative with regard to details of the remediated scour as are the resistivity data.

Figure B8. Stacked reflection sections for ten lines on the inflow side of ORLSS. Edge of the scour is indicated by the green triangle at the top of each profile.



The reflection sections from the outflow side are more interesting than those on the inflow side because the bottom topography deepens substantially moving downstream from ORLSS. In addition, there are features indicative of a rough or irregular bottom, called diffraction hyperbolae. The features appear in the depth section shown in Figure B9a below an apparent depth of 76.2 m (250 ft) on the left half of the figure. They appear as secondary, nearly linear features that trail away in both directions from the diffraction apexes, labeled "D." These artifacts can be remediated through a processing technique known as migration. The migrated section in Figure B9b shows a more representative location for these features once the diffraction hyperbolae have been mostly collapsed to their source location. The absence of diffraction hyperbolae indicated that migration was not needed on most of the ORLSS lines, so it was applied only to selected lines on the outflow side. Similarly, Figures B9c and B9d show both unmigrated and migrated sections for outflow Line 400.

Figure B9. (a) Unmigrated and (b) migrated depth sections for outflow Line 300.

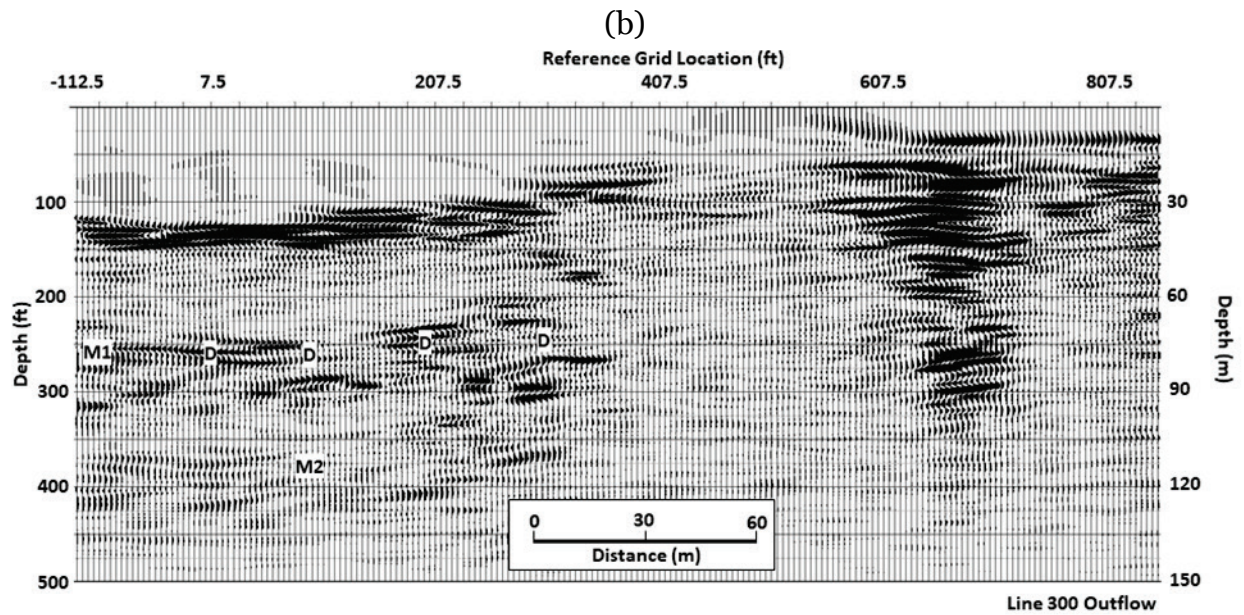
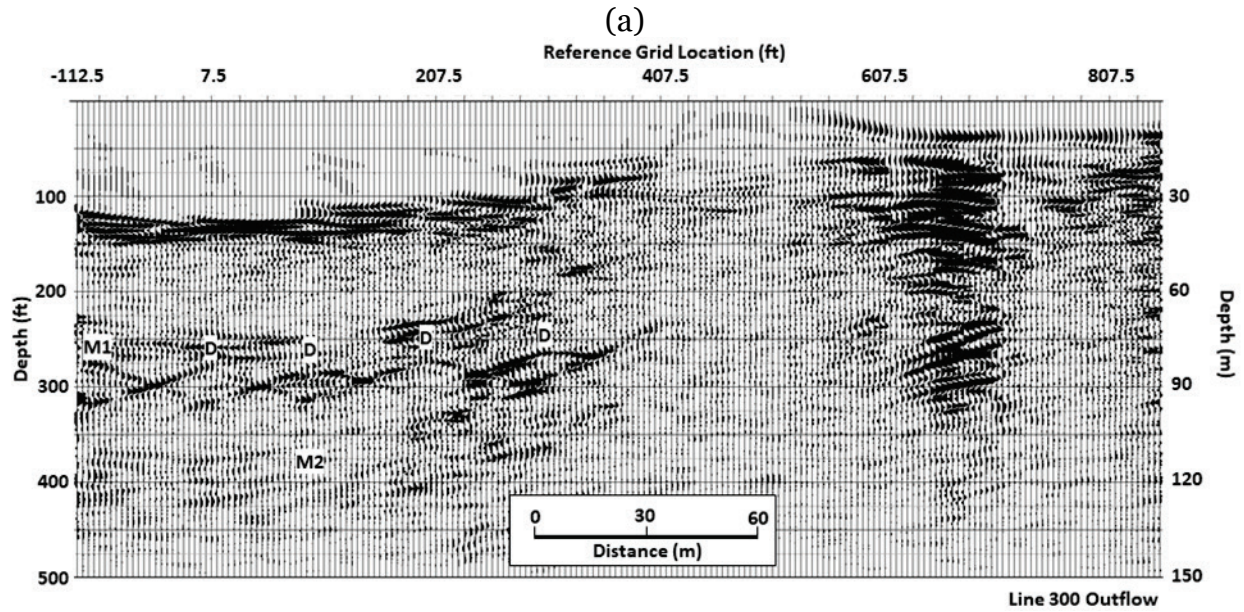
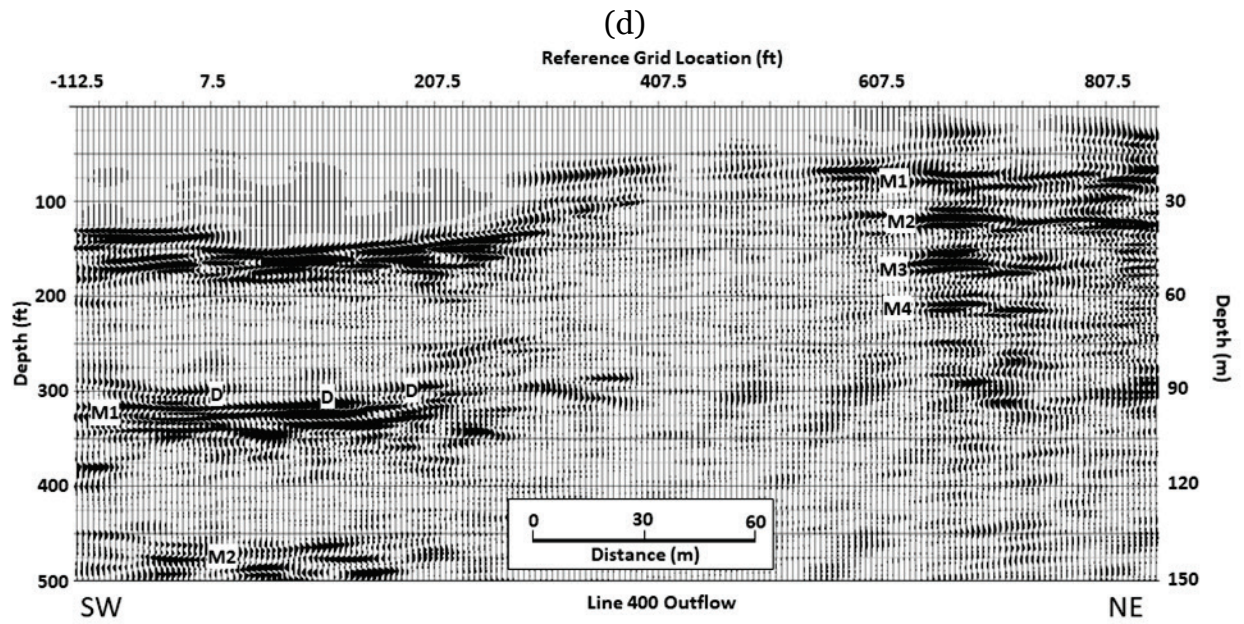
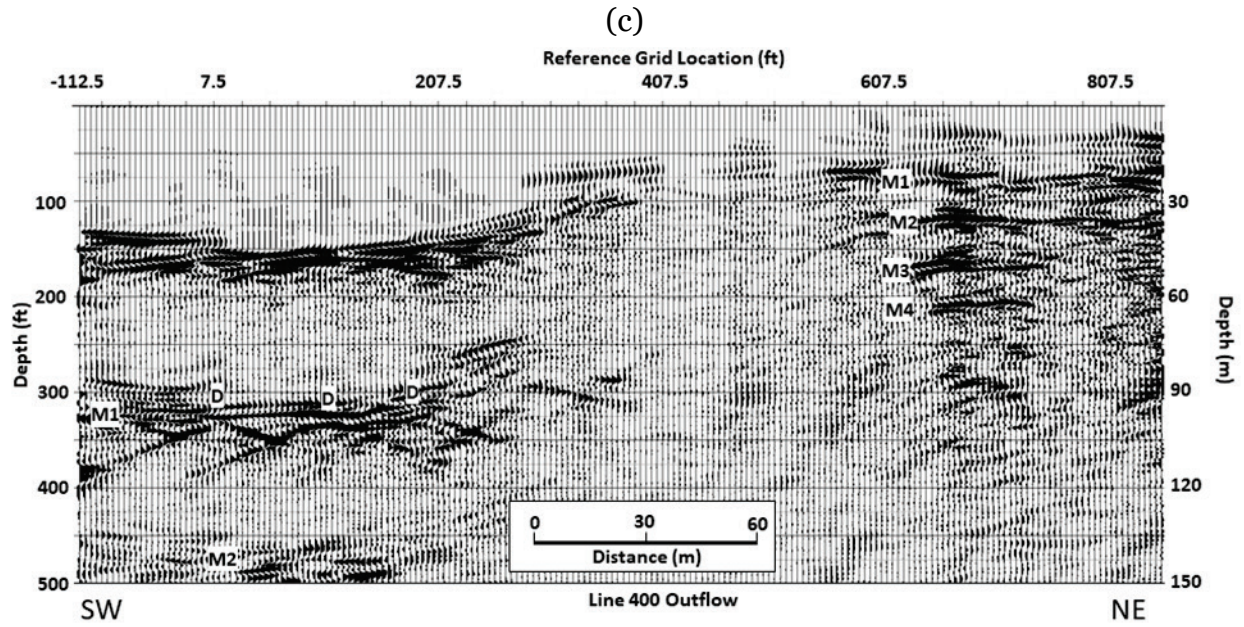


Figure B9. (c) Unmigrated and (d) migrated depth sections for outflow Line 400.



Unit Conversion Factors

Divide	By	To Obtain
cubic meters	0.02831685	cubic feet
cubic centimeters	16.3871	cubic inches
degrees Celsius	(F-32)/1.8	degrees Fahrenheit
meters	0.3048	feet
meters	0.0254	inches
meters	1,609.347	miles (U.S. statute)
meters per second	0.44704	miles per hour
megapascals	0.006894757	pounds (force) per square inch
kilograms	0.45359237	pounds (mass)
kilograms per cubic meter	16.01846	pounds (mass) per cubic foot
kilograms per cubic meter	2.757990 E+04	pounds (mass) per cubic inch
kilograms per square meter	4.882428	pounds (mass) per square foot
kilograms per square meter	0.542492	pounds (mass) per square yard
square meters	0.09290304	square feet
square meters	6.4516 E-04	square inches
square meters	2.589998 E+06	square miles
kilograms per cubic meter	1,328.939	tons (long) per cubic yard
kilograms	907.1847	tons (2,000 pounds, mass)
kilograms per square meter	9,764.856	tons (2,000 pounds, mass) per square foot

REPORT DOCUMENTATION PAGE

Form Approved
OMB No. 0704-0188

Public reporting burden for this collection of information is estimated to average 1 hour per response, including the time for reviewing instructions, searching existing data sources, gathering and maintaining the data needed, and completing and reviewing this collection of information. Send comments regarding this burden estimate or any other aspect of this collection of information, including suggestions for reducing this burden to Department of Defense, Washington Headquarters Services, Directorate for Information Operations and Reports (0704-0188), 1215 Jefferson Davis Highway, Suite 1204, Arlington, VA 22202-4302. Respondents should be aware that notwithstanding any other provision of law, no person shall be subject to any penalty for failing to comply with a collection of information if it does not display a currently valid OMB control number. **PLEASE DO NOT RETURN YOUR FORM TO THE ABOVE ADDRESS.**

1. REPORT DATE (DD-MM-YYYY) April 2022		2. REPORT TYPE Final		3. DATES COVERED (From - To)	
4. TITLE AND SUBTITLE Waterborne Geophysical Investigation to Assess Condition of Grouted Foundation: Old River Control Complex – Low Sill Structure, Concordia Parish, Louisiana				5a. CONTRACT NUMBER	
				5b. GRANT NUMBER	
				5c. PROGRAM ELEMENT NUMBER	
6. AUTHOR(S) Benjamin R. Breland, Janet E. Simms, William E. Doll, Jason Greenwood, and Ronald Kaufman				5d. PROJECT NUMBER 110712	
				5e. TASK NUMBER	
				5f. WORK UNIT NUMBER	
7. PERFORMING ORGANIZATION NAME(S) AND ADDRESS(ES) See next page				8. PERFORMING ORGANIZATION REPORT NUMBER ERDC/GSL TR-22-9	
9. SPONSORING / MONITORING AGENCY NAME(S) AND ADDRESS(ES) U.S. Army Corps of Engineers (USACE), New Orleans District (MVN) New Orleans, LA 70118				10. SPONSOR/MONITOR'S ACRONYM(S)	
				11. SPONSOR/MONITOR'S REPORT NUMBER(S)	
12. DISTRIBUTION / AVAILABILITY STATEMENT Approved for public release; distribution is unlimited.					
13. SUPPLEMENTARY NOTES Old River Low Sill Evaluation					
14. ABSTRACT The Old River Low Sill Structure (ORLSS) at the Old River Control Complex (ORCC) in Concordia Parish, LA, is a steel pile-founded, gated reinforced-concrete structure that regulates the flow of water into the Atchafalaya River to prevent an avulsion between the Mississippi River and the Atchafalaya River. A scour hole that formed on the southeast wall of ORLSS during the Mississippi River flood of 1973 was remediated with riprap placement and varied mixtures of self-leveling, highly pumpable grout. Non-invasive waterborne geophysical surveys were used to evaluate the distribution and condition of the grout within the remediated scour area. Highly conductive areas were identified from the surveys that were interpreted to consist mostly of grout. Resistive responses, likely representing mostly riprap and/or sediment, were encountered near the remediated scour area periphery. A complex mixture of materials in the remediated scour area is interpreted by the more gradual transitions in the geophysical response. Survey measurements immediately beneath ORLSS were impeded by the abundance of steel along with the structure itself. The survey results and interpretation provide a better understanding of the subsurface properties of ORLSS.					
15. SUBJECT TERMS Waterborne Subsurface Geophysics Geophysical surveys		Electrical resistivity tomography Seismic refraction Infrastructure Mississippi River Scour (Hydraulic engineering)		Grout condition Grouting (Soil stabilization) Diversion structures (Hydraulic engineering) Concordia Parish (La.)	
16. SECURITY CLASSIFICATION OF:			17. LIMITATION OF ABSTRACT	18. NUMBER OF PAGES	19a. NAME OF RESPONSIBLE PERSON
a. REPORT Unclassified	b. ABSTRACT Unclassified	c. THIS PAGE Unclassified			SAR

PERFORMING ORGANIZATION NAME(S) AND ADDRESS(ES)

Geotechnical and Structures Laboratory
U.S. Army Engineer Research and Development Center
3909 Halls Ferry Road
Vicksburg, MS 39180-6199

Oak Ridge Institute for Science and Education
P.O. Box 117
Oak Ridge, TN 37831-0117

Advanced Geosciences Inc.
2121 Geoscience Drive
Austin, TX 78726

Spotlight Geophysical Services, LLC
4618 NW 96th Avenue
Doral, FL 33178